Catalysis over Molybdenum Containing Nitride Materials

UNIVERSITY
of
GLASGOW

David Mckay

A Thesis Presented to the University of Glasgow for the Degree of Doctor of Philosophy

December 2007

Abstract

Reactions involving nitrogen transfer/ fixation are of great industrial interest, as novel processes could help industries meet their increasingly challenging economic and environmental targets. An example of this could be the direct synthesis of aniline from benzene, which would avoid the lengthy, uneconomic, and environmentally unfriendly process currently employed.

This work explores the reactivity of bulk and supported transition metal nitride catalysts, with particular emphasis on the possible reactivity of lattice nitrogen within bulk nitride catalysts. The experimental work has focussed on two main objectives: determining the most active transition metal nitride catalyst for ammonia synthesis, and hydrogenating these materials to in the absence of N_2 to produce reactive NH_x species. These materials were then tested for the possible direct synthesis of aniline from benzene by entrapment of reactive NH_X species. The second objective was to achieve nitrogen reactivity with nitride catalysts akin to the Mars-van Krevelen mechanism observed in oxidation catalysis.

It has been shown that the binary nitrides, γ-Mo_2N and β-$Mo_2N_{0.78}$, have comparable ammonia synthesis activities although measurements indicate that β-$Mo_2N_{0.78}$ may have a much greater activity on a surface area normalised basis. Meanwhile the δ-MoN phase has an intermediate surface area, but very low activity.

The influence of morphology in the ammonia synthesis reaction was investigated by testing *nanorod* forms of β- and γ-phase molybdenum nitrides and comparing their ammonia synthesis activities with molybdenum nitride powders. Morphology was found to have little effect on the reaction and the influence of structure sensitivity is thought to be limited in this case. What was apparent, was that the highly specific temperature programmed reaction synthesis required to prepare γ-Mo_2N produced an ammonia synthesis catalyst with no catalytic advantage over one that is prepared in mixtures of H_2/N_2 (β-$Mo_2N_{0.78}$).

The influence of preparation on the ammonia synthesis activity of ternary nitride catalysts was also investigated by preparing materials in NH_3 or H_2/N_2 atmospheres. Treatment of iron and cobalt molybdenum oxide under H_2/N_2 was not sufficient to yield a pure phase nitride, however $NiMoO_4$ was fully reduced to Ni_2Mo_3N. Co_3Mo_3N, prepared using NH_3, was the

most active of the ternary nitride catalysts tested, and preparing the materials in H_2/N_2 failed to increase the activity, with the exception of Ni_2Mo_3N.

Reaction of Co_3Mo_3N with H_2/Ar significantly decreased the nitrogen content of the material, and it is believed that a previously unknown eta-12 Co_6Mo_6N phase has been formed as a result of the nitrogen removal. Hydrogen was shown to be essential to induce this change, despite the fact that most of the eliminated N ended up in the form of N_2. Prolonged treatment with H_2/Ar at elevated temperature did not remove any additional nitrogen. It is believed that the incomplete loss of nitrogen is a direct consequence of the migration of nitrogen between crystallographic sites as the stoichiometry is reduced. In the case of iron and nickel-molybdenum nitrides the loss of nitrogen was evidenced by combustion analysis, however no new phases of material were formed. Similar experiments, with conducted with different molybdenum nitride polymorphs have shown the removal of nitrogen with a mixed phase of constituent metal and nitrided species, with only β-$Mo_2N_{0.78}$ fully decomposing to the pure metal. The loss of nitrogen, and hence its potential for reaction, is evident. However, in all cases the predominant form of lost nitrogen is N_2, which is believed to be a consequence of the thermodynamics of ammonia decomposition at higher temperatures. Restoration of stoichiometry by treatment with H_2/N_2 has been observed for a number of materials, i.e. Co_3Mo_3N, γ-Mo_2N. In the case of Co_6Mo_6N, the NH_3 synthesis activity has been found to be comparable with Co_3Mo_3N.

H-ZSM-5 supported nitride catalysts were also tested for ammonia synthesis and it was observed that the introduction of iron as a dopant has significant promotional effects. XPS evidence confirmed the presence of Fe^0 in the material, in addition to the molybdenum (oxy)nitride species observed for MoO_3/H-ZSM-5. FTIR spectroscopy was used to conduct isotopic nitrogen exchange experiments over nitrided H-ZSM-5 and MoO_3/H-ZSM-5. Under the conditions of the experiment, it was shown that the presence of "molybdenum nitride" facilitated the exchange of $^{15}N_2$ with zeolite framework NH_x species. This shows that supported γ-Mo_2N species can be a source of reactive and mobile N species, potentially opening up possibilities for its application as a source of spill-over nitrogen.

A potential route for the direct synthesis of aniline from benzene by hydrogenating ternary nitrides with benzene in the feed, trapping the possible reactive nitrogen species, was investigated. GCMS data showed the no reaction occurred, as only benzene was found in the

product condensate. In all cases a significant amount of carbon was incorporated/ deposited on the catalysts. In the case of the cobalt molybdenum sample, the XRD data confirmed the conversion of nitride to the carbide, however post-reaction XRD of the iron and nickel samples did not indicate carbide formation.

Contents

Figures and Tables

List of Tables

Publications

J. S. J. Hargreaves and D. Mckay, "Nitrides and oxynitrides as catalysts", Specialist Periodical Reports in Catalysis, RSC Cambridge, J J Spivey Senior Reporter, Volume 19, Chapter 3, 86-109 (2006).

D. Mckay, J. S. J. Hargreaves and R. F. Howe, "XPS evidence for molybdenum nitride formation in ZSM-5", *Catalysis Letters*, 112, 109-113 (2006).

D. Mckay, D. H. Gregory, J. S. J. Hargreaves, S. M. Hunter and X-L. Sun, "Towards nitrogen transfer catalysis: Reactive lattice nitrogen in cobalt molybdenum nitride", *Chem. Commun.* (2007), 3051-3053 (2007).

D. Mckay, J. S. J. Hargreaves, J. L. Rico, J. L. Rivera and X-L. Sun. "On the reactivity of some molybdenum containing nitrides" (2007). J. Solid. State. Chem. In Press.

Future publications anticipated.

Acknowledgements

Where to start!? There are so many people that I would like thank, as the experiences, successes, and laughs, would not have been possible without them.

Firstly I would like to say a massive thank you to my supervisor, Dr. Justin Hargreaves, for the guidance, enthusiasm, help, and support that he has given me over the last three years. I hate to embarrass him, but I really could not have wished for a better supervisor than Justin, nothing is ever any trouble to him at any time of day (or night!). Highlights for me would be, how the med building is the only place to get a decent coffee, and in-depth discussion with Graham and myself on the front-runner in the fast-food industry, "Burger King or Mcdonalds?". I have really enjoyed working with Justin for the last three years, and can't stress enough how much I appreciate his help.

I would also like to thank Professor. Russell Howe for all his help with the XPS measurements and Dr. Michael Stockenhuber for allowing me access to the facilities at Nottingham Trent University, and for kindly conducting the FTIR study. I also thank Dr. Jose L. Rico for kindly preparing and donating the α-MoO_3 *nanorods*. I am also grateful to Dr. Xiao-Ling Song and Stuart Hunter for their assistance and collaboration in the last 3 years

Thanks to Mrs. Kim Wilson for her assistance in performing the CHN analysis, Mr. Jim Gallagher for his help with the SEM, and Mr. Ron Spence for his help with the GCMS analysis.

A special thanks to Mr. Socialism, Andy Monaghan, for his friendship, help, and tremendous patter for the last 3 years. The man is walking encyclopaedia and I will miss his insights into political and ornithological matters, and the various discussions that would come under "Glasgow etiquette". Paxman hasn't got a look in!

I must also pay a special tribute to the man, the myth, the legend that is Graham Ormsby, from sharing rolls and sausage after nights out to trading joking insults across the lab; Graham has been the highlight of my social and professional life at University. Personal highlights are, "If

I finish your biggest steak, do I get a T-shirt or something?" and, "I'm looking for a black/ rubber latex mask?". There are many more Ormsby-isms that are not fit for print. I've had a great time the last 7 years mate, and I hope you get everything you hoped for with the new job, and that we stay in touch (I'm sure we will!).

A special thanks also to Alan Ferguson for his friendship over the last 7 years, I've enjoyed the "over zealous" conversations he has with TV reporters in Glasgow pubs, sitting with me through maths lectures and all the great nights out. A special thanks must also go to the lunchtime crowd, Gemma, Katrina, Nicola and Jenny for a great time at university and listening to my mad chat for the last 7 years.

I would also like to thank Sharon Burns for all the chat, help and laughs we shared during our time at university together.

There are a few members of the Jackson group whom I would also to thank for the good times had in the last 2 or 3 years, Mark "The God-Father" Facchini, Stuart "Caprice?" Blain, David "The Bear" Milroy, Dan "Boris Becker" Rosenberg, David " Em…Um….Er….YES!" Williams, Fiona "The Mythical" Wigzell, and Claire Gillan. I hope we all stay in touch guys and that everything goes well for those of you who are finishing up in the next year or so!

This acknowledgements thing is in really danger of running away with itself, so……

I owe a huge thanks to my parents/ grandparents for all their love, encouragement and support during my time at university and throughout my life. I wouldn't be here without them.

Finally I thank Deborah, for her patience, never ending support, and for all the encouragement and pep-talks over the last 5 years.

Author's Declaration

The work contained in this thesis, submitted for the degree of doctor of philosophy, is my own original work, except where due reference is made to others. No material within has been previously submitted for a degree at this or any other university.

For Mum, Dad, and Deborah.

1. Introduction- Catalysis with Nitrides and Oxynitride

1.1 General Introduction

Advances in the last 20 years in the methods of preparation have resulted in an expansion in the amount of accessible nitride materials [1-5]. For example, it is only in recent years that the first nitrides possessing the spinel structure have been prepared [6-9], although oxynitrides with this structure were previously reported [10, 11]. At present the primary catalytic interest [5, 12-14] in nitrides has centred around two general themes: (i) the well documented ability of some transition metal nitrides to exhibit catalytic properties which are similar to platinum group metals, and (ii) the acid-base properties of nitrides and oxynitrides. Within the literature, catalytic studies have been mostly concerned with the application of a relatively small number of nitrides/ oxynitrides to a restricted number of reactions. However recent years have seen an expansion in the range of reactions catalysed by nitrides and also the application of novel nitrides to established catalytic reactions. It is clear that nitride and oxynitride catalysis is an exciting and vibrant field with a number of significant advances reported in recent times. However, the catalytic behaviour of most of the reported nitride based materials is largely unknown, with most studies focussing on the various preparative procedures rather than their development as catalysts.

Nitrides can be sub-divided into ionic, covalent and interstitial types [15, 16]. An alternate general classification of nitrides, based on bonding classification, as ionic, covalent and metallic has also been applied. Ionic or "salt-like"nitrides are formed by electropositive elements such as Li, Mg, Ca, Sr, Ba, Cu, Zn, Cd and Hg and possess formulae which correspond to those expected on the basis of the combination of the metal ion with N^{3-} ions. A range of covalent nitrides are known and are exhibited by less electropositive elements such as B, S, P, C and Si. Interstitial nitrides are formed by some transition metals and refer to compounds which can be described in terms of the occupancy of interstitial sites in close packed metallic structures by nitrogen atoms. Oxygen can also be accommodated within these structures in this manner and a range of oxynitrides are known to exist, along with carbonitrides wherein both nitrogen and carbon are distributed between interstitial sites. These subdivisions are, to an extent, arbitrary

and nitrides/oxynitrides are further classified as binary (containing one metal within the main structure), ternary (containing two metals) and quaternary (containing three metals). Arguably, nitrides and oxynitrides which are best described as interstitial have attracted the greatest attention in catalytic studies, although a number of oxynitrides in which partial substitution of the oxygen lattice within oxide structures by nitrogen has been performed have also attracted interest, particularly in terms of their acid-base character. There has also been a lot of interest in nitrogen doped oxides as photocatalysts [116-120]. The main structure–types of the interstitial nitrides are given elsewhere [17]. Of these, binary molybdenum nitrides have been studied in most depth. Although a number of phases of molybdenum nitride have been characterised (γ-, β-, and δ-phases) [18, 19], it is the γ-Mo_2N phase which has been most widely reported in terms of its catalytic behaviour. Its structure can be best described as a face centred cubic array of Mo atoms with nitrogen atoms occupying one half of the octahedral interstices. Figure 1.1-1 below illustrates the structure of γ-molybdenum nitride phase.

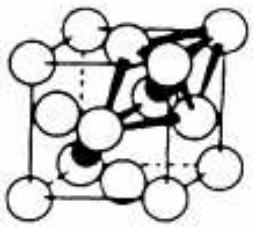

Figure 1.1-1. Representation of γ-Mo_2N phase. molybdenum (white), nitrogen (black).

As discussed later, there is often oxygen incorporated in the near-surface region of the γ-Mo_2N material where the stoichiometry may differ from the bulk, this is possibly due to the passivation procedure, which is necessary to handle the pyrophoric material in air.

It is only in the last few years that the catalytic activity of ternary nitrides has begun to be reported, with Co_3Mo_3N being studied in most detail [53-60].

1.2 Preparation of Nitride and Oxynitride Catalysts

The major preparation routes to nitrides and oxynitrides have been described in detail by Volpe and Boudart [23], Wise and Markel [34] and Choi *et al.*[24]. Historically many nitride

materials were prepared by direct reaction of the metal with nitrogen gas, this preparation route typically employed very high temperatures to cleave the strong N-N triple bond (although lithium is a known exception, forming a nitride at ambient temperature under nitrogen gas). This type of preparation was not concerned with the surface area of resultant materials and as a consequence the surface areas of these nitride materials were generally very low.

In more recent times surface area considerations have played a more important role in the preparation of nitrides/ oxynitrides, and this type of preparation method is no longer favoured. There are two different methods of preparing high surface area materials. The first is to generate a porous material or nano-structured powder via a synthesis method such as temperature programmed reduction (e.g. ammonolysis). The second is to disperse the catalytically active species (e.g. metal nitride) on a high surface area support material. At present within the literature ammonolysis is the preferred method of synthesising high surface area nitrides/ oxynitrides. However Antonelli and co-workers have documented the preparation of mesoporous titanium and niobium oxides [20-22] with metallic properties which, when treated at room temperature in flowing nitrogen, forms a nitride coat on the surface of the material (avoiding the high temperature usually applied to cleave dinitrogen). The porosity and high surface area of the parent materials was retained after reaction with dinitrogen, which makes these materials ideal for reactions concerning the catalytic incorporation of nitrogen into organic molecules, although this does not appear to have been explored to date.

Generally, the method used to prepare metal nitride and oxynitride catalysts is temperature programmed ammonolysis. This method was first documented by Volpe and Boudart, and applied to an MoO_3 precursor in the synthesis of γ-Mo_2N - which was pseudomorphic with the precursor and could be prepared with surface areas as high as 225 m^2g^{-1} [23]. The surface area of the resultant nitride materials was shown by Marchand and co-workers [18] to be strongly dependent on the synthesis parameters employed, such as space velocity and temperature ramp rate, as shown in Table 1.2-1.

As can be observed from the table, high space velocities of ammonia and low temperature ramp rates are required to maximise the surface area of the nitrided material. The high space velocity has the effect of lowering the partial pressure of water formed during the reduction of

the oxide (in this case MoO_3), while the low temperature ramp rates minimises sintering by solid state reaction.

	Mo_2N-A	Mo_2N-B
Amount of commercial MoO_3 (S_g =2m^2g^{-1}) precursor (g)	2-3	2-3
Rate of temperature increase ($Kmin^{-1}$)		
-from 293 to 633K	10	20
-from 633 to 723K	1	20
-from 723K to final T	1	20
Final temperature (K)	700	780
Step time (h)	10-12	0.5
Ammonia flow rate (lh^{-1})	35	35
Specific surface area (m^2g^{-1})	115-120	15-20

Table 1.2-1. The influence of ammonolysis parameters on the surface area of molybdenum nitride [18].

A study conducted by Choi *et al.* into the preparation of molybdenum nitride has shown the influence of these synthesis parameters on the structural properties of molybdenum nitrides prepared in this manner [24]. They have concluded that the formation of molybdenum nitride proceeds through a series of parallel reactions and that use of low ramp rates with high space velocity is key to channelling the conversion of MoO_3 through the γ-$Mo_2O_yN_{1-y}$ intermediate, yielding high surface area γ-Mo_2N. The reaction scheme is summarised below in Figure 1.2-1.

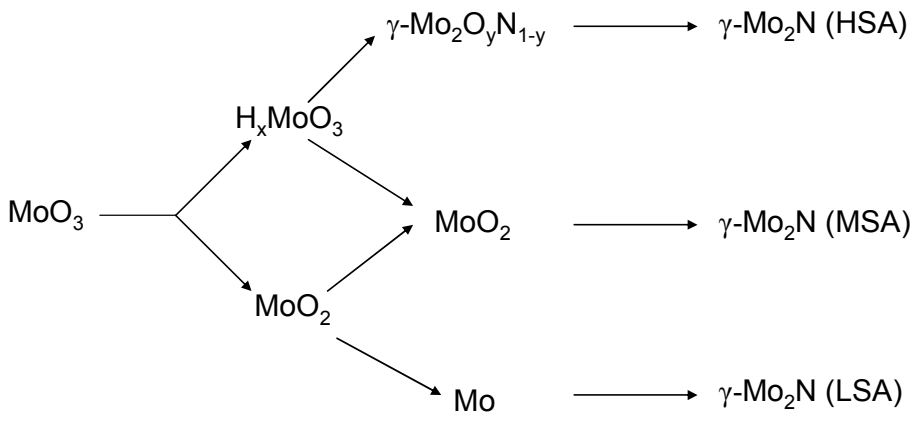

Figure 1.2-1. The inter-conversion pathways during ammonolysis of MoO_3 [24].
(where LSA, MSA and HSA refer to low, medium and high surface area respectively).

A number of studies present in the literature have indicated that molybdenum nitride prepared via the temperature programmed ammonolysis route contains a number of surface NH_x residues (partially dehydrogenated forms of surface ammonia) [25, 26]. After temperature programmed ammonolysis, nitrided materials are usually cooled to room temperature in inert gas (helium or nitrogen) or in flowing ammonia, before being subsequently passivated in a dilute oxygen mixture (typically <1% O_2). In this latter passivation stage, an oxynitride surface skin is formed which facilitates handling and also protects the pyrophoric bulk nitride from reaction with air. As described in section 1.1, a significant amount of oxygen is incorporated in the near surface region during this stage [27, 28], which is generally removed prior to catalytic application by hydrogen pre-treatment at *ca.* 400^{o}C [24, 26, 28]. In a detailed TPD and TPR study, Grange and co-workers documented large differences between the freshly prepared and passivated γ-Mo_2N [26]. Two types of NH_x adsorbed species (weakly/ and strongly adsorbed) are present on the freshly prepared γ-Mo_2N sample. The passivated γ-Mo_2N has only weakly adsorbed NH_x. It was concluded that the main effect of the passivation was to remove some of the NH_x species, with the oxygen bonding to surface Mo atoms to occupy the original positions of the NH_x species forming the protective oxide layer. Thompson and co-workers have undertaken a high resolution transmission electron microscopy and XPS study of passivated and re-reduced γ-Mo_2N and concluded that there are significant differences in the bulk and near surface structures of the materials [29]. It was proposed that the surface structures of both of these materials should be viewed as oxynitrides with the general formula Mo_2N_3-

$_xO_x$, which has a body centred lattice structure. This structure accounts not only for the compositions of the materials but also electron diffraction patterns measured by Thompson and co-workers. A diagram of the oxynitride structure is shown below in Figure 1.2-2.

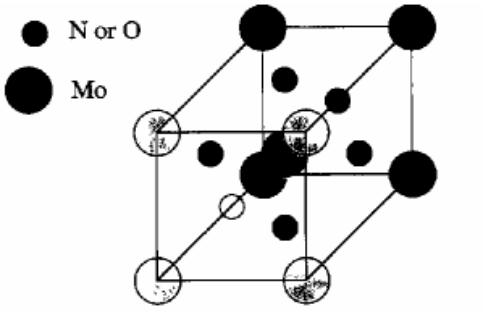

Figure 1.2-2. Proposed $Mo_2N_{3-x}O_x$ structure in which all of the interstices are filled with nitrogen or oxygen. (Note: Similar spheres indicate atoms in the same plane and similar size denotes atoms of the same type) [29]

The temperature programmed ammonolysis reaction has been applied to a number of different Mo based precursors. Jaggers and co-workers have made comparisons between various molybdenum oxide based precursors to determine the relationship between the structure and stoichiometry of the starting material, the intermediates, phase, surface area and morphology of the product [30]. MoO_3, $(NH_4)_6Mo_7O_{24}.4H_2O$, $(NH_4)_2MoO_4$ and H_xMoO_3 were investigated and it was shown that the nitrided materials exhibited high surface areas when the products were pseudomorphic with the reactants (as in the case MoO_3 and $(NH_4)_6Mo_7O_{24}.4H_2O$). Nitridation of the H_xMoO_3 precursor was shown to yield nitrided products with higher surface areas than that from MoO_3 which was attributed to the formation of MoO_2 as an intermediate during the ammonolysis of MoO_3. This conclusion agrees with the reaction scheme proposed by Thompson and co-workers shown in Figure 1.2-1, where the formation of low and medium surface area γ-Mo_2N is channelled through the MoO_2 intermediate. Jaggers and co-workers also documented the formation of mixed phase nitride species, with γ-Mo_2N and δ-MoN (which can be described as a hexagonal close packing of molybdenum with nitrogen occupying all the octahedral interstitial sites) being formed on nitridation of $(NH_4)_6Mo_7O_{24}.4H_2O$ and H_xMoO_3. However, in a similar study using MoO_3 and H_xMoO_3 precursors, Thompson and co-workers did not observe the formation of δ-MoN intermediates/ products. The synthesis of modified forms of δ-MoN has been reported previously by

Marchand and co-workers who prepared the material by ammonolysis of MoS_2 precursors according to the reaction:

$$MoS_2 + 4/3NH_3 \longrightarrow \delta\text{-}MoN + 2H_2S + 1/6N_2$$

In addition to bulk materials, temperature programmed ammonolysis has also been applied to preparation of supported γ-Mo_2N, e.g. [31-33].

Although temperature programmed ammonolysis has benefits, including avoiding sintering (due to the lower temperatures involved compared with reacting dinitrogen directly with the metal) and increased surface areas, Wise and Markel [34] have drawn attention to the problems associated with the endothermic decomposition of ammonia, which can be considerable even on a small scale. They proposed that using mixtures of H_2/N_2 for nitridation has several advantages over the use of ammonia, the main ones being that γ-Mo_2N could be prepared with reproducible surface area, and also the use of H_2/N_2 eliminates the heat transfer problems discussed previously. Despite these findings, ammonolysis continues to be the preferred method to prepare nitride catalysts, with in addition to molybdenum nitrides, VN, W_2N, TiN and NbN being prepared in this manner [35-36]. This method can also be applied to mixed oxide precursors to yield ternary nitrides [37] and oxynitrides [38]. Within the literature, it is notable that in a number of studies, nitridation has been performed by isothermal treatment of the appropriate precursor under flowing ammonia. Examples of studies adopting this procedure have been the preparation of nitrogen-containing ZSM-5 [39], nitrogen-containing NaY and the oxynitride phosphates AlPON-5 [40], ZrPON [41], AlGaPON [42]. Within these studies variation of nitridation temperature and/ or duration has been shown to exert an influence over the final nitrogen content [41, 43] which can, of course, have an important effect on the resultant catalytic properties [43]. Table 1.2-2 taken from a study by Grange and co-workers in to AlPONs shows the effect of nitridation temperature and/ or duration.

Composition	Nitridation temperature (K)	Nitridation time (h)	Surface area (m^2 g^{-1})	Total N (wt.%)	Surface N (wt.%)
$AlPO_{3.64}N_{0.24}$	1073	3	275	2.8	2.7
$AlPO_{3.55}N_{0.30}$	1073	8	275	3.6	1.3
$AlPO_{3.10}N_{0.60}$	1073	40	235	7.2	1.0
$AlPO_{2.67}N_{0.89}$	1073	65	230	11.0	1.1
$AlPO_{1.96}N_{1.35}$	1073	120	215	17.5	2.4
$AlPO_{1.71}N_{1.53}$	1073	200	195	20.0	2.6

Table 1.2-2. The influence of nitridation time on the nitrogen content of AlPONs [43].

When controlled nitridation of surface layers is required, as for example in the modification of the chemical properties of the surface of a support, the atomic layer deposition (ALD) technique can be applied [44]. This technique is based upon repeated separate saturating reactions of at least two different reactants with the surface, which leads to the controlled build-up of thin films via reaction of the second component with the chemisorbed residues of the first reactant. Aluminium nitride surfaces have been prepared on both alumina and silica supports by this method wherein reaction cycles of trimethylaluminium and ammonia have been performed with the respective supports, retaining their high surface areas [45]. This method has been applied to the modification of the support composition for chromium catalysts supported on alumina [44].

Within the catalysis literature, there are very few examples of nitridation other than ammonolysis or reaction with nitrogen at atmospheric pressure. However ammonolysis frequently leads to partial nitridation and it is difficult to reproduce the surface areas of nitrided materials accurately. As discussed previously, there are significant amounts of oxygen incorporated into the structure of nitrided materials due to passivation and/ or partial nitridation; it is clear that a number of these compounds should be viewed as oxynitrides [15].

The use of alternative preparation methods can lead to unusual polymorphs of nitrides already known to possess catalytic activity, and are therefore likely to be of catalytic interest themselves. An example of this is the reported preparation of α-Mo_2N, which possesses the α-

Mo_2C structure (an orthorhombic unit cell resulting from the ordering on interstitial nitrogen atoms in a face centred cubic array of molybdenum atoms), documented by Marchand and co-workers [18]. This polymorph of molybdenum nitride can apparently be prepared by a metathesis reaction of $MoCl_5$ and Ca_3N_2 in an excess of molten $CaCl_2$ at elevated temperature, the reaction scheme is shown below [18].

$$2MoCl_5 + 5/3\ Ca_3N_2 \xrightarrow[1123K]{CaCl_2} Mo_2N + 5CaCl_2 + 7/6\ N_2 \uparrow$$

High temperature-high pressure syntheses are also yielding novel metastable structures, such as the spinel analogues mentioned previously [6,7]. There is therefore an ever-increasing base of nitrides and oxynitrides with diverse structures and potential catalytic interest.

1.3 Catalytic Reactions with Nitride and Oxynitrides

Metal nitrides and oxynitrides have been shown to catalyse a range of reactions, due mostly to researchers investigating the well documented ability of some transition metal nitrides to exhibit catalytic properties which are similar to platinum group metals. Table 1.3-1 shows the range of reactions studied and the nitride catalysts applied.

Reaction	Catalyst
Ammonia Synthesis	V_2O_2N [46, 47], VN [48], γ-Mo_2N [49-51]
	Cs/ γ-Mo_2N [52], Cs/Co_3Mo_3N [53-60]
	Fe_3Mo_3N [54, 58], Ni_3Mo_3N [54, 58]
	Ti-TMS-1 (N_2 treated) [61]
Ammonia Decomposition	VN [48, 62,] 63, γ-Mo_2N [35, 64, 65]
	β-$Mo_{16}N_7$ [64, 65], δ-MoN [64, 65]
Hydrazine Decomposition	Mo_2N/γ-Al_2O_3 [66, 67], NbN [68]
	W_2N [66], γ-Mo_2N [67]

Amination	γ-Mo_2N, VN, W_2N, NbN, TiN [69]
	W_2N/γ-Al_2O_3, W_2N/TiO_2 [70]
Amoxidation	VAlON [71-74,]
NO Removal	γ-Mo_2N [75-77], VN [76]
	Co_3Mo_3N [75], W_2N [76, 78]
	Ni_3N [79]
Hydrotreating and Hydrogenation	γ-Mo_2N [80, 81], Mo_2N/γ-Al_2O_3 [82],
	$MoO_{1.83}N_{0.36}$ [83], VN [84]
	Co_3Mo_3N [85], YbN [86]
	EuN [86], $Mo_2N_{0.6}O_{1.46}P$ [87]
	$WN_{1.09}O_{0.8}P_{0.28}$ [88], $CoMoN_x$ [89]
Base Catalysis	AlPON [43, 90-93], ZrPON [41, 94-96]
	AlGaPON [97-102], AlVON [103-107]
	γ-Mo_2N [108], Nitrogen Incorporated ZSM-5 [39],
	SiON [109], K/Si_3N_4 [110]
Photocatalysis	TiO_2 (Nitrogen Doped Anatase) [111-116]
	TiO_2 (Nitrogen Doped Rutile) [117, 118]
	TaON [119, 120]
Nitrides and Oxynitrides as	Pd/Si_3N_4 [121-124], Pt/BN [125-127]
Supports	Pt/AlPON [43, 128], Pt/AlGaPON [129, 130]
	Pt/AlCrPON [129], Pt/ZrPON [131]
	Pt-Mo/EMT zeolite [132]

Table 1.3-1. Table of the various catalytic uses for nitride based materials.

It is clear that there has been a resurgent interest in the use of nitrides and oxynitrides as heterogeneous catalysts in recent years. This has partly been driven by the use of temperature programmed techniques to produce high surface area materials. For many nitride-based catalysts, a number of exciting developments have been reported where the activities of nitrides/oxynitrides rival, if not better, current commercial catalytic systems e.g. Cs/Co_3Mo_3N

has shown to be much more active for ammonia synthesis than the commercial iron based catalyst [53-60].

Whilst there has been an expansion in the known applications for nitride catalysts, these are still relatively limited, and it appears that much more remains to be discovered. As stated previously, interest has generally centred around the modified basicity and platinum group metal–like properties of such systems. However, it is generally unclear as to the extent which nitrides can be used as reservoirs of "active" nitrogen for nitrogen transfer reactions. Although nitrogen storage has recently been reported for transition metal-intermetallic compounds [133], the extent to which a nitride may, e.g., participate in a Mars-van Krevelen type process still remains unclear. The possible analogy with this type of oxide behaviour had been raised in early studies of ammonia synthesis over uranium nitride [134, 135] and it appears that there may be such parallels with, the often related, carbide catalysts for methane oxidation [136]. Recently, a "double" Mars-van Krevelen mechanism has been proposed for the production of acrylonitrile in propane ammoxidation over VAlON catalysts [137] and the work of Schlogl has documented the mobility of nitrogen atoms in bulk zirconium oxynitride catalysts [139]. Despite becoming more apparent from photocatalysis studies, the use of nitrogen as a "dopant" to modify the defect structure of oxides for thermally activated reactions is largely unexplored. Recent studies have detailed the unusual effects of low levels of nitrogen incorporation on the ionic conductivity of yttria stabilised zirconia [138]. Finally, the application of carbonitrides and other mixed "anion" nitrides seems to have been largely ignored.

In this thesis, the reactivity/ mobility of lattice nitrogen present in nitride based catalysts will be investigated.

2. Experimental

2.1 Introduction

The experimental techniques employed in this work are presented in three discrete sections, catalyst preparation, catalyst testing and catalyst characterisation.

2.2 Catalyst Preparation

A number of catalysts were prepared and tested in this work. They are predominantly molybdenum containing bulk nitride catalysts, although oxynitrides and H-ZSM-5 supported nitride species were also prepared. The catalysts of principal interest in these studies were bulk binary and ternary nitrides.

2.2.1 Preparation of Precursors and Nitrided Materials

(i) Experimental set-up for preparing nitrides

As outlined in the introduction, the method of preparing nitrided materials that was used was the temperature programmed reaction method, following the experimental set up first described by Volpe and Boudart [23]. The gases employed were NH_3 (>99.9%), N_2 (oxygen free, 99.998%), and 2% O_2/Ar (all purchased from BOC), which were delivered to a vertical quartz reactor (10.5 mm internal diameter) fitted with a sinter, via 1/4 inch stainless steel tubing (Swagelok). The gas flow was monitored using Brooks 5850 TR mass flow controllers and controlled using a Brooks microprocessor control and readout unit. The furnace used was a Carbolite furnace which was programmed to go through various heating regimes during the nitriding. The temperature of the material was monitored using a K-type thermocouple situated on the outside of the quartz reactor at the centre of the bed. Flexible tubing was fitted to the exit of the reactor. Due to the hazards associated with ammonia gas, the effluent gas was flowed into an empty conical flask (to create a dead volume) and then out in to an acid bath to neutralise the ammonia present. All experiments were conducted within a ventilated fume

cupboard. The diagram below shows the experimental set up for nitriding. A check valve and a one-way valve (Swagelok) were also fitted in to the line to prevent any possible back flow of gases and or liquids through the mass flow controllers.

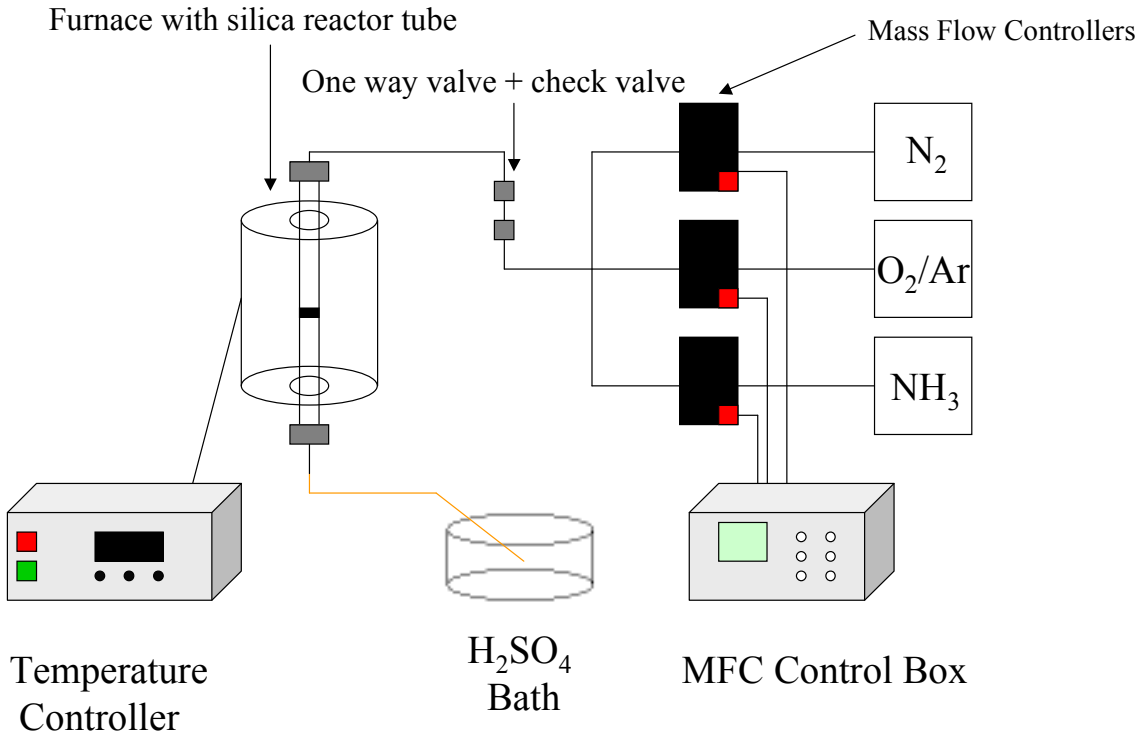

Figure 2.2-1 Apparatus used to synthesise nitrides by ammonolysis.

(ii) Nitridation of materials

The typical experimental conditions used for nitriding are outlined below.

Approximately 1.0 gram of the material to be nitrided was placed into the vertical quartz reactor (10.5 mm internal diameter). A 94 ml/min flow of NH_3 was introduced to the reactor. The furnace was programmed to heat the material in three stages. The temperature was increased from ambient to 357^{o}C at a rate of 5.6^{o}C/min (60.1 mins), then to 447^{o}C at 0.5^{o}C/min (180 mins), then to 785^{o}C at 2.1^{o}C (160.9 mins) and the furnace was held at this temperature for 5 hours. The nitrided material was then cooled in flowing ammonia to ambient temperature and on reaching this temperature, nitrogen was flushed through the system at 100

ml/min to remove any residual NH_3. To prevent pyrolysis on exposure of the nitrided material to air, the material was passivated using a mixture of 2% O_2 in argon flowing at 5 ml/min and N_2 (passed through an oxygen trap) at 95 ml/min to give a gas mixture containing <0.1% O_2, providing a protective oxide skin for the material which allowed pyrophoric and air sensitive materials to be discharged from the reactor.

2.2.2 Preparation of γ-Mo2N

MoO_3 (Sigma-Aldrich, 99.5%) was used as the precursor for γ-Mo_2N. MoO_3 was nitrided in accordance with the nitridation conditions that were outlined above. Powder X-ray diffraction (XRD) confirmed the phase of the resultant material as γ-Mo_2N which is in accordance with previous literature [23, 5, 52, 77, 140].

2.2.3 Preparation of β-$Mo_2N_{0.78}$

β-$Mo_2N_{0.78}$ was prepared *in-situ* in the fixed bed micro-reactor used for the ammonia synthesis activity evaluations. In this procedure, 0.4g of MoO_3 (Sigma Aldrich, 99.5%) was charged to the reactor and treated with 60 ml/min of a 3:1 H_2:N_2 (BOC, H_2 99.998%, N_2 99.995%) mixture at 700^oC for 2 hours.

2.2.4 Preparation of α-MoO_3, γ-Mo_2N and β-$Mo_2N_{0.78}$ Nanorods

The α-MoO_3 *nanorods* were kindly prepared and donated by Dr. Jose L. Rico from UMSNH, Morelia, Mexico. The α-MoO_3 *nanorods* had been synthesised by a hydrothermal route [141, 142]. A saturated solution of the precursor compound ($(NH_4)_6Mo_7O_{24}.4H_2O$) was prepared at room temperature and acidified to pH=5 using a 2.2M nitric acid solution. The acidified precursor was then stored at 60^oC under constant stirring for one week. The resultant solution was then transferred to a teflon-lined stainless steel autoclave and heated to 200^oC for 30-60 hours. The material was then washed using deionised water and dried for 5 hours at 60^oC to yield the MoO_3 *nanorods*.

Nanorods of γ-Mo_2N were prepared by nitriding the α-MoO_3 nanorods in accordance with the typical nitridation conditions that were outlined previously. *Nanorods* of β-$Mo_2N_{0.78}$ were prepared using the same method to prepare β-$Mo_2N_{0.78}$ powder samples.

2.2.5 Preparation of Co_3Mo_3N and Cs/Co_3Mo_3N, K/Co_3Mo_3N

Co_3Mo_3N was prepared by nitriding a cobalt molybdate hydrate precursor ($CoMoO_4.nH_2O$, confirmed by XRD). The precursor was prepared by adding together aqueous solutions of cobalt nitrate ($Co(NO_3)_2.6H_2O$, Sigma Aldrich, 98+%) and ammonium heptamolybdate ($(NH_4)_6Mo_7O_{24}.4.H_2O$, Alfa Aesar , JM 81-83% as MoO_3) and heating the mixed solution to approximately 80°C. A purple precipitate was obtained after vacuum filtration and the precipitate was washed twice with distilled water and once with ethanol and then dried overnight at 150°C. The powder was calcined at 500°C and then nitrided according to the general procedure previously described. When preparing the caesium promoted bimetallic nitride, caesium nitrate ($CsNO_3$, Sigma Aldrich, 98%) was added by impregnation to the cobalt molybdate hydrate after the calcination step, dried at 80°C and the calcination step repeated. The potassium promoted material was prepared in the same way using KNO_3 (Hopkin and Williams, 99%). The amounts of metal nitrate added were a molar ratio of Cs/Mo = 0.02 and K/Mo = 0.05, which have been reported to be the optimal amounts of alkali metal promoter for ammonia synthesis by Aika and Kojima [54].

2.2.6 Preparation of Fe_3Mo_3N and Ni_2Mo_3N

These bimetallic nitrides were prepared by nitriding the transition metal molybdates, $FeMoO_4$ and $NiMoO_4$, according to the procedure carried out by zur Loye and co-workers [143]. The molybdates were prepared by drop-wise addition of 400ml of a 0.25M aqueous solution of metal nitrate, $Fe(NO_3)_3.9H_2O$ (>98%, Sigma-Aldrich) or $Ni(NO_3)_2.6H_2O$ (Sigma-Aldrich purity not given, Cat: 244074), to a 150ml solution of $Na_2MoO_4.(H_2O)_2$ (Sigma-Aldrich, >99%). A brown (M=Fe) or Green (M=Ni) precipitate was obtained after vacuum filtration and the precipitate was washed twice with distilled water and once with ethanol and then dried overnight at 150°C. The powder ($FeMoO_4$ / $NiMoO_4$) was then calcined at 700°C for 6

hoursunder a flow of nitrogen gas (5ml/min). The resultant molybdates were then nitrided according to the general procedure previously described in Section 2.2-1.

2.2.7 Preparation of Aluminium Vanadium Oxynitride (VAlON)

V/Al oxide precursors were prepared by dissolving 0.01 moles of ammonium metavanadate (Sigma Aldrich, 99%) in 100ml of hot water. The solution was subsequently acidified to pH=3 with 50% HNO_3. 0.01 moles of aluminium nitrate (Sigma Aldrich, 98%) was then dissolved in 100ml of water and added to the solution of ammonium metavanadate and the mixture was heated to 70^{o}C under constant stirring. 1M NH_3 was added slowly to the mixture, increasing the pH to pH=7, at which point a yellow precipitate began to form, and the precipitate was left to stir in solution for 2 hours. This precipitate was then filtered off, and washed once with ethanol and then propanol, and dried overnight in an oven held at 60^{o}C [52].

The conditions used in the nitridation of the V/Al oxide precursor differ from the conditions typically used for nitriding. Between various studies, the conditions described in the literature to prepare and nitride the V/Al oxide precursor are ambiguous and lack consistency. The conditions used in this case were chosen as a "best fit" for the conditions specified in several papers by Grange [72, 96, 144, 145]. Approximately 1.0g of the precursor was loaded in to the quartz reactor, and a 94 ml/min flow of NH_3 is introduced to the reactor. The temperature was raised from ambient temperature to 500^{o}C at a rate of 1^{o}C/min and was held at this temperature for 5 hours, and subsequently cooled to ambient temperature in flowing nitrogen (50ml/min).

The XRD pattern of the precursor was amorphous and the BET surface area was >170m^2 g^{-1},

2.2.7 Preparation of δ-MoN

Studies by Marchand have shown that δ-MoN (NiAs structure) [5] can be prepared by ammonolysis of MoS_2. The conditions used in the nitridation of the MoS_2 precursor differ from the conditions typically used for the nitridation of oxides.

1.0g of MoS_2 (Sigma Aldrich, 99%) was loaded in to the quartz reactor, and a flow of NH_3 was introduced to the reactor at a rate of 94 ml/min. The temperature was raised to 785^{o}C at a

heating rate of 15°C/min, and held at this temperature for 60 hours to form hexagonal δ-MoN according to the reaction shown below.

$$MoS_2 + 4/3NH_3 \longrightarrow \delta\text{-}MoN + 2H_2S + 1/6N_2$$

Formation of hexagonal δ-MoN from the temperature programmed reaction of MoS_2 with ammonia.

The material was then cooled to ambient temperature in flowing ammonia. This is an important step, as Marchand reported in the literature that cooling the material in nitrogen resulted in the formation of γ-Mo_2N. XRD confirmed the phase of the material as δ-MoN.

2.2.8 Preparation of $Ru/Al_2O_3/TiFe_2N_x$

$Ru/Al_2O_3/TiFe_2N_x$ materials were prepared by heating 0.5g of Fe wire (Goodfellow, 99.95%) and 0.5 g of Ti metal shots (Goodfellow, 99.96%) to 1100°C under argon and dwelling at this temperature for 48 hours. After cooling in the flowing gas, the material was crushed and pulverized into fine particles (powder), and again heated to 1100°C under argon for 48 hours, and crushed into fine particles again.

The resultant material was transferred to a glove box with an inert atmosphere (nitrogen), and impregnated with 10 wt % $Al(C_2H_5)_3$ in n-hexane (Sigma-Aldrich, 1.0M in n-hexane). The material was then removed from the glove box and Al_2O_3 was formed on the surface of the material by oxidative decomposition of $Al(C_2H_5)_3$ in air at room temperature after impregnation. Ruthenium was introduced to the material by the decarbonylation of the $Ru_3(CO)_{12}$ metal cluster compound (99% Sigma-Aldrich) on the $Al_2O_3/TiFe_2$ and heating to 300°C in 5% H_2/Ar (BOC, H_2 99.998%, Ar min 99.99%) at 40 ml/min for 2 hours. The $Ru/Al_2O_3/TiFe_2$ material was then nitrided in a temperature programmed ammonolysis reaction. A 94 ml/min flow of NH_3 was introduced to the reactor and the furnace was programmed to heat the material at 5.6°C/min to 450°C and remained at this temperature for 3 hours before being cooled to room temperature in the flowing ammonia.

The conditions used to prepare and nitride the $Ru/Al_2O_3/TiFe_2$ material in the literature [146] are ambiguous and so the conditions used in this case were chosen as a "best fit" for the conditions specified.

2.2.8 Preparation of 5%-MoO_3/H-ZSM-5, Fe/5%-MoO_3/H-ZSM-5 and Ga/5%-MoO_3/H-ZSM-5 and Nitridation

Supported molybdenum containing catalysts were prepared by exchange of H-ZSM-5 (CATAL International Ltd, CT-410) with MoO_3 (Sigma-Aldrich, 99.5%). The concentration of MoO_3 was calculated with respect to the amount of zeolite to be added to achieve a Mo loading of 5%, supported on H-ZSM-5 (i.e. 0.075g MoO_3 in every gram of catalyst prepared). After exchange, the catalysts were dried in an oven at 120^{o}C and calcined at 500^{o}C for 5 hours. Iron and gallium were used as dopants and doped catalysts were prepared by impregnation after the calcination step using $Fe(NO_3).9H_2O$ (Sigma Aldrich, 98+%) and $Ga(NO_3)$ (Sigma Aldrich, 99.9%) respectively, the molar ratio of dopant to molybdenum was 0.25. The doped catalysts were again dried and calcined using the same conditions previously described.

Subsequently samples were nitrided following the same conditions described in the section 2.2.1 and also *in-situ* using the same method used to prepare β-$Mo_2N_{0.78}$ powder and *nanorod* samples.

2.2.9 Nitridation of H-ZSM-5

H-ZSM-5 was nitrided and tested for ammonia synthesis and studied by *in-situ* FT-IR. Two methods were used to nitride the material due to conflicting reports on the procedure used to incorporate nitrogen into the zeolite structure [39, 40]. Both methods of preparation involved a temperature programmed reaction heating the zeolite to 850^{o}C at 5^{o}C/min in NH_3 at a flow rate of 94 ml/min. The nitrided zeolite was then cooled to ambient temperature in the flowing ammonia or nitrogen (94 ml/min).

2.3 Catalyst Characterisation

The following techniques were used to characterise, describe and verify the properties of materials in this work and evaluate the result of the various reactions carried out.

2.3.1 Powder X-ray diffraction (XRD)

Powder X-ray diffraction was carried out on all synthesised materials to identify phases of the pre- and post-reaction samples. XRD patterns were obtained using a Siemens D5000 X-ray diffractometer (40kV, 40mA) using a CuK_α X-ray source (1.5418Å). *In-situ* measurements utilised an Antonn-Parr XRK cell fitted to the diffractometer
The scanning range used was $5^o < 2\theta < 85^o$ with a step size of 0.02 ^{o} and counting time of 1 sec per step.

2.3.2 Rietveld Refinement

Scan times of 15 hours were used for Rietveld refinement. The scanning range used was $10^o < 2\theta < 120^o$ with a step size of 0.02 ^{o}. Rietveld refinements against XRD data were performed using GSAS and EXPGUI packages by Professor D. H. Gregory

2.3.3 Surface Area Determination

The surface area of the catalysts was determined where appropriate by applying the Brunauer, Emmett and Teller (BET) method to nitrogen physisorption isotherms determined at liquid nitrogen temperatures. Isotherms were measured using a Micromeritics Flow Prep 060 Gemini BET machine. The samples were degassed in N_2 at 110^oC overnight to remove any adsorbed moisture prior to analysis.

2.3.4 Fourier Transform Infrared Spectroscopy (FTIR)

Fourier transform infrared spectroscopy was used to confirm the presence of ammonia gas during the ammonia synthesis reactions using a JASCO FTIR 4100 spectrometer. The experimental apparatus was modified slightly to allow the exit gas to flow through a gas I.R cell and out to vent. The cell was flushed with the exit gas during the reaction and gas was collected and transferred to the spectrometer for analysis.

2.3.5 *In-situ* FTIR studies

In-situ FTIR studies were carried out with the kind help of Dr. Michael Stockenhuber at Nottingham Trent University. The *in-situ* FTIR studies were carried out using an ATI Research Series FTIR spectrometer operating in transmission mode using a resolution of $4cm^{-1}$. The spectrometer was equipped with an *in-situ* stainless steel cell with calcium fluoride windows, capable of a base pressure $< 10^{-7}$mbar.

2.3.6 X-ray photoelectron spectroscopy (XPS)

X-ray photoelectron scattering measurements were conducted using facilities kindly made available by Professor Russell Howe at the University of Aberdeen. Samples were pressed into self supporting disks which were mounted on nickel sample stubs using double sided tape. All samples were evacuated at 10^{-7} mbar (base vacuum 10^{-9} mbar) before being introduced to the analysis chamber. XPS spectra were obtained using a VG ESCALAB II spectrometer with Al K_α X-rays (10kV, 20mA, un-monochromatised). Correction for sample charging was made by setting the C 1s binding energy to 285.0 eV (giving a Si 2p binding energy for ZSM-5 of 103.0 eV).

Sample sputtering used an argon ion gun operating at 4 kV accelerating voltage and ion current of around $20A\mu cm^{-2}$. Curve fitting of the observed spectra was performed using Gaussian line shape functions constrained by the intensity ratios and the peak splittings required for Mo 3d, intensity ratio 2:1 and splitting of ca. 17.2 eV for Mo3p). Binding energies

were reproducible to within 0.2 eV. Atomic ratios were estimated by dividing peak areas by the appropriate atomic sensitivity factors.

2.3.7 Determination of Nitrogen Content

The CHN content of samples was determined by combustion using an Exeter Analytical CE-440 elemental analyser with the help of Mrs Kim Wilson at the University of Glasgow.

2.3.8 Scanning Electron Microscopy (SEM)

SEM images of the powder and *nanorod* forms of both γ - and β- molybdenum nitrides were taken using a Philips XL30E-Scanning electron Microscope.

2.3.9 GCMS

GCMS analysis was conducted on liquid samples (dissolved in 1:10 ratio with methanol) using a ThermoQuest Trace GC, Trace MS fitted with a AS2000 autosampler. The column used in the instrument was a SGE Solgel Wax 30metre, 0.25mm ID, 0.25μm film run at a constant pressure of 14.5 p.s.i. The injector was heated to 200^{o}C and the split ratio was 50:1. The oven started at a temperature of 40^{o}C and was held for 5 minutes and increased at 10^{o}C/min to 170^{o}C and held for 41.5 minutes.

2.4 Catalyst Testing

2.4.1 Reactor Design

(i) Ammonia Synthesis Reactions

The performance of the catalysts used for ammonia synthesis was investigated using an experimental procedure similar to that used by Aika and Kojima [141]. The reactor consisted of

taps, pressure gauges and mass flow controllers (Brooks 5850TR) The temperature of the material was monitored using a K-type thermocouple situated on the outside of the quartz reactor at the centre of the bed. ¼ inch stainless steel tubing was used to deliver the gas to the silica reactor (10.5mm internal diameter) and the temperature was regulated using a Carbolite furnace. The vent gas from the reactor was passed through a sulfuric acid bubbler and the decrease in conductivity, corresponding to the consumption of H^+ by NH_3, was measured by a conductivity meter. All gases were vented through a fume cupboard.

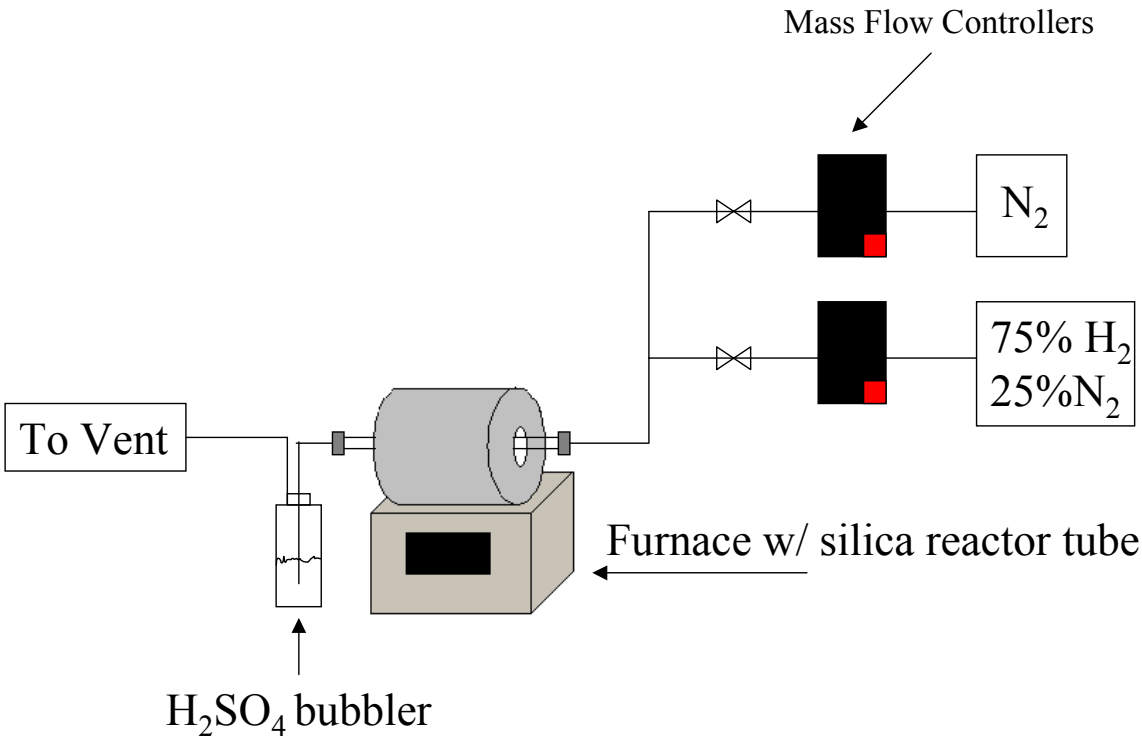

Figure 2.4-1 Apparatus used to conduct ammonia synthesis experiments

Experimental Procedure

0.4g of catalyst was placed in to the silica reactor tube and was held centrally within the heated zone of the furnace. The catalysts were pre-treated at 700°C with the reactant gas (H_2/N_2 (BOC, H_2 99.998%, N_2 99.995%) in a ratio of 3:1 respectively) at 60ml/min for 2

hours and then cooled to a reaction temperature, 400^{o}C, in the flowing gas (approximately 20 mins) in accordance with previous literature. On reaching the reaction temperature, the vent gas from the reactor was flowed through a sulfuric acid solution (0.00108 Mol L^{-1}, 200ml at ambient temperature) and the ammonia yield was calculated by detecting the conductivity decrease of protons in the sulfuric acid solution with respect to time. The activity data was taken after 30 mins, when the catalysts were thought to be stabilized at every temperature and every 60 mins thereafter. A linear decrease in conductivity versus time was observed during the measurement using H_2/N_2 as the reactant gas

(ii) Lattice Nitrogen Reactivity Studies

The reactivity of lattice nitrogen within various bulk nitride catalysts was investigated using the same apparatus described in Figure 2.4-1. 0.4g of catalyst was placed in to the silica reactor tube and was held centrally within the heated zone of the furnace. The catalysts were pre-treated at 700^{o}C with the reactant gas (H_2/N_2 in a ratio of 3:1 respectively) at 60ml/min for 2 hours, and cooled to 400^{o}C. At this point the feed gas used was switched from H_2/N_2 (BOC, H_2 99.998%, N_2 99.995%) to H_2/Ar (3:1) (BOC, H_2 99.998%, Ar min 99.99%), and conductivity measurements were made at 400^{o}C for 4 hours. The temperature of the reaction was then increased and held at that temperature in the following increments, 500^{o}C (1 hour dwell), 600^{o}C (1.5 hour dwell) and finally increased to 700^{o}C (1 hour dwell). From conductivity calibration data, the percentage of nitrogen lost from the catalyst that could be attributed to the formation of ammonia could be calculated and compared with the actual amount of nitrogen lost from the catalyst as determined from combustion analysis.

(iii) Synthesis of Aniline from Benzene

Experiments investigating the synthesis of aniline from benzene were carried out using a similar experimental set-up as the ammonia synthesis experiments, with slight modifications (see Figure 2.4-1). 0.4g of catalyst was placed in to the silica reactor tube and was held centrally within the heated zone of the furnace. The catalysts were pre-treated at 700^{o}C with the reactant gas (H_2/N_2 in a ratio of 3:1 respectively) at 60ml/min for 2 hours, and cooled to

400°C. At this point the feed gas, H_2/N_2 (3:1), the feed gas flowed into a benzene bubbler (99+%, Sigma-Aldrich) and over the catalyst. The temperature of the reaction was then increased using the temperature profile documented in the lattice nitrogen reactivity studies. An ice bath was used at the exit of the reactor to condense products which were subsequently analysed by GC-MS.

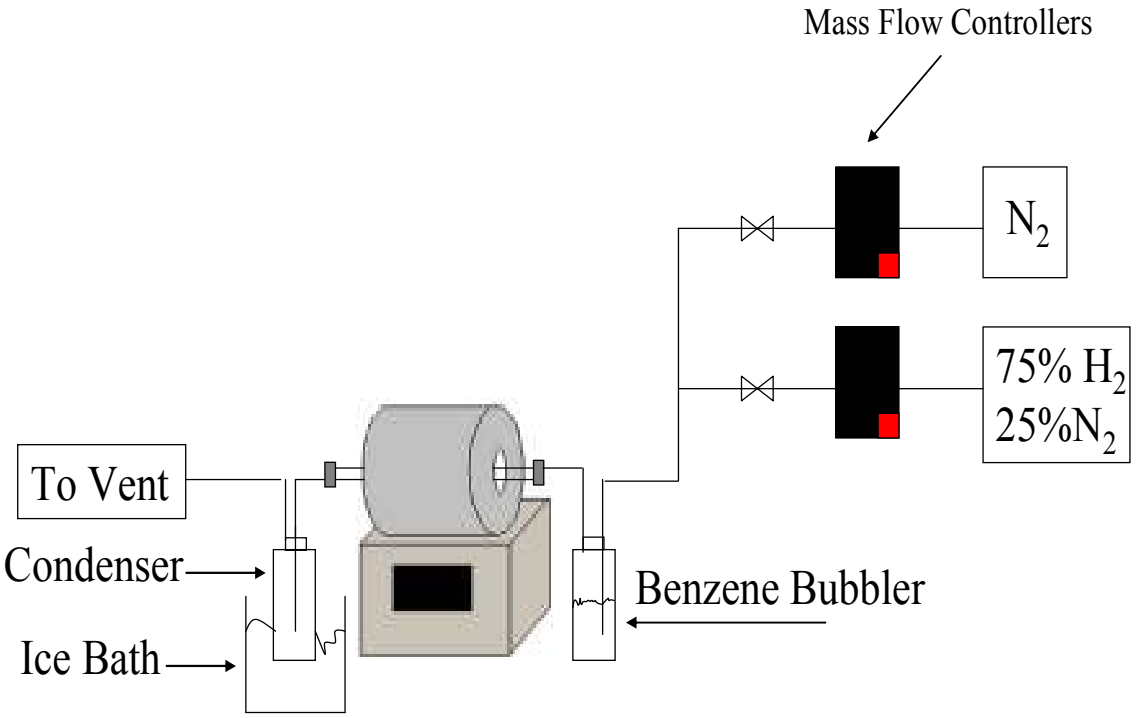

Figure 2.4-2. Apparatus used to conduct aniline synthesis experiments

3. Ammonia Synthesis Activity of Molybdenum Containing Nitride Materials

3.1 General Introduction

Transition metal nitride materials have been studied in the literature for a range of different applications involving their mechanical, optical, magnetic and catalytic properties [5, 15,147, 148]. The latter interest has arisen largely due to the synthesis of high surface area of γ-Mo_2N, which has similar catalytic properties to group VIII metals such as Pt [12]. γ-Mo_2N is prepared via ammonolysis of oxide precursors using low temperature ramp rates and high ammonia space velocities, in a method which was first documented by Volpe and Boudart [23]. These highly specific parameters are crucial in attaining high surface areas by minimising the partial pressure of water which is generated during the preparation from oxidic precursors. Water is believed to reduce surface area via the effects of hydrothermal sintering. Studies by Wise and Markel [34] have shown that H_2/N_2 mixtures, rather than NH_3, can be used to prepare high surface area γ-Mo_2N again employing similar conditions involving low temperature ramp rates and high space velocities. Hillis *et al* also observed the preparation of γ-Mo_2N using mixtures of H_2/N_2 as a consequence of carrying out ammonia synthesis studies over reduced molybdenum dioxide [49]. In the study by Wise and Markel, comparisons were drawn between both methods of nitride preparation, and the conclusion that using mixtures of H_2/N_2 is preferred to NH_3 in large scale preparation due to the difficulties associated with heat transfer caused by endothermic processes occurring with ammonia at high temperatures was reached.

A great deal of the literature published on nitrides centres on the preparation of materials, with the catalytic behaviour of most reported nitride based materials being largely unknown. The catalytic application of transition metal nitride and oxynitride catalysts can be split in to two general areas of interest. A number of studies have investigated the application of interstitial nitrides such as γ-Mo_2N and Co_3Mo_3N in reactions which are typical of metals, such as those involving hydrogen transfer. The use of nitrides in this context is based on the suggested similarity between the electronic structure of molybdenum nitrides and group VIII metals as mentioned above. The second general area of interest is in the application of oxynitride

materials as base catalysts. Oxynitrides are of interest in this area because of the ability to control the levels of nitrogen doped into the system, and hence their basicity. Amongst systems in this category attracting interest having been studied to date are AlVON [74], ZrPON [41] and even nitrogen containing microporous structures such as aluminophosphates [40] and H-ZSM-5 [39].

The work conducted in this chapter focuses on the ammonia synthesis activities of a series of binary and ternary nitrides. In the case of the binary nitride materials, the ammonia synthesis activities of three different polycrystalline forms of molybdenum nitride, γ-Mo_2N, β-$Mo_2N_{0.78}$ and δ-MoN, have been investigated and compared, and possible structure sensitivity of these materials has also been investigated. Structure sensitivity has previously been reported by Volpe and Boudart on γ-Mo_2N samples of varying surface area [51]. The stoichiometry reported in the literature for β-molybdenum nitride is inconsistent, most studies report the stoichiometry as β-$Mo_2N_{0.78}$, and the X-ray diffraction patterns presented are in good agreement with those β-molybdenum nitride materials prepared in this chapter [19,149,150]. However one of the first reported syntheses of the polymorph was heating mixtures of Mo metal and calcium nitride, said to catalyse the reaction, in a nitrogen atmosphere for 1 day at 450^{o}C and 2 weeks at 750^{o}C reports the stoichiometry as $Mo_{16}N_7$ by measuring the nitrogen content of the material gravimetrically and volumetrically [210]. Thompson *et al* have prepared thin films of β-molybdenum nitride and also assigned the formula $Mo_{16}N_7$. In that study the material was synthesised using Ion Beam Assisted Deposition (IBAD), which involved the deposition of Mo atoms and low energy N ions on to a singles Si (100) crystal [152]. It is interesting to note that both studies which report the formation of $Mo_{16}N_7$ do not include any XRD patterns (although Karam and Ward have tabulated the data [151]), and so a comparison of phases is not possible. However the calculated stoichiometric nitrogen content of $Mo_{16}N_7$ is 6.00 wt. %, which is slightly higher than the observed nitrogen content of the β-molybdenum nitride samples prepared in this chapter (N = 5.38 wt. %). Another study by Inamaru *et al* reports the formation of β-$Mo_2N_{0.85}$ (N = 5.84 wt. %) by deposition of Mo metal by pulsed laser deposition of Mo metal under nitrogen radical irradiation on a silicon substrate [153]. The β-molybdenum nitride materials in this chapter will be assigned to the β-$Mo_2N_{0.78}$ stoichiometry, which is most commonly used stoichiometry within the literature.

Nanorod forms of γ-Mo_2N and β-$Mo_2N_{0.78}$ were also prepared and comparisons between powder and nanorod samples were made to elucidate any possible influence of morpholgy upon the reaction. Zeolite supported molybdenum nitride catalysts have also been tested to investigate the effect of increasing the surface area of the material via high dispersion of the active phase on the support, and also the effect of dopants on their ammonia synthesis activity. The ternary nitride catalysts that have been tested, Co_3Mo_3N, Fe_3Mo_3N, and Ni_2Mo_3N, are more well established ammonia synthesis catalysts, largely due to work carried out by Aika and Kojima [54], and Jacobsen and co-workers [58].

On reviewing the literature available on the ammonia synthesis of molybdenum containing nitride catalysts, there is no evidence of a comparative study of these different binary and ternary nitride catalysts determining the influence of structure sensitivity on ammonia synthesis.

3.2 Results and Discussion- Ammonia Synthesis of Binary Molybdenum Nitrides

3.2.1 Introduction to γ-Mo_2N, β-$Mo_2N_{0.78}$ and δ-MoN

In recent times the widespread catalytic properties of binary (monometallic) nitrides has attracted much attention. Owing to the presence of nitrogen atoms in the interstitial lattice sites of the parent metals, the materials possess chemical properties similar to those of the platinum group metals. Binary nitrides of molybdenum [51], vanadium [69] and tungsten [76] have been applied to a range of reactions including CO hydrogenation, NO dissociation and ammonia synthesis, with rates competing with more traditionally used catalysts. Of the binary nitride materials reported in the literature, molybdenum nitride has been studied in the greatest detail in terms of its catalytic application. Different polymorphs of molybdenum nitride reported include γ-Mo_2N, β-$Mo_2N_{0.78}$ [150] and δ-MoN [5], but it is the γ-Mo_2N phase that has been studied in most detail.

Most studies of γ-Mo_2N are concerned with structural properties and the different synthetic routes available. The preferred method used in the literature to prepare high surface area γ-Mo_2N is the temperature programmed ammonolysis of MoO_3 (described in the experimental section). The conditions described within the literature for the preparation of γ-Mo_2N differ in specific detail, but all apply slow temperature ramp rates and high ammonia space velocities. The significance of these synthesis parameters is highlighted in a study by Thompson *et al.* [24] probing the effect of these different parameters on structural properties. γ-Mo_2N is an active ammonia synthesis catalyst at ambient pressure and other binary nitride materials such as vanadium nitride and uranium nitride have also shown ammonia synthesis activity, however those studies were conducted at high pressures [46, 134].

A potential route used to prepare β-$Mo_2N_{0.78}$ is the temperature programmed reaction of MoO_3 in a mixture of H_2/N_2, however Wise and Markel have reported the formation of γ-Mo_2N using the same method, although much more specific preparation conditions were employed in this synthesis [34]. The decomposition of γ-Mo_2N to form β-$Mo_2N_{0.78}$, and eventually Mo metal, has also been reported in the ammonolysis of MoO_3 at temperatures greater than 800^oC [210]. Decomposition of γ-Mo_2N to β-$Mo_2N_{0.78}$ has been reported by cooling γ-Mo_2N in inert gas or heating the material to high temperatures (up to 1000^oC) in an inert atmosphere [19]. Catalytically, β-$Mo_2N_{0.78}$ has mainly been studied for the bulk and alumina supported hydrodesulfurisation of thiophenes [150-153].

There is little literature available on the catalytic properties of δ-MoN. The available literature deals primarily with synthesis techniques and the electronic and structural properties [154-155].

3.2.2 Effect of Pre-treatment on γ-Mo_2N

Throughout this project the synthesis of nitride materials, in particular γ-Mo_2N, was shown to be more difficult than originally anticipated. Typically, an incomplete nitridation occurred, with the MoO_2 phase (identified by XRD) being present in the as-prepared γ-Mo_2N sample. As described previously in the experimental section, the pyrophoricity of γ-Mo_2N requires that the material be passivated in a dilute oxygen mixture (< 1%), allowing the nitride to be subsequently exposed to the air by forming a protective oxide or oxynitride skin around the bulk material. This layer is generally removed prior to catalytic application by hydrogen pre-

treatment at c.a 400°C [29, 54, 153]. It can be postulated then, that the same pre-treatment at 700°C outlined in the conditions documented by Aika and Kojima for ammonia synthesis [54], would go someway to removing the residual MoO_2 from the bulk γ-Mo_2N structure.

An *in-situ* hot-stage XRD experiment was carried out to investigate the effect of the pre-treatment on a γ-Mo_2N sample prepared as outlined in the experimental chapter which contained as significant fraction of MoO_2, following pre-treatment conditions used by Aika and Kojima [54] for ammonia synthesis (3:1 H_2/N_2, 60 ml/min) as closely as possible. Due to constraints of the hot-stage XRD set-up, the gas employed for the reduction was 5% H_2/N_2 at 20 ml/min, rather than the 3:1 H_2/N_2 mixture used in the ammonia synthesis reaction. The results are presented in Figure 3.2-1.

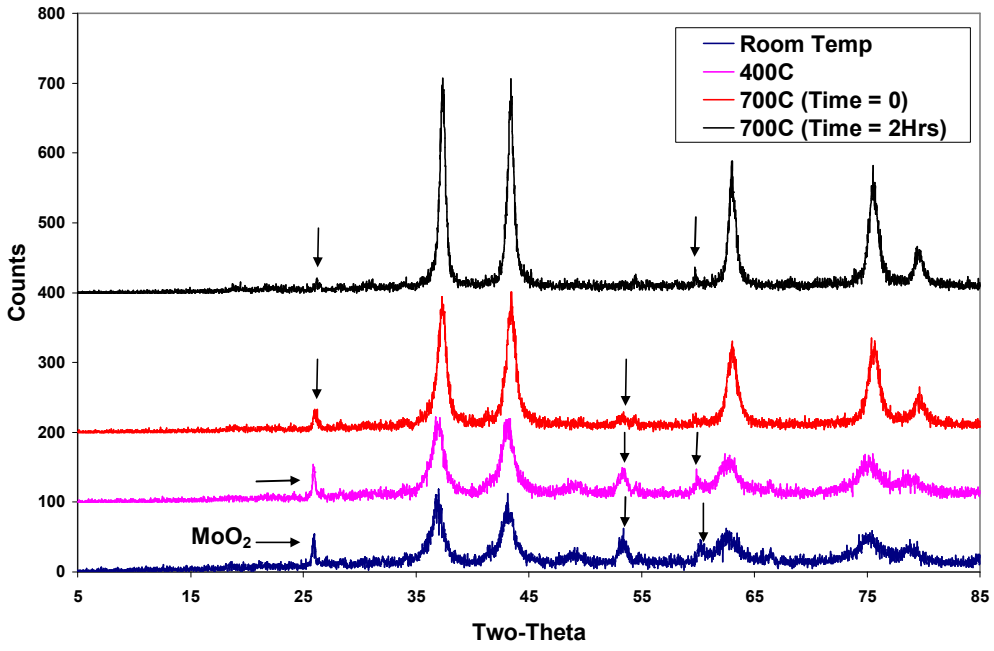

Figure 3.2-1 XRD pattern of γ-Mo_2N during in-situ hot stage experiment following the effects of reduction at 700C, H_2/N_2. The arrows indicate MoO_2 reflections.

The XRD patterns shown in the figure clearly show the MoO_2 reflections present at room temperature (e.g. at 26° two-theta). The temperature was increased under flowing 5% H_2/N_2

gas (ca. 20ml/min) to 700°C and held at this temperature for 2 hours, at which point it was clear that most of the residual oxide present had been removed; only very weak MoO_2 reflections remained and the lattice parameters of γ-Mo_2N remain unchanged. As there were no problems in the preparation of the other polymorphs of binary molybdenum nitride (the β- and δ-phases) tested in this section, the effect of pre-treatment was not investigated.

3.2.3 Reaction Data γ-Mo_2N, β-$Mo_2N_{0.78}$ and δ-MoN Powders

The ammonia synthesis experiments were carried out according to the conditions documented by Aika and Kojima [54], and are described in the experimental section. Ammonia synthesis rates were derived from conductivity versus time plots, and a calculation is applied to the gradient from the plot using calibration data detailed in Appendix 1.

A typical conductivity versus time plot for the steady state ammonia synthesis of γ-Mo_2N at 400°C is shown in Figure 3.2-2.

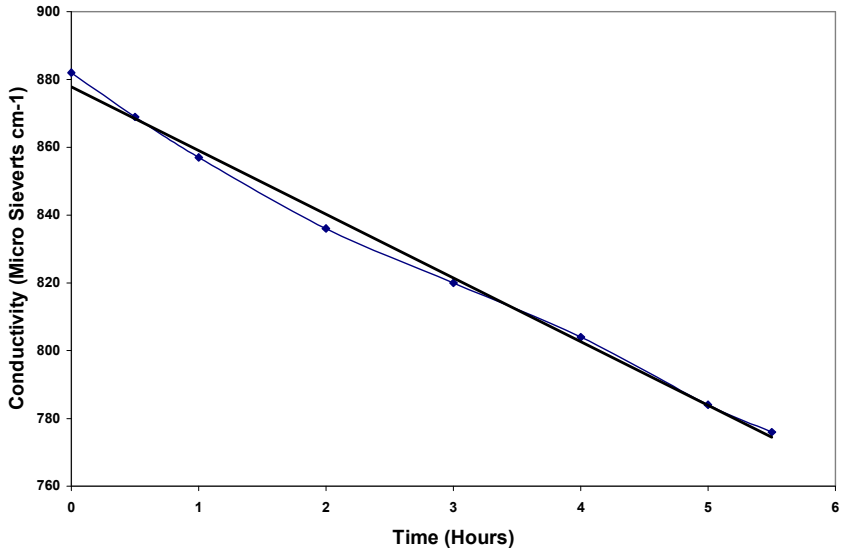

Figure 3.2-2. The change in conductivity of a 0.00108M H_2SO_4 solution as a function of time for the ammonia synthesis of γ-Mo_2N

The presence of ammonia in the exit stream of these reactions was confirmed by attaching an FTIR cell to the exit of the micro-reactor and collecting a gas sample. Spectra confirming the presence of ammonia can be found in Appendix 2.

The steady state rates of ammonia synthesis at 400^{o}C and ambient pressure for the γ-, β-, δ-powder phases of molybdenum nitride are presented in Table 3.2-1.
Despite the well known properties of molybdenum for the dissociation of dinitrogen and also molybdenum nitride being a relatively active ammonia synthesis catalyst, a comparative study of these materials does not exist in the literature. In general most catalytic studies of molybdenum nitride materials have focussed on the γ-Mo_2N phase, with Aika reporting the ammonia synthesis activity of γ-Mo_2N to be 48 μmol $h^{-1}g^{-1}$ under conditions comparable to those used in this work [150].

Catalyst	NH_3 synthesis rate (μmol h^{-1} g^{-1})
β-$Mo_2N_{0.78}$	35 / 36
γ-Mo_2N	34 / 34
δ-MoN	4 / 4
MoS_2	Trace / Trace

Table 3.2-1 Ammonia synthesis rates of different molybdenum containing phases at 400^{o}C and ambient pressure. (Values after slashes denote duplicate rates from repeat reactions).

On inspection of the table, it is apparent that there are some significant differences between the activities of these catalysts. The mass normalised activity of β-$Mo_2N_{0.78}$ is comparable to that of γ-Mo_2N, which is in turn significantly greater than the δ-MoN phase.

The ammonia synthesis activity of the MoS_2 precursor material, which is used to synthesise δ-MoN, is also included in the table to make comparisons with those experiments described in the experimental section in which the β-$Mo_2N_{0.78}$ polymorph is prepared *in-situ*. MoS_2 produces only trace amounts of ammonia during the reaction and the XRD data (section 3.2.3) shows that its crystal structure remains unchanged.

3.2.4 XRD Patterns

The post-reaction XRD analysis of all three forms of molybdenum nitride is shown in Figure 3.2-3. In all cases, except for the δ-MoN, in which a minority of γ-Mo_2N phase (indicated by arrows) is formed upon reaction, which has also been reported by McMillan and co-workers [176], the materials were found to be the single phase required, confirming the phase assignments made. On further inspection of the post-reaction δ-MoN, there was no crystallographic evidence of the MoS_2 precursor in the XRD patterns. However, sulfur residues on the surface of the material cannot be ruled out as a possible reason for the comparatively poor ammonia synthesis activity of δ-MoN. It is clear from the diffraction patterns that the materials synthesised all have very different crystal structures as expected.

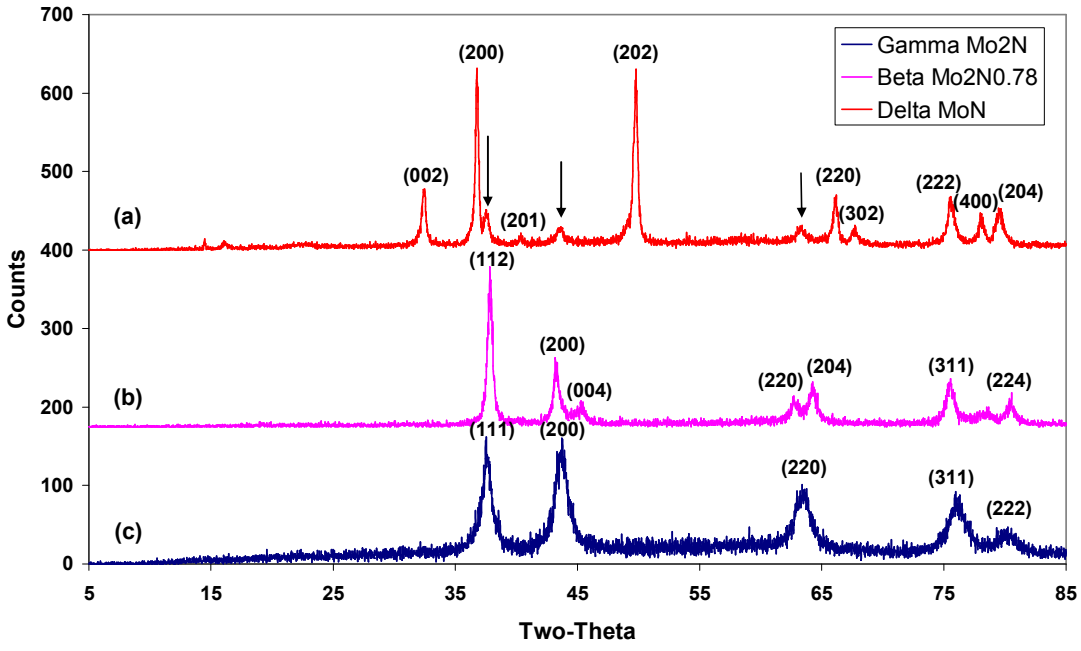

Figure 3.2-3 Powder x-ray diffraction patterns of the binary molybdenum nitrides (a) δ-MoN, (b) β-$Mo_2N_{0.78}$ and (c) γ-Mo_2N

McMillan and co-workers have recently investigated the distribution of nitrogen atoms within the γ-Mo_2N structure by powder neutron diffraction (PND). They concluded that the phase is a face centred cubic arrangement of molybdenum atoms, with nitrogen atoms distributed within

one half of the resultant octahedral interstitial sites [156]. Studies conducted by Marchand and co-workers shows the hexagonal δ-MoN phase to have a distorted NiAs type structure [157]. β-$Mo_2N_{0.78}$ is based upon a body centred tetragonal unit cell [5].

It is clear that in addition to the structural differences between these materials, there are pronounced differences in the stoichiometries between the three phases. As outlined previously, β-$Mo_2N_{0.78}$ can be formed via the high temperature denitrogenation of γ-Mo_2N under inert atmospheres [19, 158].

3.2.5 BET Surface Area Measurements

Since the molybdenum nitride phases are air sensitive, they are passivated prior to reaction in a dilute O_2/Ar mixture (<1%) according to the procedure described in the experimental section. They also potentially react with air on discharge from the ammonia synthesis reactor. The pre- and post-reaction BET surface area measurements for these materials may not, then, be a representative measurement of the reacting samples. However, on analysis of the post-reaction BET surface area of materials reported in Table 3.2-2, it can be seen that the surface area of β-$Mo_2N_{0.78}$ is approximately one tenth of that of γ-Mo_2N. These measurements indicate that β-$Mo_2N_{0.78}$ may have a much greater activity on a surface area normalised basis, since it has a comparable mass normalised rate to γ-Mo_2N.

Catalyst	BET Surface Area (m^2 g^{-1})
β-$Mo_2N_{0.78}$	9
γ-Mo_2N	85
δ-MoN	18

Table 3.2-2 BET Surface areas of various phases of molybdenum nitride

It is interesting however, on further inspection of the table that δ-MoN has an intermediate surface area, but the material has the lowest activity. As mentioned earlier, the potential adverse effects of sulfur residues on the ammonia synthesis activity, however, cannot be ruled

out, given that the material is synthesised from a sulfide precursor. The possible presence of sulfur was investigated using EDAX analysis of the post reaction samples, which provided inconclusive results as the energy peaks for sulfur and molybdenum overlap, making it difficult to determine the presence of sulfur. It was not possible to detect sulfur in the material by combustion analysis as the facilities available did not allow the detection of sulfur confidently.

3.2.6 Post-Reaction Nitrogen Analysis

The results of the post-reaction nitrogen analysis of the different binary molybdenum containing phases and the calculated unit cell volumes of these materials are presented in Table 3.2-3.

Catalyst	Calculated Stoichiometric Nitrogen Content (wt. %)	Post-Reaction (H_2/N_2, 400°C) Nitrogen Content (wt. %)	Unit Cell Volume (Å^3)
γ-Mo_2N	6.80	5.78(3)	71.09
β-$Mo_2N_{0.78}$	5.39	5.71(3)	139.11
δ-MoN	12.74	13.33(3)	175.45
MoS_2	0	0	

Table 3.2-3. Post ammonia synthesis nitrogen content of binary molybdenum containing phases after 5.5 hour reaction. The values in parentheses indicate standard error of technique.

The nitrogen content of the post reaction samples is in relatively good agreement with the calculated nitrogen contents for these materials. In the case of γ-Mo_2N the slightly lower nitrogen content could be explained by the incorporation of oxygen in to the structure on discharge from the reactor. In contrast the β- and δ-molybdenum nitride samples have a slightly higher nitrogen content which could be due to sorbed NH_x on the surface of the material. The unit cell volume of the molybdenum nitride phases increases in the order γ-Mo_2N< β-$Mo_2N_{0.78}$< δ-MoN. The zero nitrogen content of the post-ammonia synthesis MoS_2

sample supports the XRD data presented in section 3.2.3, confirming that no nitridation of the MoS_2 occurred during ammonia synthesis.

The aim of this section was to conduct a comparative study on the ammonia synthesis activities of various forms of molybdenum nitride. It is apparent from the data presented, that the ammonia synthesis activities of the β- and γ- molybdenum nitride phases are comparable on a mass normalised basis, with δ- phase exhibiting a comparatively low activity. Furthermore, when the influence of surface area is taken into account, the β-phase is by far the most active catalyst. This then implies that the lengthy, highly specific temperature programmed ammonolysis reaction required to prepare the high surface area γ-phase, produces an ammonia synthesis catalyst which, at best, has no advantage to one prepared by the direct reaction of the oxide precursor with H_2/N_2 at high temperatures.

The XRD data provides details of the crystallographic structure of materials; however it provides little information about the surface structure of materials which is hugely important in catalysis. This is highlighted in a study by Thompson *et al.* on the surface structure of bulk molybdenum nitrides. The surface structure of passivated samples of γ-Mo_2N, which was argued to be representative of the nitrided surface, was reported to be body centred [159]. Further study demonstrated that the near surface structure of the material differed both in crystal structure and also in composition from the bulk structure [29], the γ-Mo_2N bulk structure being a face centred cubic arrangement, while the lattice structure near the surface was body centred. On this basis, it is then possible that the surface phases do not correspond to the bulk ones, and although the bulk structures of the phases are very different, their surface structures may not be.

3.2.7 SEM Images and XRD Data of γ-Mo_2N, β-$Mo_2N_{0.78}$ Powders and Nanorods

Structure sensitivity with molybdenum nitride catalysts of varying surface area for ammonia synthesis has been reported previously in a study carried out by Volpe and Boudart [51]. They

demonstrated that γ-Mo_2N samples of low surface area had a higher intrinsic activity. In structure sensitive reactions, it can be anticipated that the morphology of the catalyst crystallites would have a significant impact on the activity. Accordingly, this aspect has been investigated with the two more active polymorphs of molybdenum nitride, γ-Mo_2N and β-$Mo_2N_{0.78}$, by employing a *nanorod* MoO_3 precursor and nitriding the material using the same method to produce the powder polymorphs.

The post-reaction XRD patterns of the *nanorod* forms of γ-Mo_2N and β-$Mo_2N_{0.78}$ are shown in Figure 3.2-4. These diffraction patterns confirm the formation of the desired nitride phases and match exactly with the powder molybdenum nitride samples in Figure 3.2-3.

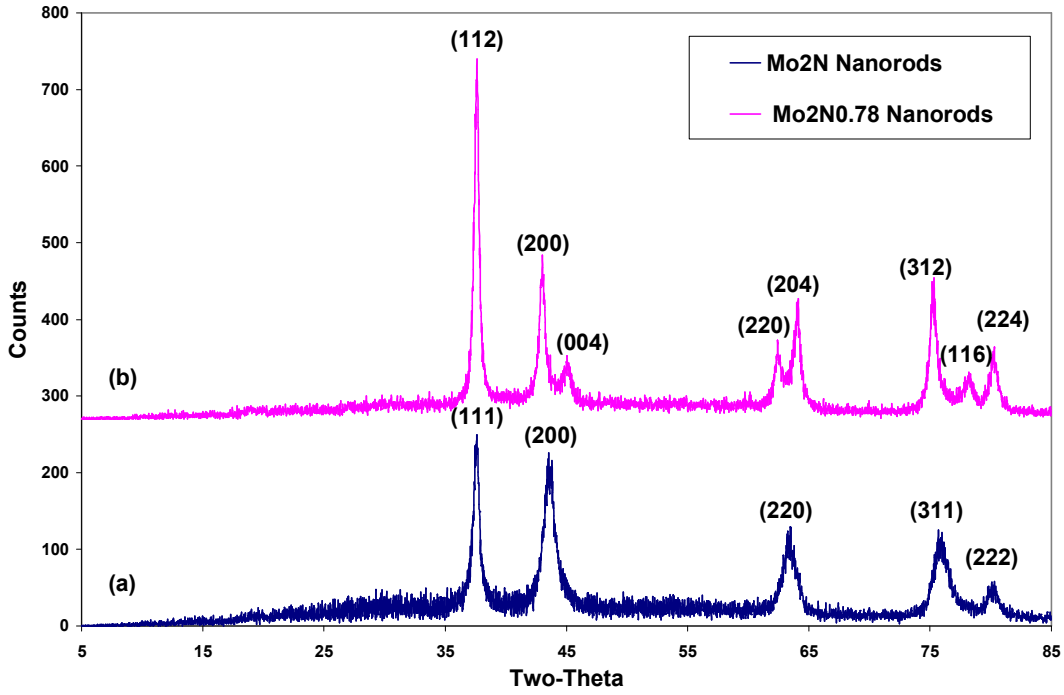

Figure 3.2-4 Powder X-ray diffraction patterns of molybdenum nitride nanorods (a) γ-Mo_2N and (b) β-$Mo_2N_{0.78}$

Representative SEM images of the post-reaction powders and "*nanorods*" of γ-Mo_2N are shown in Figures 3.2-5 (a) and (b). The difference in the shape of the crystallites between the powder samples and the *nanorods* is immediately apparent.

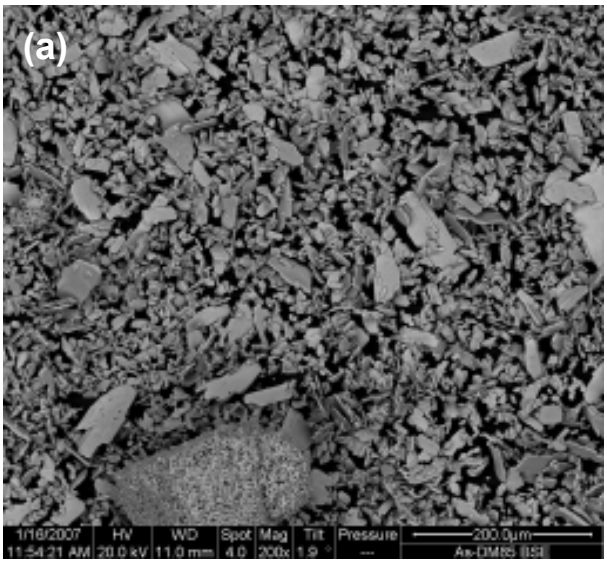
(a)

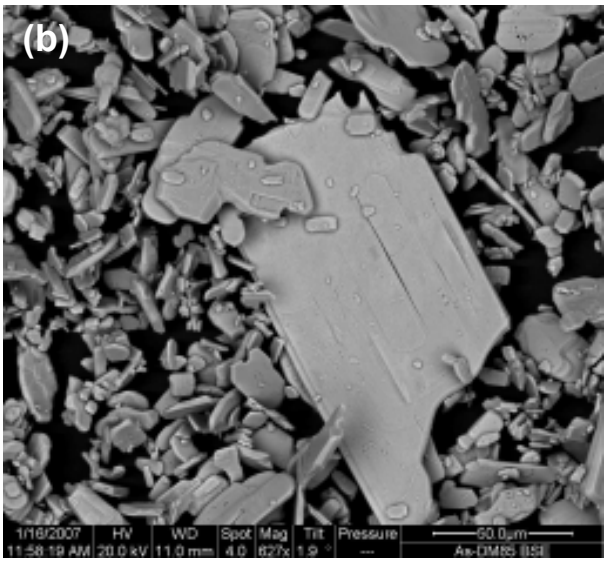
(b)

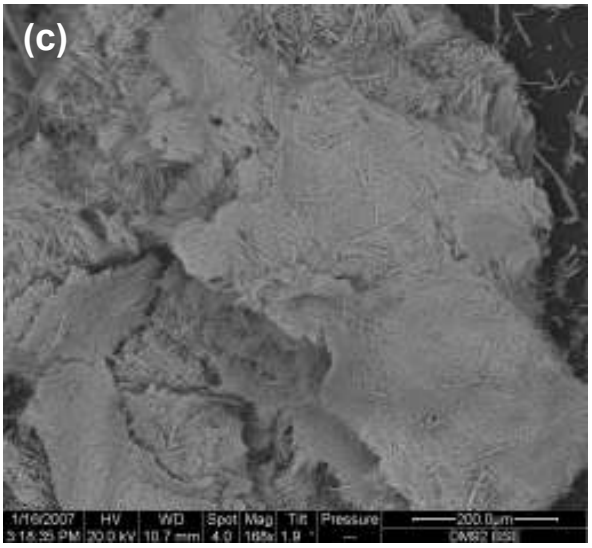
(c)

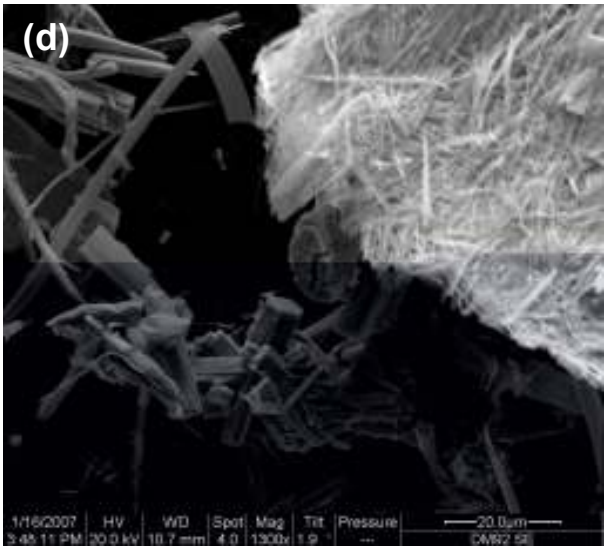
(d)

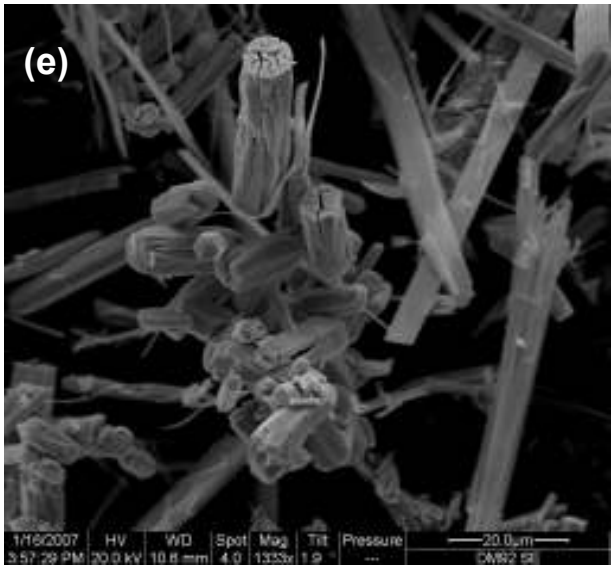

Figure 3.2-5 (a)-(b) γ-Mo_2N synthesised from MoO_3 powder and (c)-(e) γ-Mo_2N *nanorods* as synthesised from MoO_3 *nanorods*.

In Figure 3.2-5 (a)-(b) the γ-Mo_2N powder sample is made up of plate like crystals which are orientated in an irregular manner. Examining the material more closely emphasises the platelet morphology of the γ-Mo_2N powder and shows that the particles have no uniform size. In Figure 3.2-5(c)-(e) the *nanorods* of γ-Mo_2N also exhibit a wide distribution of crystallite sizes, with large aggregates of *nanorod* material. The transformation to γ-Mo_2N via the ammonolysis of the *nanorods* of MoO_3 precursor is pseudomorphic as expected [160], as the retention of morphology on nitridation of precursor oxides has been previously reported for powder nitride samples [137]. In the micrographs of the γ-Mo_2N *nanorod* sample there is also evidence of crystal fracturing, Figure 3.2-5(e). This is consistent with the corresponding powder diffraction pattern in Figure 3.2-4 where the reflection widths of the γ-Mo_2N *nanorods* indicate that the crystallites are multidomainic (see later). However if the XRD patterns of γ-Mo_2N powder and γ-Mo_2N *nanorods* are compared (Figures 3.2-3 and 3.2-4), there is pronounced reflection width anisotropy apparent which is indicative of acicular morphology of diffraction domains in the case of the *nanorod* forms.

SEM images of the post ammonia synthesis reaction powder and *nanorod* β-$Mo_2N_{0.78}$ samples are shown in Figure 3.2-6.

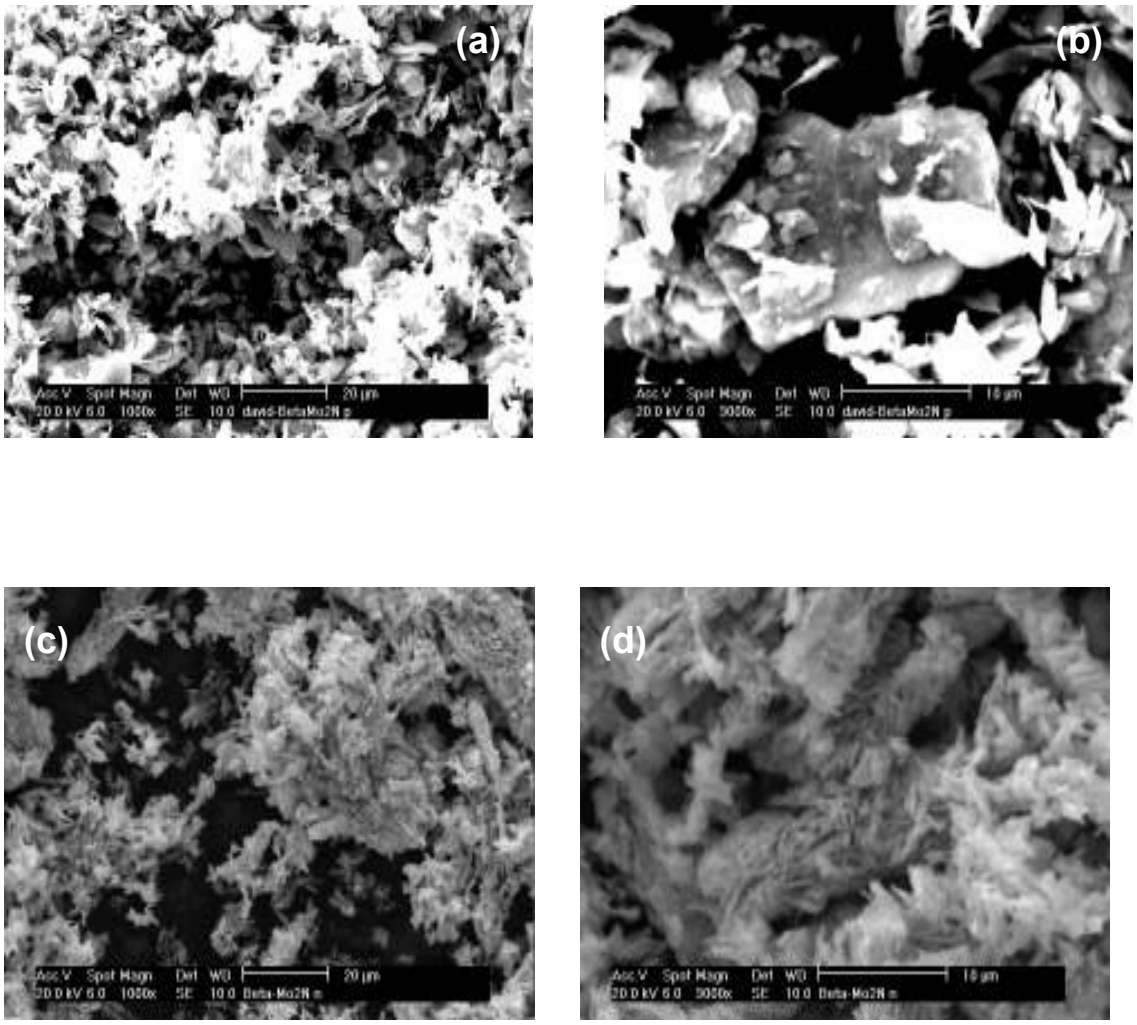

Figure 3.2-6 (a)-(b) β-$Mo_2N_{0.78}$ synthesised from MoO_3 powder and, (c)-(d) β-$Mo_2N_{0.78}$ *nanorods* synthesised from MoO_3 *nanorods*.

On inspection of the micrographs of the powder β-$Mo_2N_{0.78}$ phase in Figure 3.2-6 (a)-(b), synthesised by the nitridation of the standard MoO_3 powder in a mixture of H_2/N_2, it is apparent that it also exhibits the plate like morphology observed previously in the case of the powder γ-Mo_2N sample. However, the β-$Mo_2N_{0.78}$ powder morphology is much less well defined, and takes on a rougher appearance. The same general observation is true for the *nanorod* MoO_3 derived sample, although there are rods present, they are less well defined than

for the corresponding γ-Mo_2N *nanorod* sample. On comparison of the diffraction patterns for the β-$Mo_2N_{0.78}$ and γ-Mo_2N samples (Figures 3.2-3 and 3.2-4), it is clear the reflection widths of the β-molybdenum nitride materials are generally narrower than the γ-phase counterparts, which is a result of larger diffraction domains and/ or a lower degree of disorder within the crystal structures.

As mentioned previously, when the XRD patterns of powder and *nanorod* γ-Mo_2N samples are compared, the (111) reflection appears to be narrower in the case of the latter. If the all the line widths in the powder diffraction patterns are assumed to arise from Scherrer broadening (a limiting assumption), the apparent diffraction domains (crystallite sizes) can be calculated as detailed in Table 3.2-4.

Catalyst	Calculated crystallite size based on (111) reflection (Å)
γ-Mo_2N (powder)	439
γ-Mo_2N (*nanorods*)	488
β-$Mo_2N_{0.78}$ (powder)	702
β-$Mo_2N_{0.78}$ (*nanorods*)	702

Table 3.2-4. Molybdenum nitride crystallite size calculated from width of the (111) reflection

One possible explanation for the less well defined, coarse morphology, exhibited by the β-$Mo_2N_{0.78}$ materials lies in the synthesis conditions. As was described in the experimental section, the β-molybdenum nitride phase was prepared *in-situ* by treating of MoO_3 (powder or *nanorods*) with the H_2/N_2 mixture at 700°C using a non-controlled temperature ramp rate. Unlike the highly specific conditions employed in the ammonolysis of MoO_3, it is anticipated that a transient high partial pressure of water could ensue, which would result in lower surface areas, and possibly the irregular morphology observed in the micrographs.

3.2.8 Reaction Data γ-Mo_2N, β-$Mo_2N_{0.78}$ Nanorods

The steady state rates of ammonia synthesis at 400°C and ambient pressure for both *nanorod* and powder forms of γ- and β-phase molybdenum nitride are presented and compared in Table 3.2-5.

Catalyst	NH_3 synthesis rate (μmol $h^{-1}g^{-1}$)
β-$Mo_2N_{0.78}$ (*nanorods*)	41 / 37
β-$Mo_2N_{0.78}$ (powder)	35 / 36
γ-Mo_2N (*nanorods*)	30 / 34
γ-Mo_2N (powder)	34 / 34

Table 3.2-5. Ammonia synthesis rates of different molybdenum nitride phases and morphologies. (Values after slashes indicate duplicate data from repeat reactions).

As in the powder nitride samples, the β-phase *nanorods* are slightly more active than the γ-phase nanorods on a mass normalised basis. When comparing the activities of the powder and *nanorod* samples it is true that the *nanorod* β-phase is more active than its powder derived counterpart on a mass normalised basis, however the difference between the two phases and the different morphologies is relatively small, and it could be argued that there is no significant difference in the activities of the samples.

3.2.9 BET Surface Area Measurements

As described in section 3.2-5 for the BET surface area measurements of the powder molybdenum nitride samples, these *nanorod* samples are also air sensitive and the surface areas measurements may not be representative of the reacting samples.

Catalyst	BET Surface Area (m^2 g^{-1})
β-$Mo_2N_{0.78}$ (*nanorods*)	7
β-$Mo_2N_{0.78}$ (powder)	9
γ-Mo_2N (*nanorods*)	63
γ-Mo_2N (powder)	85

Table 3.2-6. Post-reaction BET surface areas of binary β- and γ-molybdenum nitride powders and *nanorods*

The BET surface areas of the molybdenum nitride *nanorod* samples are slightly lower than the corresponding powder samples. As in the powder samples, the specific surfaces areas of the β-$Mo_2N_{0.78}$ *nanorods* are approximately one tenth of γ-Mo_2N *nanorods*, which indicates that the β-$Mo_2N_{0.78}$ may have a much higher activity on a surface area normalised basis.

3.2.10 Post-Reaction Nitrogen Analysis

The results of the post-reaction nitrogen analysis, calculated stoichiometric nitrogen content and calculated unit cell volumes of the β- and γ-molybdenum nitride phases are presented in Table 3.2-7.

Catalyst	Calculated Stoichiometric Nitrogen Content (wt. %)	Post-Reaction (H_2/N_2, 700°C) Nitrogen Content (wt. %)	Unit Cell Volume ($Å^3$)
β-$Mo_2N_{0.78}$ (*nanorods*)	5.39	5.57(3)	140.77
β-$Mo_2N_{0.78}$ (powder)	5.39	5.71(3)	139.11
γ-Mo_2N (*nanorods*)	6.80	5.89(3)	70.38
γ-Mo_2N (powder)	6.80	5.78(3)	71.09

Table 3.2-7. Comparison of post-ammonia synthesis nitrogen content and calculated unit cell volumes of powder and *nanorod* molybdenum nitride samples.

The post-ammonia synthesis nitrogen content of the *nanorod* molybdenum nitride phases is comparable with the powder samples, and is in good agreement with the calculated stoichiometries for the relevant polymorphs. The slightly lower nitrogen content observed for the γ-Mo_2N samples can possibly be explained by an increased incorporation of oxygen in the structures on discharge from the reactor due to their higher surface areas when compared with the surface areas of β-$Mo_2N_{0.78}$ samples in Table 3.2-6.

The aim of this section was to probe the influence of surface morphology by testing *nanorod* forms of β- and γ-phase molybdenum nitrides and comparing their ammonia synthesis activities with molybdenum nitride powders. The influence of catalyst morphology on the activities of these materials appears to have little effect on the reaction and, at least in this case, the influence of structure sensitivity is limited. As in the powder samples, the β-$Mo_2N_{0.78}$ *nanorod* samples are just as active as their γ-Mo_2N counterparts on a mass normalised basis and possibly much more active per unit surface area, which again emphasises that the lengthy, highly specific temperature programmed reaction method produces an ammonia synthesis catalyst which, at best, has no advantage over catalysts prepared by the direct reaction of the oxide precursor with H_2/N_2 at high temperatures.

3.3 Results and Discussion – Ammonia Synthesis Activities of Bimetallic Nitrides/ Oxynitrides

3.3.1 Introduction to Co_3Mo_3N, Fe_3Mo_3N, Ni_2Mo_3N, AlVON, and Laves Phases

Since the first reported synthesis of bimetallic molybdenum containing nitride materials of iron, cobalt and nickel by Mittasch [42], research has shown these materials to have excellent ammonia synthesis properties. Most of the ternary nitride catalysts that have been studied in detail in the literature share similar ammonia synthesis properties. Despite the early reports of the favourable ammonia synthesis activities of ternary nitride catalysts – in some cases more

active than the commercially used doubly promoted iron catalyst – there have been very few studies on such materials, and a full understanding is incomplete.

The work carried out by Mittasch documents the increased ammonia synthesis activity of nitrided alloys of molybdenum containing iron, cobalt and nickel. Following the advances in the synthesis of molybdenum nitride materials by Boudart [23] to produce high surface area materials, Aika and Kojima were able to apply similar conditions to synthesise high surface area Co_3Mo_3N and carry out ammonia synthesis reactions at ambient pressure. Aika and Kojima also demonstrated the effect of alkali metal doping on Co_3Mo_3N, using caesium to dramatically increase the ammonia synthesis activity of the material [52]. In a parallel study, Jacobsen and co-workers also documented the ammonia synthesis activities of M_xMo_3N (M = Co:Mo = 1, Fe:Mo = 1, NiMo =2/3) and the effect of alkali metal doping, using caesium as a promoter for Co_3Mo_3N, although those reactions were conducted under industrial conditions at higher pressures [58].

A rationale for the high activity of the Co_3Mo_3N catalyst for ammonia synthesis was postulated by Jacobsen and co-workers, who described a volcano shaped relationship between the ammonia synthesis activity and the nitrogen adsorption energy, showing a CoMo alloy to have the optimum nitrogen adsorption energy (Figure 3.3-1), and therefore is the optimal ammonia synthesis catalyst [59].

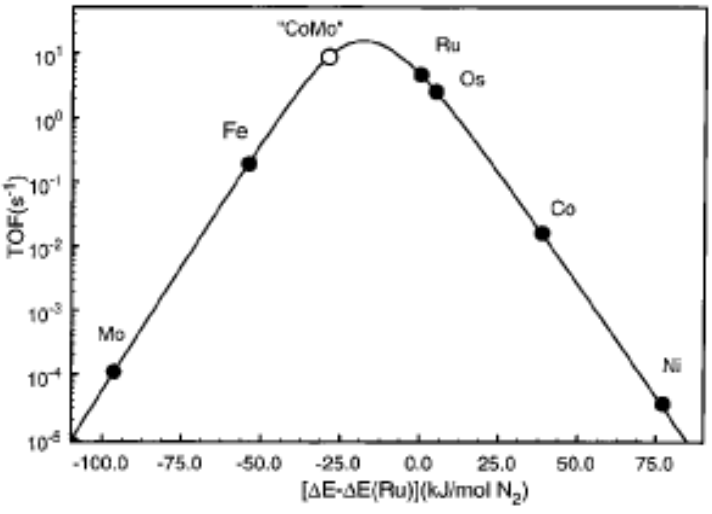

Figure 3.3-1. Calculated turnover frequencies for ammonia synthesis as a function of the adsorption energy of nitrogen [59].

It has been reported that isothermal N_2 adsorption experiments have shown that the bulk nitrogen of the ternary nitride does not participate in the ammonia synthesis reaction [60]. Consequently, the primary role of nitrogen atoms in the catalyst was postulated to be to induce the required ordering, and is not believed to significantly affect other properties [5].

Despite the early studies by Mittasch, and also later the work of Jacobsen *et al.* reporting the ammonia synthesis properties of both Fe_3Mo_3N and Ni_2Mo_3N, there are very few catalytic studies of these ternary nitride materials. Most studies of these materials centre on the preparation and characterisation of their electronic and magnetic properties.
Fe_3Mo_3N has been shown to be iso-stuctural with Co_3Mo_3N, using Rietveld refinement [29]. However, the structure of nickel molybdenum nitride is under debate. Bem *et al* synthesised nickel molybdenum nitride by ammonolysis of an oxide precursor, indexing the final material as "Ni_3Mo_3N" [143]. However, Weil and Jutma have also prepared "Ni_3Mo_3N" under different synthetic conditions presenting an XRD pattern of their final product, clearly different from that reported by Bem *et al* (i.e. no phase segregation, no Ni metal impurity) [164]. The correct stoichiometry of the material formed on ammonolysis of the NiMo oxide was subsequently shown to be Ni_2Mo_3N, as reported by Herle *et al.* [165].

Vanadium-aluminium oxide precursors were also chosen to be nitrided and tested due to a recently published article documenting the evidence for the participation of lattice nitrogen from vanadium aluminium oxynitrides (VAlON) in propane ammoxidation. Those studies employed isotopically labelled ammonia, and measurements were conducted using a TAP (Temporal Analysis of Products) reactor [137]. Grange and co-workers documented the formation NH_x species (x = 1,2) formed during the reaction which are directly involved in the nitrogen insertion process, and also the formation of co-ordinated NH_3, formed by the weak adsorption of ammonia on the surface which is involved in non-selective pathways. A reaction cycle is shown in Figure 3.3-2. This gives cause for the material to be tested as an ammonia synthesis catalyst, the catalytic activity will determine if the catalyst is suitable for testing the "reactivity" of lattice nitrogen within the material and elucidate the potential of the material to participate in a nitrogen equivalent Mars-van Krevelen mechanism, using ammonia synthesis as a test reaction. Indeed Grange proposed a double Mars-van Krevelen mechanism involving

both oxygen and nitrogen from the lattice in the ammoxidation of propane using a VAlON catalyst [137].

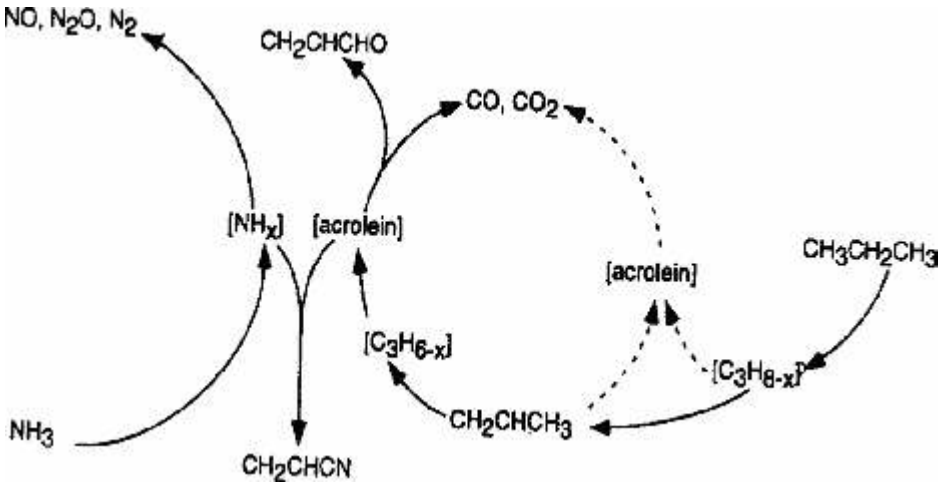

Figure 3.3-2. Reaction mechanism for propane ammoxidation over VAlON catalysts as derived from TAP experiments. Solid lines indicate reaction paths involving lattice oxygen, and dashed lines denote pathways with adsorbed oxygen. Square brackets are used to symbolize surface intermediates [137].

Work carried out by Machida and co-workers has shown that the Laves type material, $Ru/Al_2O_3/TiFe_2$, exhibits nitrogen storage properties by both ammonolysis and by interaction with nitrogen at temperatures between 450-500^oC [146]. It was also reported that these materials could reversibly desorb nitrogen by hydrogenation while maintaining the structure of the parent material. The nitrogen species generated in this desorption step was shown to have reacted with the hydrogen to form ammonia owing to the high activity of the atomic nitrogen stored in the intermetallic material. This ammonia production is not surprising given the presence of both and iron and ruthenium within the material, and it was therefore felt warrantable to examine the catalytic efficacy of these materials in ammonia synthesis.

In this section, the ammonia synthesis activities of bimetallic nitride and oxynitride materials and their precursors will be presented. These studies will be of fundamental importance when discussing the reactivity of lattice nitrogen within these materials in forthcoming chapters.

3.3.2 XRD - Effect of Ammonia Synthesis Treatment on Co_3Mo_3N, Fe_3Mo_3N and Ni_2Mo_3N and Corresponding Oxide Precursors

As described in section 3.2.1, the preparation of nitride materials, namely γ-Mo_2N, via the ammonolysis of oxide precursor materials proved difficult in securing a single phase nitride material. With the exception of Ni_2Mo_3N, the synthesis of the ternary nitride materials was no different, ammonolysis of oxide precursors yielded poorly crystalline materials or mixed phase oxynitride materials. XRD patterns were obtained post-ammonolysis and post-ammonia synthesis to investigate if the effect of the treatment carried out in the ammonia synthesis reactions was sufficient to remove any residual oxide precursor from the material and leave a single phase nitride.

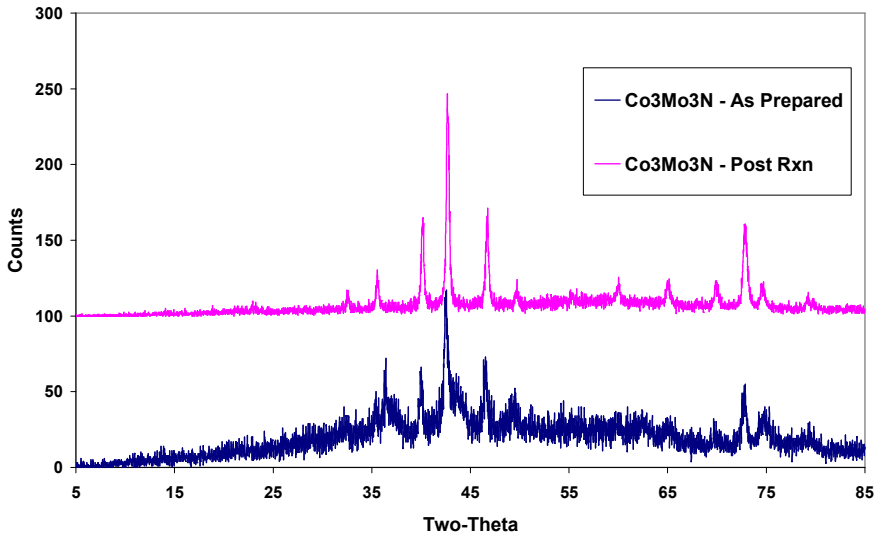

Figure 3.3-1 (a) XRD pattern showing effect of ammonia synthesis on as prepared Co_3Mo_3N.

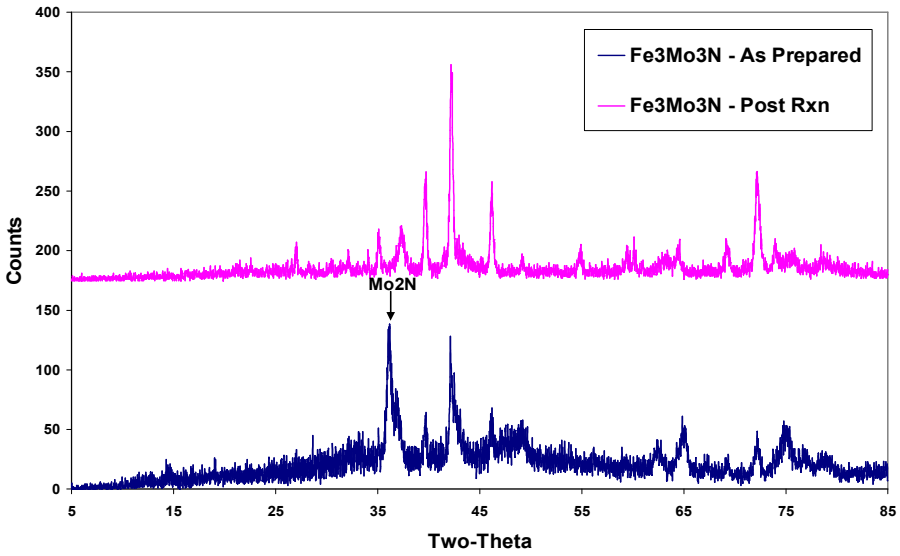

Figure 3.3-1 (b) XRD pattern showing effect of ammonia synthesis on as prepared Fe_3Mo_3N (arrow correspond to γ-Mo_2N reflection)

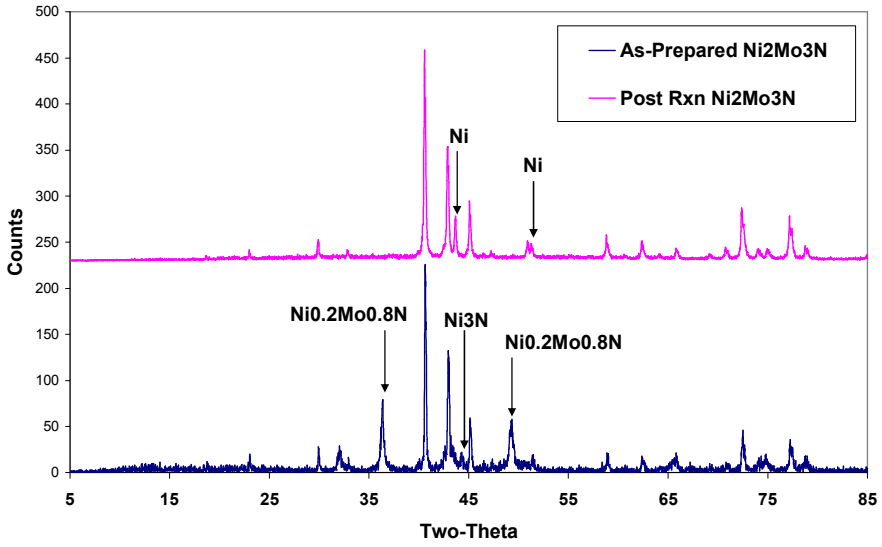

Figure 3.3-1 (c) XRD pattern showing effect of ammonia synthesis on as prepared Ni_2Mo_3N. (arrows correspond to impurities in the sample)

The XRD patterns shown in Figures 3.3-1 (a) and (b), demonstrate the poorly crystalline phases of the as-prepared Co_3Mo_3N and Fe_3Mo_3N ternary nitride samples. By looking at the

post-reaction XRD patterns, it is clear that like the binary nitrides, the conditions employed in the pre-treatment of the ammonia synthesis reaction (H_2/N_2, 700^{o}C for 2 hours), are sufficient to produce a pure phase nitride.

As previously described, there have been conflicting reports on the stoichiometric nature of nickel molybdenum nitride as a result of ammonolysis of the NiMo oxide precursor; it was first believed to take on the form Ni_3Mo_3N. However, further structural refinement showed that the synthesised material contained a small amount of metallic nickel [165], and the XRD data obtained was in agreement with the previously assigned Ni_3Mo_3N. Due to nickel phase segregation occurring during the ammonolysis of the NiMo oxide precursor, the formation of a nitride phase with Ni:Mo ratio of 1:1 was deemed unlikely. Instead the correct assignment of the material produced was found to be Ni_2Mo_3N, which has the β-Mn structure, with some metallic nickel impurity present [165]. In Figure 3.3-1 (c) the XRD patterns of the as-prepared and post-ammonia synthesis nickel molybdenum nitride are presented. The as-prepared sample shows, unlike the iron and cobalt examples, a very crystalline structure, however the sample is not without impurity with some Ni_3N (44.58^o), and $Ni_{0.2}Mo_{0.8}N$ (36.56, 44.48^o) reflections present (indicated by arrows) which have been previously reported in the synthesis of nickel molybdenum nitride [163]. On ammonia synthesis these impurities are removed and the final material consists only of the Ni_2Mo_3N + Ni material.

The precursor oxides, used to synthesise the bimetallic nitrides of Co, Ni, Fe by ammonolysis, were also charged directly in to the ammonia synthesis reactor (0.4g), and subjected to the same treatment as the nitrides for an ammonia synthesis reaction (700^{o}C for 2 hours then 400^{o}C for 5.5 hours under H_2/N_2).

The pre- and post-reaction XRD patterns of the bimetallic oxide precursor materials are shown in Figure 3.3-2 (a-c). It is immediately clear, that in the case of NiMo oxide precursor, the ammonia synthesis conditions were sufficient to completely nitride the oxide precursor and transform the material into the Ni_2Mo_3N phase. In the case of the CoMo and FeMo oxide precursors, the XRD patterns obtained upon carrying out the ammonia synthesis reaction are much less crystalline than the pattern observed from the ammonia synthesis of their NiMo

counterpart. The diffraction patterns obtained for both materials are reminiscent of their corresponding oxide precursor and the as-prepared ternary nitrides prepared by the ammonolysis route. The conditions applied in the ammonia synthesis reaction appear to have only partially nitrided the oxide precursors. The arrows shown in the XRD patterns of the oxides nitrided in H_2/N_2, in Figures 3.3-2 (b)-(c), indicate those reflections that are characteristic of the fully nitrided bimetallic material.

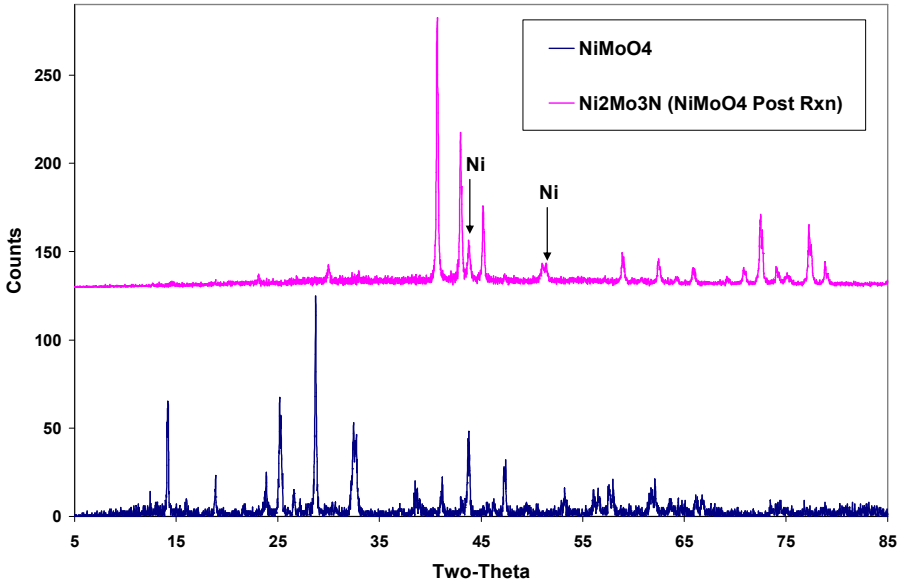

Figure 3.3-2 (a) XRD pattern showing full nitridation of $NiMoO_4$ after ammonia synthesis reaction

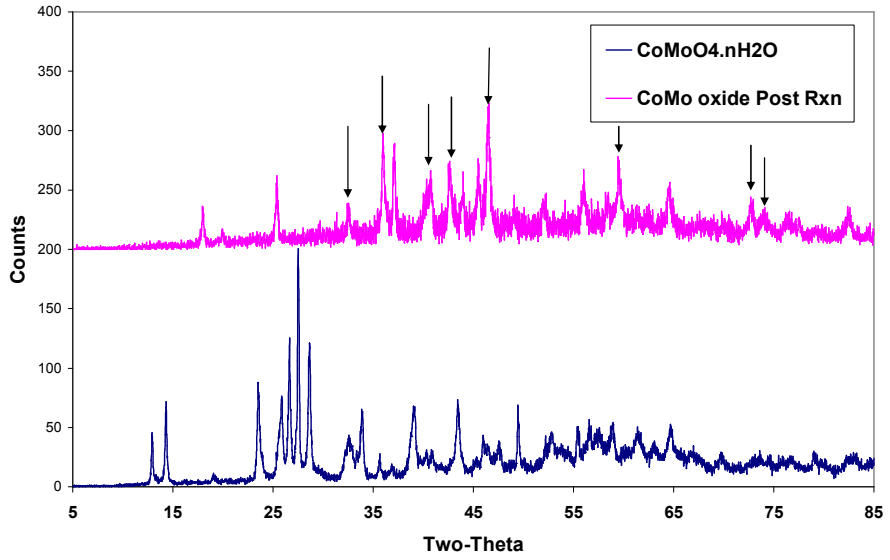

3.3-2 (b) XRD pattern showing effect of ammonia synthesis on $CoMoO_4.nH_2O$.
(arrows indicate those reflections characteristic of fully nitrided Co_3Mo_3N)

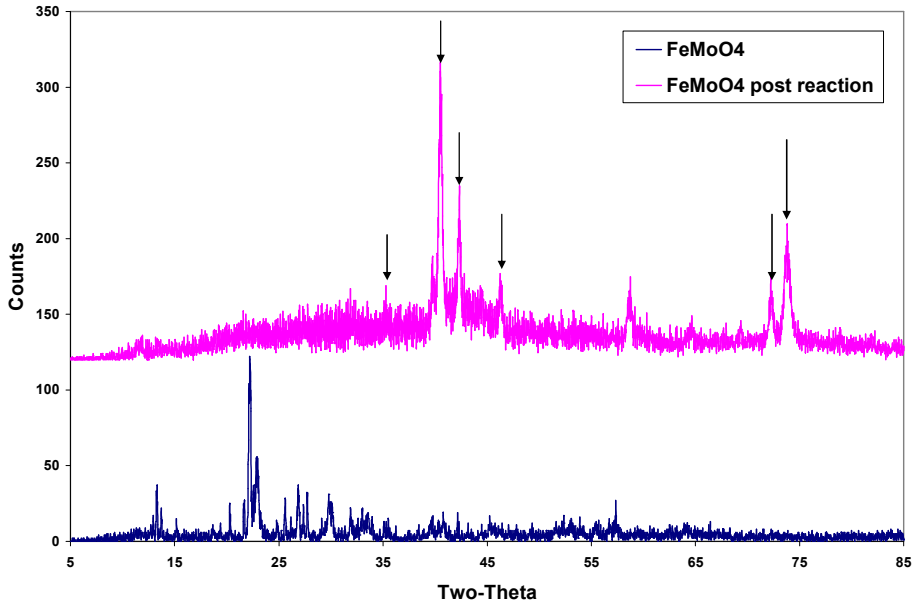

3.3-2 (c) XRD pattern showing effect of ammonia synthesis on $FeMoO_4$.
(arrows indicate those reflections characteristic of fully nitrided Fe_3Mo_3N)

3.3.3 Results and Discussion - Ammonia Synthesis Activity of Co_3Mo_3N, Fe_3Mo_3N and Ni_2Mo_3N and Mixed Oxide Precursors

The ammonia synthesis reactions carried out using the ternary nitride catalysts and their precursors were conducted as a comparative study with respect to the binary molybdenum nitride catalysts. The procedure used to determine the ammonia synthesis rates was identical to that of the binary nitrides and is described in the experimental section.

The steady state ammonia synthesis rates at 400^{o}C and ambient pressure for the bimetallic nitrides and their oxide precursors are presented in Table 3.3-1. From the data presented in the table, it is clear that there are significant differences in the activities of these catalysts. On examination of the ammonia synthesis activities of the bimetallic nitride catalysts prepared by ammonolysis, the Co_3Mo_3N catalyst is the most active material of both the binary and ternary nitride materials prepared by ammonolysis, as the literature has suggested. However, the rate at which ammonia is produced by Co_3Mo_3N is not as high as that reported by Aika and Kojima [52] (652 μmol h^{-1} g^{-1}, compared with the 167 μmol $h^{-1}g^{-1}$ observed in this case) using comparable conditions.

Catalyst	NH_3 synthesis rate (μmol $h^{-1}g^{-1}$)
Co_3Mo_3N	167 / 164
Fe_3Mo_3N	95
Ni_2Mo_3N	28 / 27
$CoMoO_4.nH_2O$ (partial nitridation)	134 / 137
Ni_2Mo_3N (by N_2/H_2 treatment of NiMo oxide)	45 / 48
$FeMoO_4$ (partial nitridation)	9
VAlON	Trace / Trace
$Ru/Al_2O_3/TiFe_2N_x$	Trace / Trace

Table 3.3-1 Ammonia synthesis rates of ternary nitride powders and their oxide precursors. Values after slashes indicate duplicate data from repeat reactions.

Reproducing the promotional effects of alkali metal doping on Co_3Mo_3N reported by Aika and Kojima proved problematic, and therefore the results are not presented in the table. Aika and Kojima have studied the promotional effects thoroughly, and found that caesium was a more effective promoter than potassium suggesting an electronic effect. An optimum amount of 2 mol % (Cs/Mo = 0.02 mol ratio) was found to yield the maximum promotional effect [52]. Aika and Kojima have also shown that the activity is decreased by further alkali addition in the case of K^+ and Cs^+ [52]. It was shown that there are at least two negative effects of alkali addition resulting from structural changes. Alkali addition decreases the surface area and retards the complete formation of the Co_3Mo_3N phase, instead producing Co metal and Mo_2N phases, although these reflections are less apparent when lower levels of Cs^+ are used [52]. In this project the effect of both dopants were studied. The dopants were added to $CoMoO_4.nH_2O$ by impregnation prior to nitridation as described by Aika [52], and also using an alternative method, by adding the dopant after nitridation as described by Jacobsen [59], both methods had the same negative effect on the ammonia synthesis activity of the materials (2 mol % Cs = 61 µmol $h^{-1}g^{-1}$, 5 mol % K = 51 µmol $h^{-1}g^{-1}$) although no obvious structural changes were observed in the materials, as shown in Figure 3.3-3.

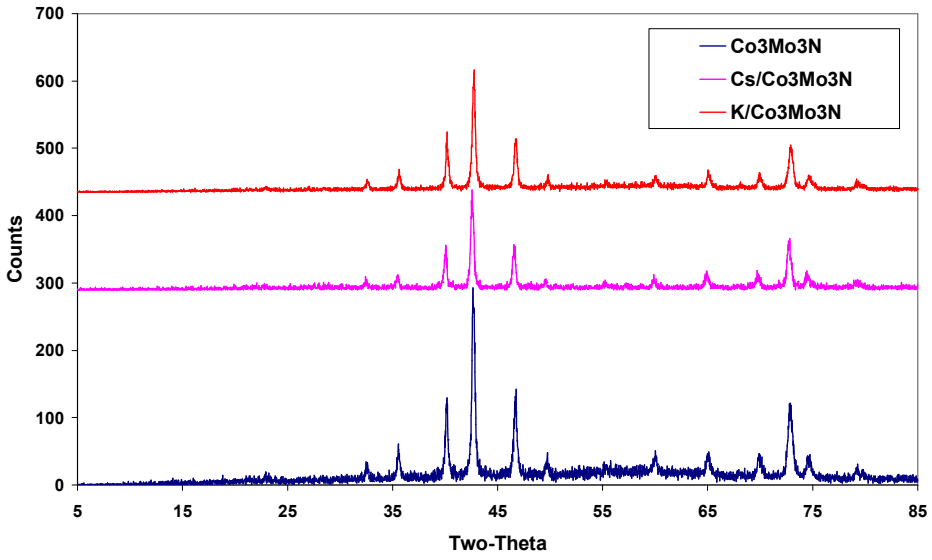

Figure 3.3-3. This should be K^+ and Cs^+ doped Co3Mo3N

In view of the inability to duplicate the beneficial effects of alkali metal addition, activity studies have concentrated on unpromoted ternary nitride systems.

The VAlON and Laves type $Ru/Al_2O_3/TiFe_2N_x$ catalysts only produce trace amounts of ammonia during the reaction and therefore will not be pursued further in determining the reactivity of lattice nitrogen using ammonia synthesis as a test reaction in the latter part of this thesis.

The activities of Fe_3Mo_3N and Ni_2Mo_3N are much lower than that of Co_3Mo_3N. This can possibly be rationalised by Jacobsen and co-workers' theory of alloying metals to generate an optimum nitrogen binding strength [59]. It is on this basis then, that Fe_3Mo_3N and Ni_2Mo_3N would be expected therefore, to have non-optimal binding strengths (with iron being stronger than cobalt and nickel being weaker than cobalt).

The oxide precursors of the bimetallic nitride materials were also tested for ammonia synthesis on the basis of the results shown in section 3.2 documenting the *in-situ* formation of β-$Mo_2N_{0.78}$ and subsequent ammonia synthesis, from an oxide precursor.

Inspection of the ammonia synthesis activity of the bimetallic oxide precursors, shows a similar general trend with the bimetallic nitride materials prepared by ammonolysis, with the CoMo oxide precursor being the most active of the precursor materials tested. However, there is a difference in the activities of the iron and nickel molybdenum oxide precursors, with NiMo oxide being the more active catalyst on nitridation in N_2/H_2 and the FeMo oxide producing only a small amount of ammonia during the reaction. The complete nitridation of the $NiMoO_4$ to form Ni_2Mo_3N (Identified by XRD in Figure 3.3-2 (a)) compared with the partial nitridation of $FeMoO_4$ in mixtures of N_2/H_2 could explain the higher activity of the NiMo oxide precursor.

Comparing the ammonia synthesis activities of the ternary nitride powders synthesised by ammonolysis with those oxides nitrided *in-situ* as part of an ammonia synthesis reaction is not trivial. Unlike the Ni_2Mo_3N samples which can be compared on a mass normalised basis (where appropriate corrections are applied), an accurate comparison of the ammonia synthesis activities of Co_3Mo_3N / Fe_3Mo_3N versus the N_2/H_2 treated CoMo / FeMo oxides is not

possible as the post-reaction XRD data shows that the materials are not fully nitrided and therefore the absolute phase composition of the resultant materials is not known. The ammonia synthesis rates quoted in Table 3.3-1 for the N_2/H_2 treated CoMo / FeMo oxides is based on 0.4g of precursor oxide and the assumption of complete nitridation, for ease of comparison with the pure phase nitride materials.

The activities shown for the ternary nitride materials tested match up well with the trend reported by Jacobsen and co-workers, Co_3Mo_3N > Fe_3Mo_3N > Ni_2Mo_3N, when conducting ammonia synthesis experiments under industrial conditions, at high pressures [58]. As described previously this trend is not repeated when considering the activities of the bimetallic oxides, CoMo > NiMo > FeMo. This reason for this change could lie in the degree of nitridation when H_2/N_2 is employed in the ammonia synthesis reaction. Indeed there has been a previous report of the synthesis of Ni_2Mo_3N from NiMo oxide using mixtures of H_2/N_2 [166] but, to the author's knowledge no such literature exists for the synthesis of Fe_3Mo_3N, with the lack of any significant nitridation possibly explaining the very low activity.

3.3.4 BET Surface Area Measurements

The post-reaction BET surface areas of the ternary nitrides and their corresponding precursors is presented in Table 3.3-2. As in the binary nitride catalysts, these materials are air sensitive and the surface areas quoted may not be representative of the actual reacting samples.

Catalyst	BET Surface Area (m^2 g^{-1})
Co_3Mo_3N	18
Fe_3Mo_3N	3
Ni_2Mo_3N	1
Post Reaction $CoMoO_4.nH_2O$	13
Post Reaction $FeMoO_4$	2
Post Reaction $NiMoO_4$ (Ni_2Mo_3N)	3

Table 3.3-2. Post reaction BET Surface areas of various ternary nitrides and precursors

The BET surface area of those materials synthesised by ammonolysis, exhibit the same trends as those reported by Jacobsen for the same materials, $Co_3Mo_3N > Fe_3Mo_3N > Ni_2Mo_3N$, and the ammonia synthesis rates of these materials have been shown to follow the same trend [58]. Surface area measurements of the post-ammonia synthesis reaction precursor materials yield entirely different results. Again the CoMo sample has the highest surface area, but the FeMo and NiMo materials have inter-changed, with the Ni_2Mo_3N prepared *in-situ* in H_2/N_2 having a higher surface area than the nickel molybdenum nitride sample prepared by ammonolysis, and also the post-ammonia synthesis reaction $FeMoO_4$.

This could explain the surprisingly high activity exhibited by the Ni_2Mo_3N sample prepared *in-situ* when compared to that of the partially nitrided $FeMoO_4$ and the Ni_2Mo_3N sample prepared by the ammonolysis route.

3.3.5 Post-Reaction Nitrogen Analysis

The results of the post-reaction nitrogen analysis of the ternary nitrides and the bimetallic oxides that were tested for ammonia synthesis along with the calculated stoichiometric nitrogen content for those materials are included in Table 3.3-3.

Sample	Stoichiometric nitrogen content (wt%)	Post N_2/H_2, 400°C reaction nitrogen (wt%)
Co_3Mo_3N	2.92	2.80(3)
Fe_3Mo_3N	2.98	3.52(3)
Ni_2Mo_3N	4.33	2.57(3)
$CoMoO_{4-n}H_2O$	Nil	1.51 (3)
$NiMoO_4$ (Ni_2Mo_3N after NH_3 Synthesis)	Nil	2.31(3)
$FeMoO_4$	Nil	0.62(3)

Table 3.3-3. Nitrogen content of various nitrides and precursors following H_2/N_2 reaction at 400°C for 5.5 hours.

The observed nitrogen content of the ternary nitride materials match up well with the stoichiometric amounts, although in some instances increased nitrogen content could be explained by adsorbed NH_x species. However, the nitrogen content of the Ni_2Mo_3N sample appears to be significantly lower than the calculated stoichiometric nitrogen content. The possible formation of related products such as Ni_3N and $Ni_{0.2}Mo_{0.8}N$ - which have been reported in less pure Ni_2Mo_3N samples [163, 165], which then decompose during the synthesis and are not visible in the XRD data could explain the reduced nitrogen content. Another possible explanation could be the oxidation of bulk Ni, although again, there is no XRD evidence of nickel oxide. The nitrogen content quoted in the table is in good agreement with the value presented for "Ni_3Mo_3N" in the literature by Zhang *et al* [166]. However, it appears that the assignment of the nickel molybdenum nitride material documented by Zhang *et al* is incorrect, as the XRD data presented for pure "Ni_3Mo_3N" matches exactly with the literature documenting Ni_2Mo_3N [163, 165], and also the XRD pattern shown in Figure 3.3-2 (a).

Confirmation of the complete/ partial nitridation of some of the precursor oxide materials shown in the XRD patterns in section 3.3.2 is given by the post-reaction nitrogen content of the materials in the table. The CoMo oxide precursor has a sub-stoichiometric amount of nitrogen present in the material, and has only half the nitrogen content of the Co_3Mo_3N material synthesised by ammonolysis, the post-reaction XRD having already shown that ammonia synthesis was not sufficient to produce a pure phase cobalt molybdenum nitride. In the case of the FeMo oxide precursor, there is very little nitrogen incorporated into the material by carrying out ammonia synthesis, highlighting the lack of any significant evidence for nitridation in the post-reaction XRD pattern and possibly explaining the comparatively low activity of FeMo oxide. Unlike the previous bimetallic oxide materials, the post-ammonia synthesis nitrogen content of the $NiMoO_4$ precursor is comparable to that of the Ni_2Mo_3N materials synthesised by ammonolysis available in the literature. Indeed, it has already been shown in the post-reaction XRD of the $NiMoO_4$ precursor that the material undergoes complete nitridation to the corresponding bimetallic nitride. However, from the data presented in Table 3.3-1, the ammonia synthesis activities of both these materials are very different, with larger post-reaction BET surface area a possible explanation for the increased activity of the Ni_2Mo_3N prepared by H_2/N_2 treatment.

It is apparent from the data presented that in the case of CoMo and FeMo oxide, the ammonia synthesis activities exhibited after nitridation in H_2/N_2 are lower than those observed when the catalysts are prepared by ammonolysis (much lower in the case of FeMo oxide). The opposite effect is observed in the case Ni_2Mo_3N, with preparation in H_2/N_2 being favoured over ammonolysis due to higher ammonia synthesis activity. This then implies that, unlike the binary molybdenum nitride catalysts, that the highly specific temperature programmed ammonolysis preparation route has an advantage over nitridation in mixtures of H_2/N_2, with the exception of Ni_2Mo_3N, which is a more active ammonia synthesis catalyst using H_2/N_2 as the preparative route.

3.4 Ammonia Synthesis Activity of Bulk Gallium Nitride and H-ZSM-5 Supported Molybdenum and Iron Nitride Catalysts

3.4.1 Introduction to γ-Mo_2N/H-ZSM-5, β-$Mo_2N_{0.78}$/H-ZSM-5 and dopants

Zeolites are microporous, crystalline, aluminosilicate solids which consist of silicon and aluminium in their framework, with cations, water, and / or other molecules contained within the pores. The pores have molecular dimensions, which makes zeolites excellent catalysts for specific applications, and other principal applications for zeolites include ion exchange and gas filtration. Other advantages of zeolites in terms of catalysis is their density of catalytic sites and their stability at high temperatures, with decomposition temperatures being generally in excess of 700^{o}C. The acidic properties of zeolite materials, which can be of Lewis or Brønsted nature, are also beneficial in catalysis [167]. H-ZSM-5 is a synthetic zeolite material with two sets of intersecting pores of dimension 5.1 x 5.5 Å.

Generally, materials require a high specific surface area to be useful as heterogeneous catalysts. There are two different methods of preparing high surface area materials. The first is to generate a porous material or nano-structured powder via a synthesis method such as temperature programmed reduction (e.g. ammonolysis). The second is to disperse the catalytically active species (e.g. metal nitride) on a high surface area support material (e.g. H-ZSM-5). The typical surface areas of bulk nitride materials is in the range of 30-100 $m^2\ g^{-1}$,

supported nitrides can easily have surface areas well in excess of 100 m^2g^{-1} [168]. Catalysis involving transition metal nitrides has been shown to be strongly related to the structural properties of the material, which are affected by the conditions employed during synthesis. Supporting a transition metal nitride may alter its surface structure, therefore changing the catalytic activity with respect to that exhibited by the bulk material [169]. Most examples of supported nitride materials available in the literature however, use bulk phase oxides such as γ-Al_2O_3 and TiO_2 as supports. The use of zeolites as a support for molybdenum nitride to achieve high surface areas is rare.

Au *et al* [169] carried out studies of zeolite supported molybdenum nitrides for the reduction of NO with H_2, using various Mo loadings ranging from 2-30 wt. %. While higher metal loadings demonstrated greater initial activity, these materials deactivated quickly with time on stream. The 2 wt. % Mo was the most stable material with catalytic activity remaining constant for the test period of 15 hours. The reason described for the deactivation of catalysts with Mo loading above 2 wt. % was due to incorporation of greater amounts of oxygen in the nitride lattice of the materials which could not be removed by reduction at 400^oC in H_2 [169].

In this section the use of Fe and Ga dopants on the zeolite supported molybdenum nitrides is studied to investigate any possible promotional effects for ammonia synthesis. Fe and Ga doped MoO_3/H-ZSM-5 have previously been shown to promote hydrogen production in the dehydroaromatisation of methane in which molybdenum carbide or oxycarbide are proposed to be active [172]. Indeed it is logical to investigate the possible promotional effects for ammonia synthesis using Fe as a dopant given the enhanced ammonia synthesis activity exhibited by Fe_3Mo_3N, and also the use of the iron based catalyst employed in the Haber process. Even in nature the dinitrogen reducing enzyme nitrogenase requires the presence of iron in conjunction with molybdenum for nitrogen fixation [177]. Zeolite supported gallium catalysts are also active in the Cyclar process converting liquefied petroleum gas (propane and butane) into aromatics like benzene and toluene, making LPG a good feedstock for petrochemical applications [173]. The role of the gallium containing phase is currently unclear, although facilitated hydrogen desorption has been suggested. It can therefore be reasoned that the use of Fe and Ga as

dopants on nitrided MoO_3/H-ZSM -5, and also the use of bulk gallium nitride, which is better known for its application as a semiconductor, is justified.

3.4.2 XRD Patterns of Pre- and Post-Ammonia Synthesis H-ZSM-5 Supported Nitrides

X-ray powder diffraction studies carried out on all the calcined 5% MoO_3/H-ZSM-5 precursors and post reaction γ-Mo_2N/H-ZSM-5 and β-$Mo_2N_{0.78}$/H-ZSM-5, and also the H-ZSM-5 support are shown in Figures 3.4-1, 3.4-2 (a) and (b).

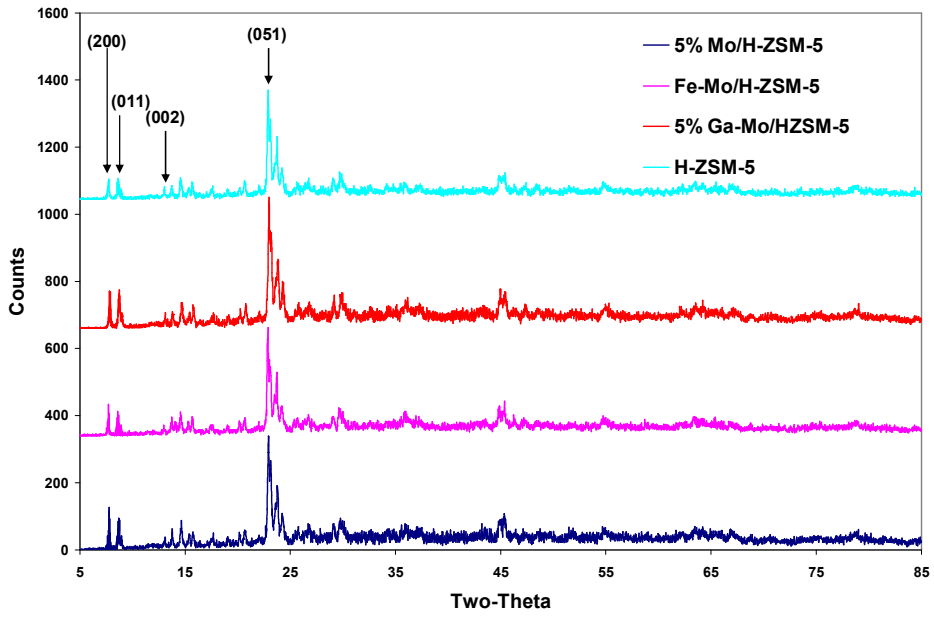

Figure 3.4-1 XRD patterns of calcined MoO_3/H-ZSM-5 catalyst doped with 5% Fe and Ga

The XRD patterns of the standard materials shown in Figure 3.4-1 exhibit the characteristic reflections of the H-ZSM-5 zeolite, with the main 2θ^o values occurring between 7-9 and 23-25^o 2θ. There is no explicit evidence of the MoO_3 crystallites or any dopant material in the diffraction pattern of the calcined samples, suggesting that these compounds are well dispersed. Further inspection of the XRD patterns however, shows a change in the relative intensity of the reflections from 7-9^o 2θ in comparison to those seen at 23-25^o 2θ after

introduction of the active phase on the zeolite support, suggesting that material that may have been occluded within the channel structure in the fresh zeolite is removed after Mo incorporation, calcination, and subsequent ammonolysis.

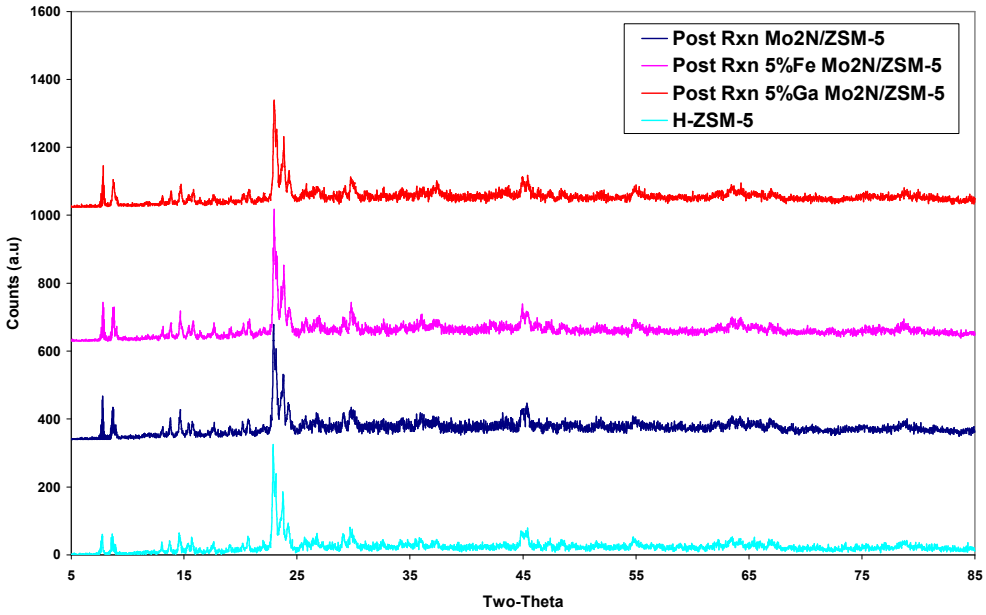

Figure 3.4-2(a) XRD patterns of γ-Mo_2N/ZSM-5 catalyst doped with 5% Fe and Ga

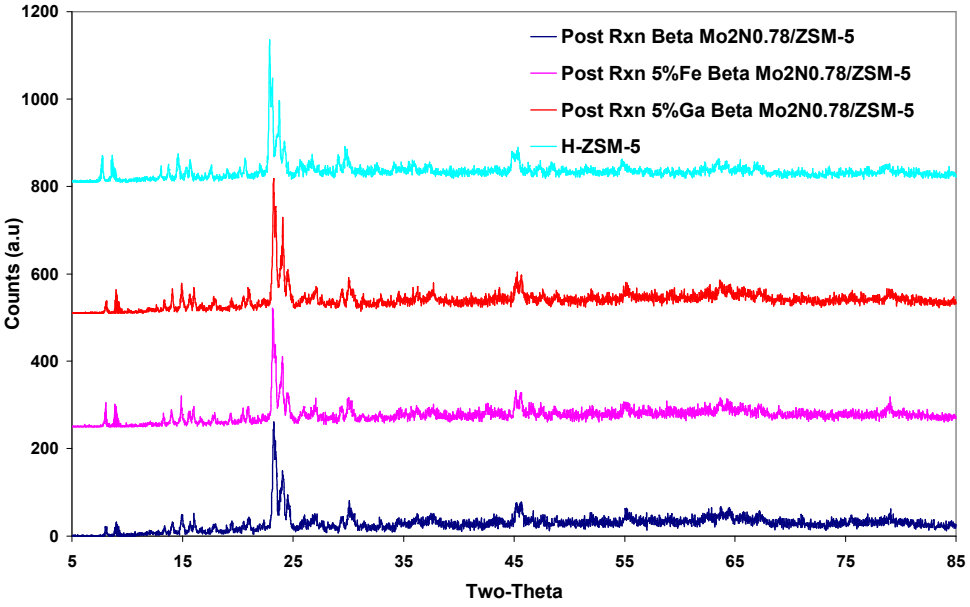

Figure 3.4-2(b) XRD patterns of β-Mo_2N/H-ZSM-5 catalyst doped with 5% Fe and Ga and H-ZSM-5 support.

The most intense reflections present in γ-Mo_2N and β-$Mo_2N_{0.78}$ phases would be observed at ca. 37, 44 and 38, 43° 2θ° respectively. From the X-ray diffraction patterns of the post-reaction supported molybdenum nitrides there is no evidence of any oxide, nitride or dopant metal crystallite species. This is not surprising given that the molybdenum species are not observed in the calcined catalysts prior to reaction and is in agreement with the work of Shi [158] where no molybdenum nitride reflections are observed below a 30% Mo loading. The characteristic reflections of the H-ZSM-5 support material are still present in the diffraction pattern and the zeolite structure has remained intact after ammonolysis and subsequent ammonia synthesis. Again the lack of evidence of molybdenum nitride in the XRD patterns could be due to the crystallite size of the material being too small to be detected by XRD. Another explanation could be due to a strong interaction between Mo species and the support, and as the MoO_3 crystallites breakdown during ammonolysis / ammonia synthesis, an amorphous phase of containing molybdenum oxide and nitride could be generated.

Post-reaction XRD patterns of H-ZSM-5 subject to ammonolysis and subsequent ammonia synthesis are presented in Figure 3.4-3.

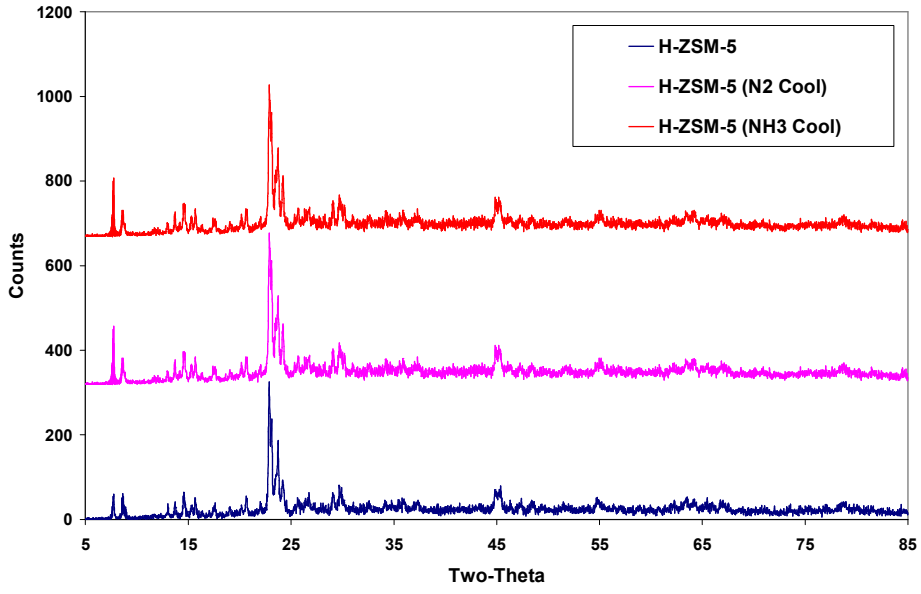

Figure 3.4-3. XRD Comparison of fresh and "nitrided" H-ZSM-5

The X-ray diffraction patterns shown in Figure 3.4-3, indicate that ammonolysis and subsequent ammonia synthesis of H-ZSM-5 materials does not destroy the crystal structure of

the zeolite. Again there is a change in the relative intensity of reflections between 7-9^{o} 2θ compared with those reflections between 23-25^{o} 2θ after ammonolysis of the zeolite, suggesting species within the channel structure of the fresh zeolite has been removed after ammonolysis.

By looking more closely at the XRD patterns of the nitrided and fresh zeolite materials presented example in Figure 3.4-4(a)-(d), the diffraction patterns shows that the relative intensities of selected reflections, indicative of the H-ZSM-5 structure (23-25^{o} 2θ), have increased in some cases. Furthermore it can be observed that the diffraction peaks shift to higher angles 2θ^{o} after impregnation of the Mo species on to the zeolite support, and shift back to lower angles after ammonolysis and subsequent ammonia synthesis when compared to the fresh H-ZSM-5 support material (Figure 3.3-4 (a) and (b)). This change in the relative intensities of the three strongest peaks, and also the peaks shifting to lower diffraction angles, indicates an increase in lattice parameter (according to a possible effect described later), and therefore the nitridation of the Mo species and/ or the incorporation of nitrogen in to the zeolite [39, 40].

An extra shoulder peak (indicated by arrows) is also observed in the XRD patterns of those materials in which molybdenum is present, and also after the fresh zeolite is nitrided (Figure 3.4-4 (a), (c), (d)). This shoulder peak is indicative of a phase transition of the zeolite from orthorhombic (fresh H-ZSM-5) to monoclinic forms (MoO_3/H-ZSM-5, γ-Mo_2N/H-ZSM-5, β-Mo_2N/H-ZSM-5 and nitrided H-ZSM-5). The opposite phase change (monoclinic to orthorhombic) has been observed previously in the literature and is believed to be induced by both temperature effects and the presence of organic adsorbates [178-182]. Within the literature this symmetry change has also been shown to be reversibly induced by loading/ unloading H-ZSM-5 powder samples with ammonia and various organic molecules [179]. The formation of coke within the channel system of H-ZSM-5 has also shown to be responsible for such framework changes [182].

There is no significant variation in these observations with the addition of Fe or Ga present in the material, and no shift in reflections was observed for “nitrided” H-ZSM-5 material.

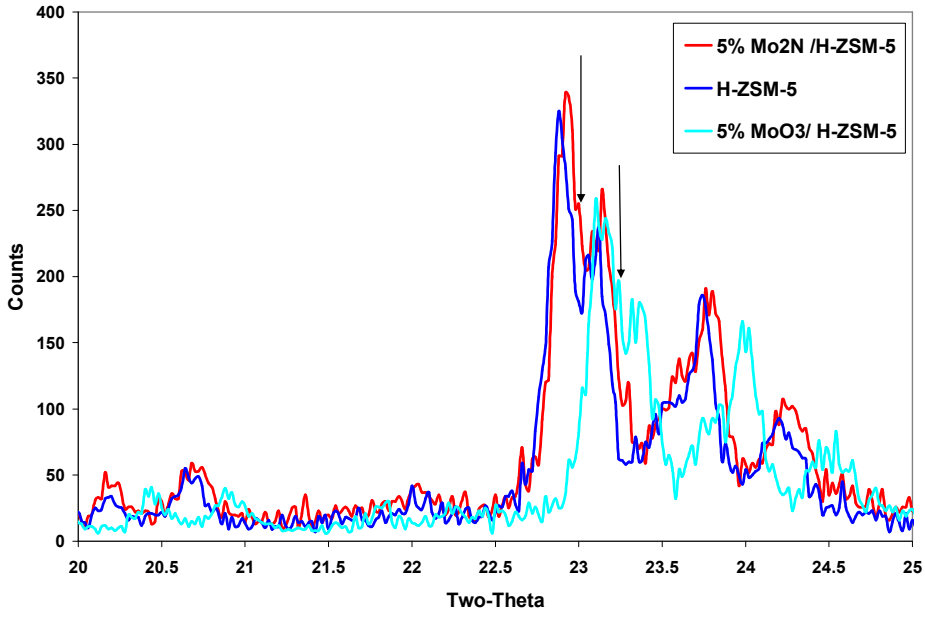

Figure 3.4-4(a) XRD pattern demonstrating decrease in diffraction angle and increase in peak intensity after ammonolysis and ammonia synthesis. A phase transition can also be observed from orthorhombic (H-ZSM-5) to monoclinic (MoO_3/H-ZSM-5 and γ-Mo_2N/H-ZSM-5).

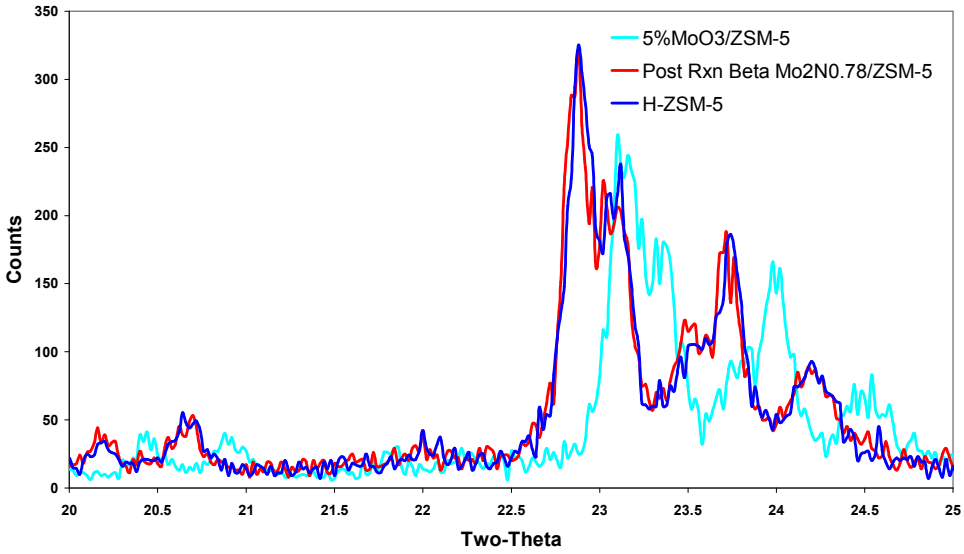

Figure 3.4-4(b) XRD pattern demonstrating decrease in diffraction angle and increase in peak intensity after ammonia synthesis of precursor.

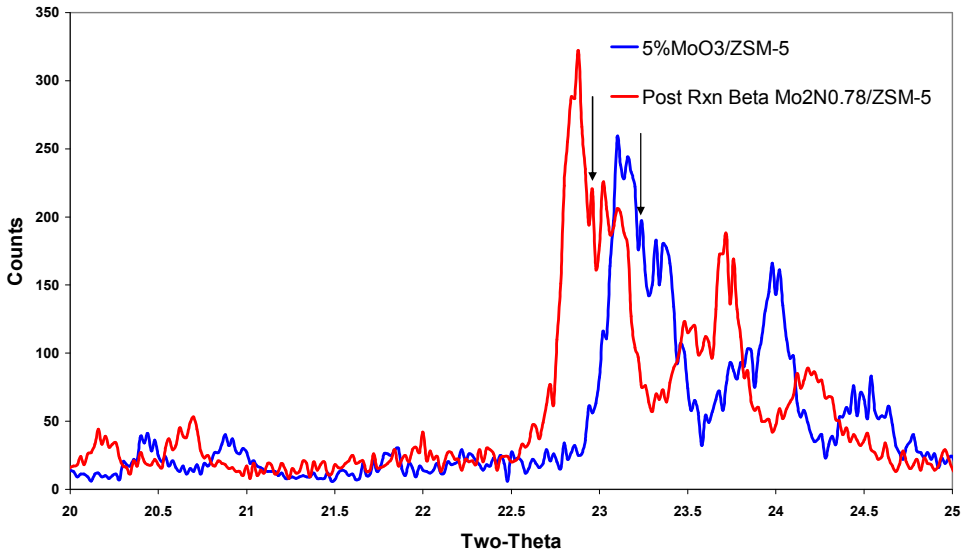

Figure 3.4-4(c). XRD patterns which highlight shoulder peaks not visible in Figure 3.3-4 (b) which indicate a phase transition from orthorhombic (H-ZSM-5) to monoclinic (MoO_3/H-ZSM-5 and β-Mo_2N/H-ZSM-5).

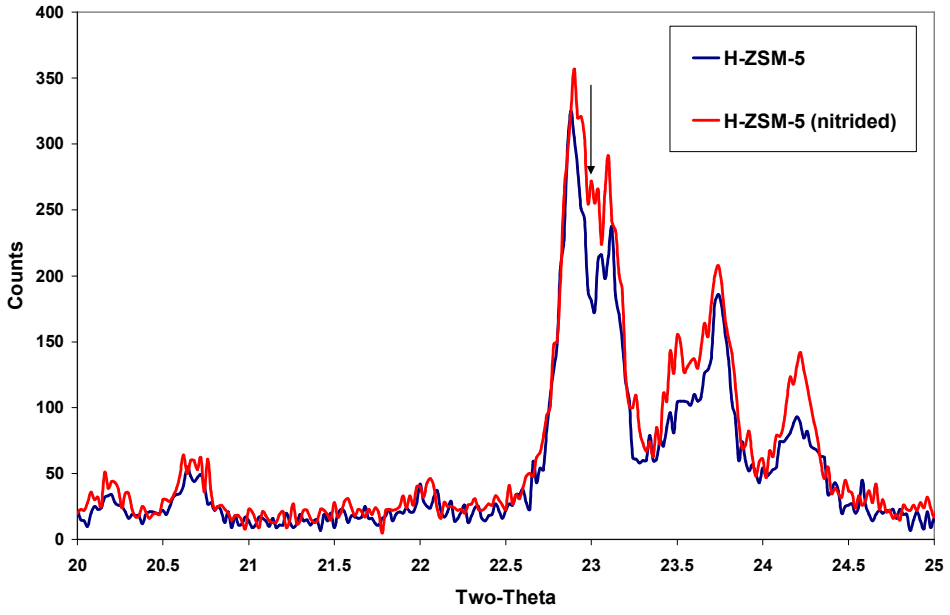

Figure 3.4-4(d). XRD patterns which, by highlighting shoulder peaks, indicate a phase transition from orthorhombic H-ZSM-5 (fresh) to monoclinic H-ZSM-5 (nitrided).

The observed shift in reflections to higher angles on impregnation of the active Mo species, and subsequent shift back to lower angles on nitridation of the MoO_3/H-ZSM-5 material can be further emphasised by listing the most obvious XRD reflections present in the patterns and noting the angles of reflection in $2\theta^o$ range which are shown in Table 3.4-1. The relevant reflections are indicated in Figure 3.4-1.

Miller indices (h k l)	H-ZSM-5 Angle of reflection $2\theta^o$	5% MoO_3/H-ZSM-5 Angle of reflection $2\theta^o$	γ-Mo_2N/H-ZSM-5 Angle of reflection $2\theta^o$	β-$Mo_2N_{0.78}$/H-ZSM-5 Angle of reflection $2\theta^o$
(011)	7.74	8.05	7.80	7.72
(200)	8.64	8.93	8.68	8.63
(002)	13.04	13.38	13.08	13.06
(051)	22.88	23.14	22.92	22.88

Table 3.4-1. Observed diffraction angles for named reflections in fresh H-ZSM-5 and molybdenum containing H-ZSM-5

Within the literature, it has been proposed that molybdenum oxide precursors are initially deposited on the external surface of H-ZSM-5 and transform to molybdenum oxo species which are redistributed between the external surface and internal channel structure [183-186]. There have been many studies which have sought to address the form of MoO_3/H-ZSM-5 catalyst precursors. Iglesia *et al.* have proposed that the active form of the catalyst takes the form of $Mo_2O_5^{2+}$ species which bridge two Al framework sites [185-187]. Similar observations were made by Ha *et al.* [188] who suggested that $Mo_2O_5^{2+}$ or MoO_2^{+} are formed upon catalyst activation. The combination of materials to form clusters, $Mo_5O_{12}^{6+}$, which are located at the channel intersections within the channel structure and crystallites of molybdenum oxide on the external surface, has been reported by Li *et al.* [189]. It is possible that the activated form of MoO_3/H-ZSM-5 can take on many different forms. There have been very few studies aimed at an investigation of the local environment of transition metal exchanged zeolites or those containing extra framework transition metal oxo species. Studies by Burns *et al.* using Al K-edge EXAFS, has shown that the average framework structure of H-ZSM-5 is strongly

perturbed by the presence of the molybdenum species, and changes the long Al-O bond distance from 1.98 to 1.89 Å, with the Al being drawn to the Mo species [190]. It has been reported previously that aluminium can be directly extracted from the H-ZSM-5 framework by increasing the Mo loading or the severity of the thermal treatment [190, 191]. The shifts observed in the XRD patterns in Figure 3.4-4 (a)-(d) and in the angles of reflection shown in Table 3.4-1 could also be a direct consequence of the framework changing due to the presence of Mo(VI) in MoO_3, and therefore distancing of the unit cell as a consequence of the polarisation effect. As documented previously in Figure 3.4-4, the unit cell parameters increase after nitridation, shifting the XRD reflections to lower angles $2\theta^o$, and the XRD patterns match well with the standard H-ZSM-5, which could be due to the reduction in molybdenum oxidation state on transformation from an oxide to a nitride.

It is clear from the lack of research available in the literature that the true nature of zeolite supported molybdenum nitrides is yet to be fully characterised.

Supported molybdenum nitride species have been studied previously using XPS and EXAFS techniques, which can provide information on the oxidation state of the molybdenum species dispersed on the support, and therefore determine the degree of nitridation of the supported molybdenum oxo species [169, 174, 175, 192, 193]. Other methods used to determine to what extent the supported molybdenum oxide is nitrided include temperature programmed reduction with hydrogen to determine the surface properties and structures of transition metal nitrides [19, 171].

Despite the work carried out previously in the literature to confirm the formation of molybdenum nitride on a support, there is little evidence provided on the location or form of this nitride species.

3.4.3 XPS Measurements on Fresh / Nitrided Bulk and Supported Molybdenum Containing Catalysts

Zeolite dispersed molybdenum nitrides were first prepared by Becue *et al.* using chemical vapour deposition to introduce $Mo(CO)_6$ into the pores of zeolite EMT (a hexagonal polytype of zeolite Y), followed by reaction with ammonia [192]. XPS and TPR methods were used to show that some nitride species were formed. Okamoto and co-workers subsequently used a

similar method to prepare molybdenum nitride species in zeolite NaY, although their Mo K-edge EXAFS measurements were unable to distinguish between O and N in the first coordination shell of molybdenum [193].

The $Mo(CO)_6$ precursor route cannot be used to introduce molybdenum into smaller pore zeolites such as H-ZSM-5, however Shi and co-workers have reported on the activity of H-ZSM-5 supported molybdenum nitrides prepared from MoO_3 (as applied in this study also) for NO reduction with H_2 [169].Shi reached the conclusion that increased molybdenum loading on H-ZSM-5 results in an increased degree of nitridation of the molybdenum and has deduced that strong interactions between the Mo species and the zeolite support hinder the complete nitridation of the supported MoO_3 crystallites [169]. However studies conducted on supported and un-supported γ-Mo_2N by Fu *et al.* using Mo K-edge EXAFS and XRD has shown both materials to be in good agreement with the face centred cubic structure of γ-Mo_2N, however it should be noted that these materials also have high molybdenum loadings on the H-ZSM-5 [175]. These workers describe the use of XPS and TPR techniques to show evidence of nitride formation, but no evidence was provided about the location of the molybdenum species.

It has been shown by XPS and Mo K-edge EXAFS that the molybdenum oxide precursor in H-ZSM-5 is converted to molybdenum carbide during the reaction for methane conversion to benzene. It is reasonable then, to suggest that zeolite dispersed molybdenum nitride species can also be obtained, by ammonolysis or *in-situ* nitridation with H_2/N_2, where the transition metal component is located within the zeolite pores rather than as an external phase [174]. The key to this would be achieving migration of molybdenum oxo species into the zeolite during high temperature calcination prior to conversion to the carbide or nitride [194]. The binding energy quoted in textbooks for the Mo 3d region is 230-233eV, and for 3p region 396-413 eV[225].

Figure 3.4-6 shows spectra in the Mo 3d region of MoO_3 and of the bulk sample of γ-Mo_2N before and after ion beam sputtering.

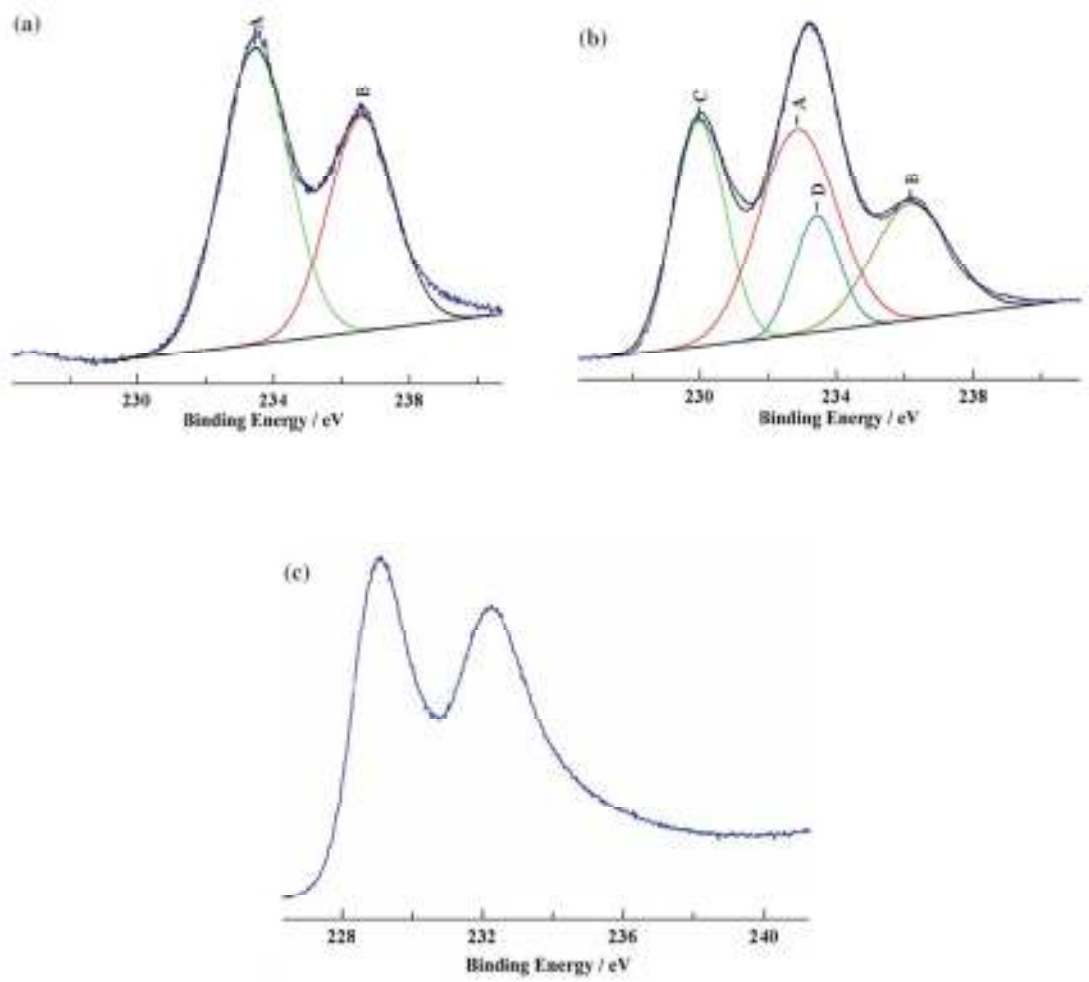

Figure 3.4-6. XPS spectra in the Mo 3d region of (a) MoO_3, (b) nitrided MoO_3 and passivated (γ-Mo_2N), (c) after argon ion etching.

The parent oxide shows a single spin-orbit doublet (Mo $3d_{5/2}$ and Mo $3d_{3/2}$ with an intensity ratio of 3:2) with a Mo $3d_{5/2}$ binding energy of 233.0 eV. The corresponding spectrum of the as-prepared γ-Mo_2N (Figure 3.4-6 (b)) shows a superposition of this doublet and a second doublet at lower binding energy (Mo $3d_{5/2}$ ~ 229.8 eV). The exact absolute binding energy values depend on the binding energy reference chosen to correct for sample charging, but the difference of 3.2 ± 0.4 eV between Mo^{+VI} in MoO_3 and the lower binding energy component in the nitrided sample is closely similar to that reported by others [76, 143, 192].

Argon ion etching can be employed to remove any surface contaminants that may be present on the sample, this technique is also known as depth profiling and can provide information in

the uniformity of elemental composition. The residual Mo^{+VI} doublet in Figure 3.3-6 (b) is attributed to the passivating oxide layer, as shown by the fact that this component is readily removed by brief argon ion etching (Figure 3.4-6 (c)). The single doublet remaining after etching shows a slightly lower binding energy (Mo $3d_{5/2}$ ~ 229.3 eV) which may be due to further reduction by the ion bombardment. Corresponding spectra in the Mo 3p region are presented in Figure 3.4-7. In this case, the parent oxide shows a single spin-orbit doublet (Mo $3p_{3/2}$ and Mo $3p_{1/2}$, with an intensity ratio of 2:1) characteristic of Mo^{+VI}. (Mo $3p_{3/2}$ = 399.0 ± 0.2 eV referenced to C 1s = 285.0 eV).

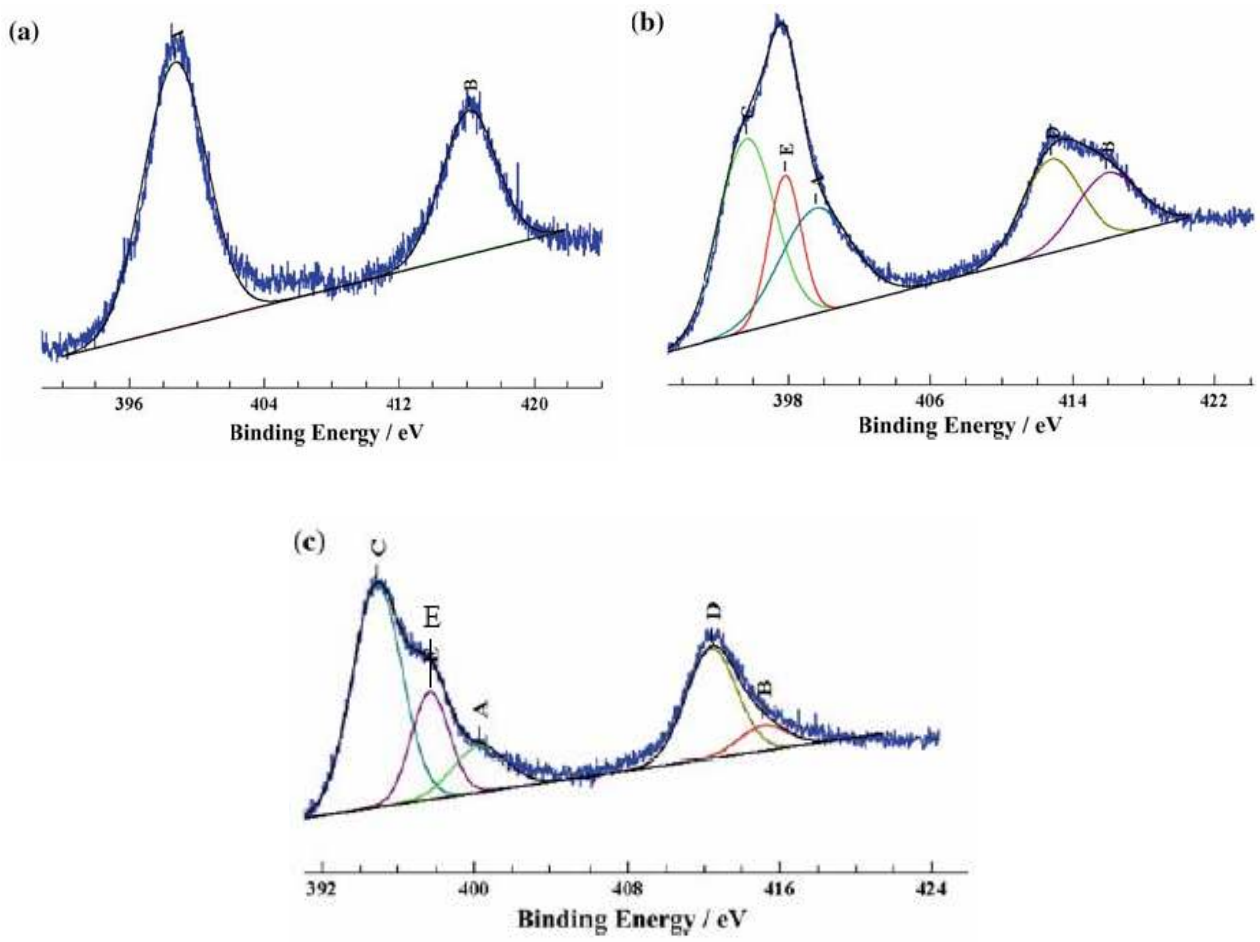

Figure 3.4-7. XPS spectra in the Mo 3p region of (a) MoO_3, (b) nitrided MoO_3 and passivated (γ-Mo_2N), (c) after argon ion etching. E marks the N 1s peak.

The as-prepared bulk nitride (Figure 3.4-7 (b)) shows, as expected from the Mo 3d spectra, two overlapping doublets in the Mo 3p region. These Mo 3p components are assigned to the passivating oxide layer and the underlying nitride. The observed peak shape could be correctly simulated however only by including a third component as a single peak (marked E in the figure) at 398.0 ± 0.2 eV. This peak is due to N 1s electrons from γ-Mo_2N (Becue et al. report a value of 397.8 eV for bulk γ-Mo_2N [192]). After argon ion etching, the Mo 3p region shows largely a single doublet with the N 1s peak present as a shoulder on the $3p_{3/2}$ component (Figure 3.4-7 (c)), although curve fitting indicates the continued presence of a small amount of the oxidised species. Determination of the N:Mo ratio from the relative intensities of the Mo $3p_{3/2}$ and N 1s peaks cannot be done accurately, but an upper limit of around 1.0 is estimated, suggesting that the surface layers probed by XPS are nitrogen-rich compared with the expected bulk stoichiometry of γ-Mo_2N.

Figure 3.4-8(a) shows the Mo 3d spectrum of MoO_3/H-ZSM-5 (4 wt% Mo) after calcination at 700°C.

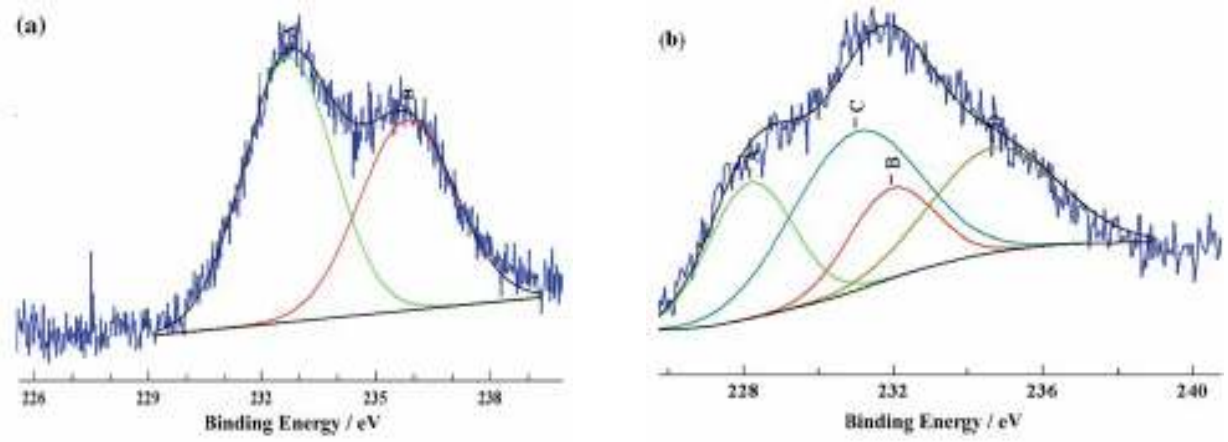

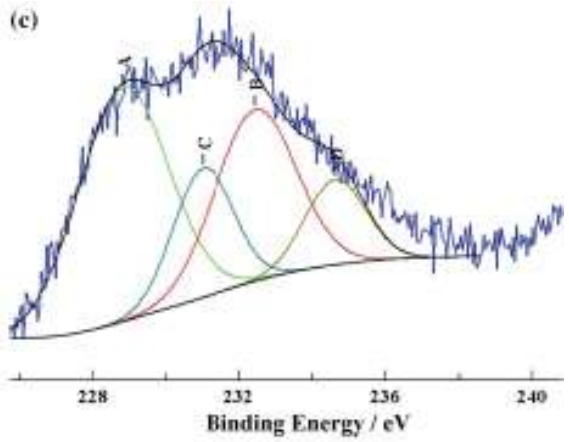

Figure 3.4-8. XPS spectra in the Mo 3d region of (a) MoO_3/H-ZSM-5 after calcination at 700°C, (b) after nitridation and passivation, (c) after argon etching.

The Mo $3d_{5/2}$ binding energy of 233.0 eV is that expected for Mo^{+VI}. The surface Mo:Si ratio measured from integrated intensities of Mo 3d and Si 2p binding energy peaks was 0.054, almost twice the value expected (0.029). This suggests that the calcination process does not succeed completely in dispersing the oxide phase within the zeolite pores. A similar conclusion was reached by Howe and co-workers in a study of earlier study of methane aromatisation catalysts [214]. The enrichment of molybdenum on the external surface of the zeolite was confirmed by observing a decrease in the Mo 3d signal intensity (to a Mo:Si ratio of 0.027) when the calcined catalyst was briefly argon ion etched.

Figure 3.4-8 (b) shows the Mo 3d spectrum recorded from a nitrided MoO_3/H-ZSM-5 sample. Nitrided samples showed a considerable reduction in Mo 3d (and 3p) signal intensities compared with the calcined catalyst (e.g. the Mo:Si ratio estimated for the sample shown in Figure 3.4-8(b) is 0.020). The broad Mo 3d envelope could be simulated by including two overlapping Mo 3d doublets with the same splitting and intensity ratios. The lower binding energy doublet (Mo $3d_{5/2}$ ~ 228.2 eV) appears to be shifted to lower binding energy from that seen with the bulk γ-Mo_2N in Figure 3.4-6, although the lower signal to noise in the zeolite dispersed samples means that the curve-fitting process is subject to larger uncertainty. The higher binding energy component (Mo $3d_{5/2}$ = 231.0 eV) is 2.0 eV shifted to lower binding energy relative to the calcined catalyst, suggesting that this species has an oxidation state lower than +6, and is not the same as the passivating oxide layer on the bulk nitride. This

difference between the zeolite dispersed and bulk samples was also seen in different behaviour on argon ion etching (Figure 3.4-8 (c)). Although the contribution of the higher binding energy doublet was reduced on etching, it could not be removed to the extent that was possible with the bulk sample (Figure 3.4-6(c)). The Mo:Si ratios estimated for etched samples were comparable (~0.02) with those of freshly nitrided samples.

Spectra measured in the Mo 3p region (shown in Figure 3.4-9), showed similar effects.

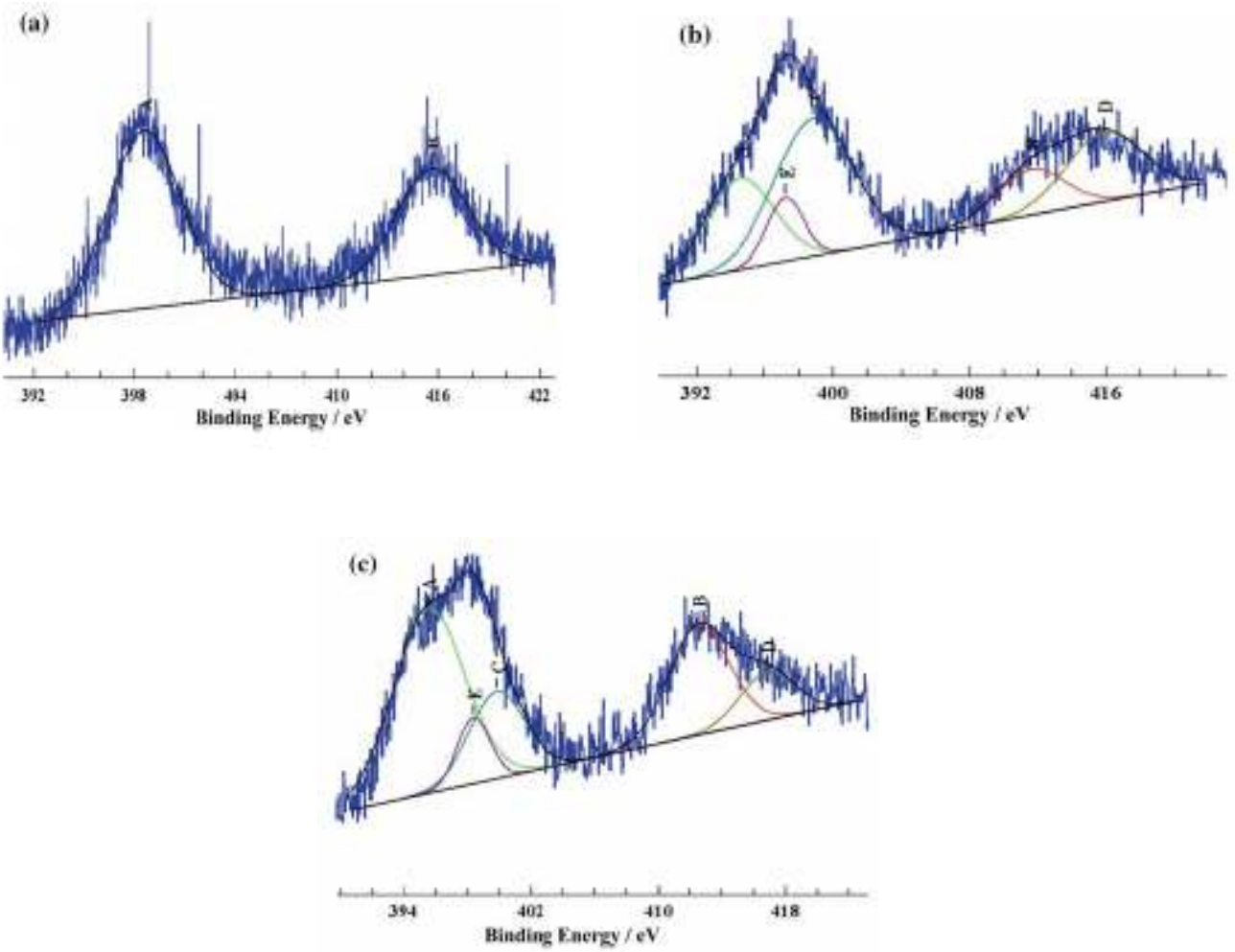

Figure 3.4-9. XPS spectra in the Mo 3p region of (a) MoO_3/H-ZSM-5 after calcination at 700°C, (b) after nitridation and passivation, (c) after argon ion etching. E marks the N 1s peak

The freshly calcined catalyst gave a single Mo 3p doublet with binding energies similar (within 0.5 eV) to the bulk oxide. The spectrum of the freshly nitrided sample could be fitted

with two doublets plus a fifth peak (marked E) due to N 1s, at ~398.0 eV. The lower binding energy doublet (Mo $3p_{3/2}$ ~ 395.0 eV) is close to that seen with the bulk nitride, but argon ion etching could not remove the higher binding energy doublet (compare with Figure 3.4-7 (c)). The N:Mo ratios estimated from relative areas of the N 1s and lower binding energy Mo 3p3/2 component were ~1.0 for the freshly nitrided catalyst, and ~0.5 for the etched sample.

Similar measurements were undertaken on MoO_3/H-ZSM-5 zeolite samples nitrided with the same protocol used for preparing the bulk nitride, i.e. cooling the sample in flowing ammonia rather than in flowing nitrogen following the high-temperature treatment. Such samples gave similar spectra in the Mo 3d region to those reported here. The Mo 3p region for these samples was however dominated by a much more intense N 1s peak which is attributed to NH_3 adsorbed in the zeolite during the cooling step. Argon ion etching reduced the intensity of this peak and allowed the lower binding-energy Mo 3p doublet to be observed, but N:Mo ratios of 20 or higher were estimated for these samples.

From the XPS data presented, it is suggested that there is an analogy between zeolite dispersed molybdenum carbide catalysts and preparing zeolite dispersed molybdenum nitride or oxy-nitride species. The zeolite supported molybdenum nitride species did however, show some differences from the bulk γ-Mo_2N material but it was impossible to fully remove the partially oxidised molybdenum component from the zeolite catalysts by argon ion etching, which suggests that the supported nitrides are best described as oxynitrides, which possibly interact strongly with the zeolite lattice.
The Mo 3d spectra observed presented are significantly different than those reported by Shi and co workers [169], who considered they were observing a mixture of γ-Mo_2N and MoO_3 on the surface of the zeolite.

3.4.4 Ammonia Synthesis Activities of γ-Mo_2N/H-ZSM-5 and β-$Mo_2N_{0.78}$/H-ZSM-5 Based Catalysts

The ammonia synthesis reactions carried out using the supported molybdenum nitride catalysts and their precursors were conducted as a comparative study with respect to the binary

molybdenum nitride catalysts. The method used to calculate the ammonia synthesis rates of the zeolite supported molybdenum nitrides is different to that used in the bulk phase binary nitride materials. It is assumed that the MoO_3 present in the H-ZSM-5 support is fully reduced to the corresponding nitride, and the rates calculated are normalised to the weight of Mo expected to be present in the fully nitrided material. It should be noted however, that this value may not be representative of the amount of Mo present in these catalysts.

The steady state ammonia synthesis rate at 400^{o}C and ambient pressures for the supported molybdenum nitrides, and those samples doped with Ga and Fe, is presented in Table 3.4-3. There are two different H-ZSM-5 samples listed in the table, one is nitrided in ammonia and cooled to room temperature in the flowing gas, the other is cooled in nitrogen. The reason for this was to assess the possible contribution of NH_3 desorption to the measured ammonia synthesis rate.

Catalyst	NH_3 synthesis rate (μmol $h^{-1}g^{-1}$ of Mo)
H-ZSM-5 (NH_3 cool)	Trace/ Trace
H-ZSM-5 (N_2 cool)	Trace/ Trace
γ-Mo_2N/H-ZSM-5	720 / 670
5% Fe-γ-Mo_2N/H-ZSM-5	1080 / 1010
5% Ga-γ-Mo_2N/H-ZSM-5	720 / 690
β-$Mo_2N_{0.78}$/H-ZSM-5	720 / 720
5% Fe-β-$Mo_2N_{0.78}$/H-ZSM-5	960 / 1000
5% Ga-β-$Mo_2N_{0.78}$/H-ZSM-5	600 / 640

Table 3.4-3. Ammonia synthesis rates of supported nitride powders and doped materials. Values after slashes indicate duplicate data from repeat reactions.

On inspection of the table, the nitrided H-ZSM-5 material produces only trace amounts of ammonia throughout the reaction, regardless of the cooling procedure employed. There is no question then that it is the active molybdenum nitride phase, or an interaction between active phase and support material, that exhibits the ammonia synthesis activity of these materials, as the contribution of the support alone is negligible.

When considering the amount of active catalyst that is present on the support, the activity of the supported molybdenum nitride catalysts is remarkably high, and is much higher than the bulk binary molybdenum nitride materials given in Table 3.2-1, although it should be noted that the activities presented in Table 3.4-3 are normalised to the weight of Mo.

The supported nitride materials exhibit the same trend for both the γ-Mo_2N and β-$Mo_2N_{0.78}$ supported materials, the Fe doped samples being the most active catalysts, followed by the supported molybdenum nitride itself. The gallium dopant seems to have no effect on the γ-Mo_2N/H-ZSM-5 material and a negative effect on the catalytic activity of the β-$Mo_2N_{0.78}$/H-ZSM-5 material. When comparing the γ- and β-supported materials directly, the difference between the activities of both nitrided polymorphs is relatively small. The activities of the supported β-molybdenum nitrides is similar to their γ-phase counterparts.

When comparing the activity of bulk gallium nitride material (2 μmol $h^{-1}g^{-1}$) with the Fe/H-ZSM-5 catalyst (3 μmol $h^{-1}g^{-1}$), it was found that the activities of both materials are very low in comparison to the bulk and supported molybdenum catalysts.

3.4.5 XPS Measurements on Fe-Mo_2N/H-ZSM-5

Iron acts a promoter for the ammonia synthesis of γ-Mo_2N/H-ZSM-5 as described in section 3.4.4. XPS measurements were conducted to determine the oxidation state of iron in the catalyst and to investigate what effect the presence of iron has on the molybdenum present in the catalyst.

Figure 3.4-10 (a) shows the Mo 3d spectrum recorded from a nitrided Fe-MoO_3/ H-ZSM-5 sample

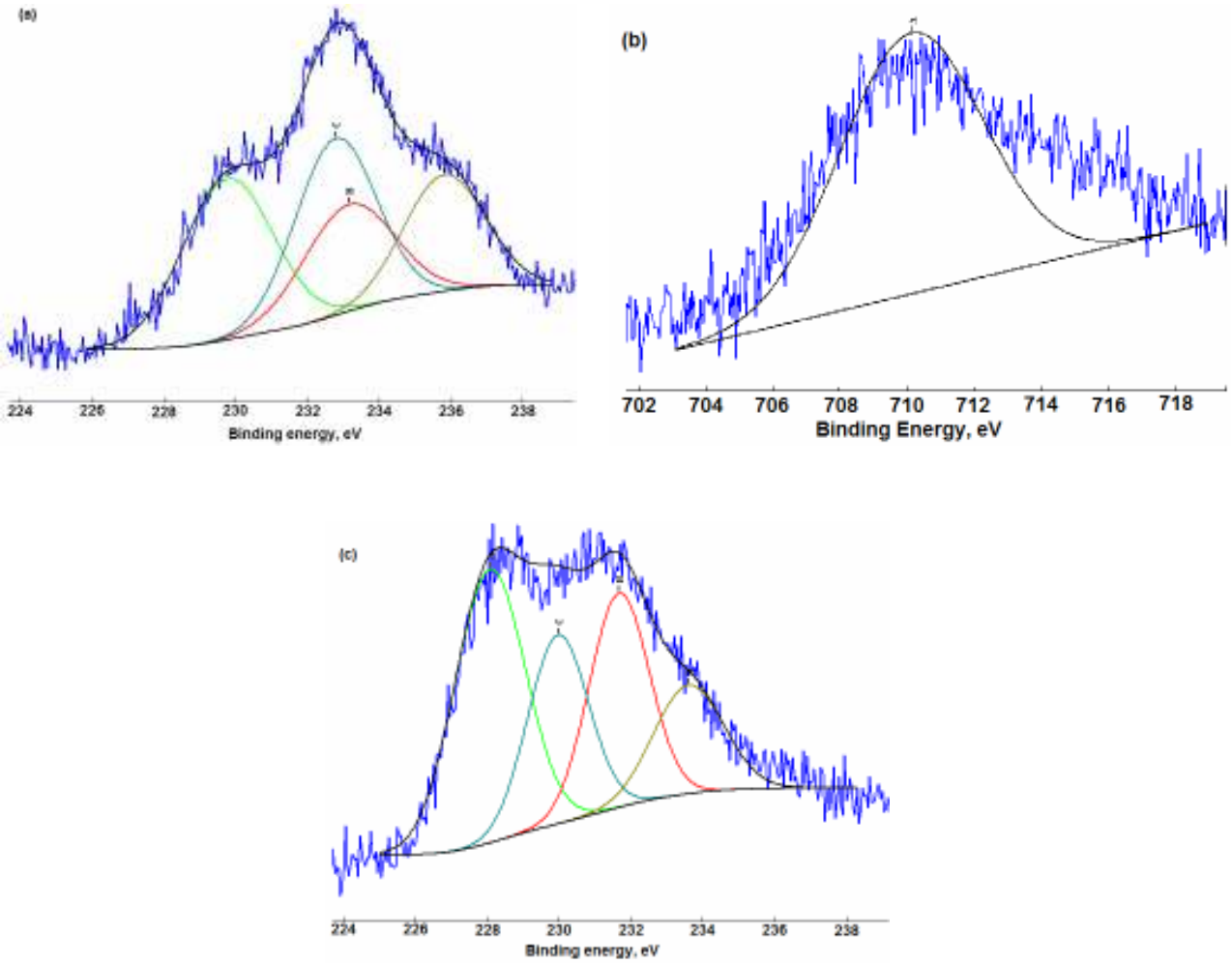

Figure 3.4-10. XPS spectra in the (a) Mo 3d region of Fe-MoO_3/ H-ZSM-5 after nitridation and passivation, (b) Fe 2p region of Fe-γ-MoO_3/ H-ZSM-5, (c) Mo 3d region of nitrided Fe-MoO_3/ H-ZSM-5 after argon ion etching.

The spectra shown in Figure 3.4-10 (a) show similarities with the nitrided MoO_3/H-ZSM-5 catalyst. Once again, the broad Mo 3d envelope could be simulated by including two overlapping Mo 3d doublets with the same splitting and intensity ratios. The lower binding energy doublet (Mo $3d_{5/2}$ ~ 229.8 eV) matches well with the lower binding energy observed in the bulk γ-Mo_2N spectra in Figure 3.4-6. The higher energy binding component (Mo $3d_{5/2}$ ~ 232.9 eV) matches well with the doublet attributed to Mo^{VI+} in the bulk γ-Mo_2N (233 eV,

Figure 3.4-6 (b)), which was related to the passivating oxide layer. Although the contribution of the higher binding energy doublet was reduced on etching (Figure 3.4-10 (b)), it could not be removed to the extent that was possible with the bulk nitride sample (Figure 3.4-6(c)). Figure 3.4-10 (b) confirms the presence of Fe^0 in the nitrided sample, with Fe $2p_{3/2}$ ~710 eV. Spectra measured in the Mo 3p region (shown in Figure 3.4-11 overleaf), showed similar effects.

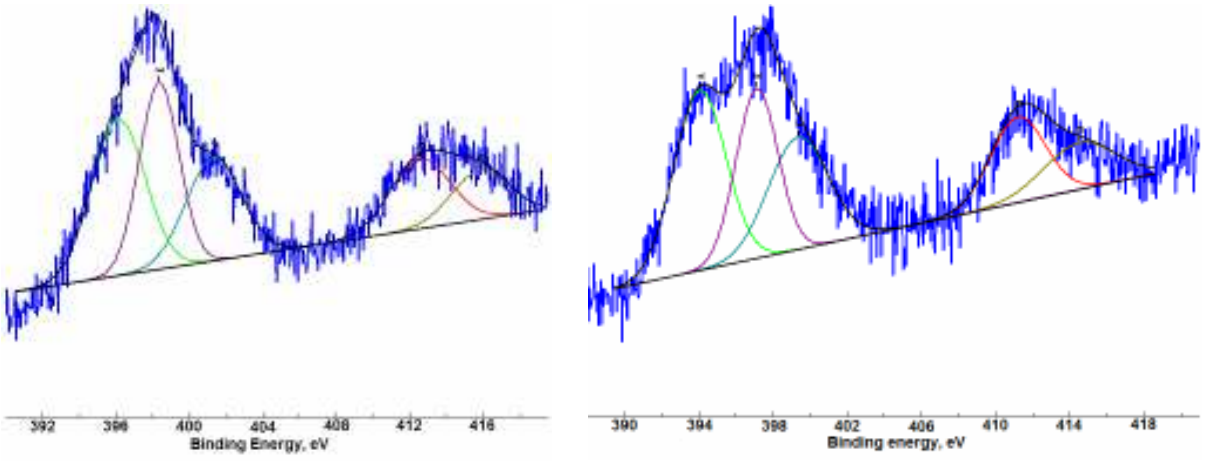

Figure 3.4-11. XPS spectra in the Mo 3p region of (a) of Fe-MoO_3/ H-ZSM-5 after nitridation and passivation, (b) after argon ion etching. E (purple) marks the N 1s peak.

The spectrum of the freshly nitrided catalyst was similar of the 3p region of the nitrided MoO_3/H-ZSM-5. The sample could be fitted with two doublets, and an additional peak (marked E, purple) due to N 1s at ~ 398.2 eV. The lower binding energy doublet (Mo $3p_{3/2}$ 396 eV) is close to that observed in the bulk γ-Mo_2N sample (Figure 3.4-6); however argon ion etching could not remove the higher binding energy doublet (attributed to passivating oxide layer). The N:Mo ratios estimated from the relative areas of the N 1s and lower binding energy Mo $3p_{3/2}$ ~ 1.25 for the freshly nitrided catalyst (this could be due to strongly adsorbed N species caused by ammonolysis), after argon ion etching this ratio is reduced to ~ 1.

3.4.6 Post-Reaction Nitrogen Analysis

The results of the post-reaction nitrogen analysis of the supported molybdenum nitrides and the calcined supported oxide precursor materials along with the calculated stoichiometric nitrogen content for those materials, assuming MoO_3 is completely nitrided, are presented in Table 3.4-4.

Catalyst	Stoichiometric nitrogen content (wt%)	Post N_2/H_2, 400°C reaction nitrogen (wt%)
H-ZSM-5 (NH_3 cool)	Nil	1.38 (3)
H-ZSM-5 (N_2 cool)	Nil	1.73 (3)
γ-Mo_2N/H-ZSM-5	0.17	0.35 (3)
β-$Mo_2N_{0.78}$/H-ZSM-5	0.13	0.38 (3)

Table 3.4-3. Nitrogen content of supported nitrides and nitrided ZSM-5 following H_2/N_2 reaction at 400°C

It is interesting to note that the post-reaction nitrogen content is considerably higher in the absence of molybdenum, which could possibly be due to the Brønsted acid sites present in H-ZSM-5 being weakened by the introduction of MoO_3. Indeed, the presence of MoO_3 has been shown to decrease the Brønsted site strength by Burns *et al.*, using NH_3 TPD, even though the Brønsted sites did not appear to be removed by MoO_3 [190]. The calculated nitrogen content for the zeolite supported γ-Mo_2N and β-$Mo_2N_{0.78}$ catalysts appear to suggest that the complete nitride formation is possible. However, in both cases the observed nitrogen content of the sample exceeds that of the calculated stoichiometric amount that would be present assuming the Mo species were completely nitrided. A possible explanation could lie in the post-reaction nitrogen content of the support material alone.

Nitridation of zeolites has been reported as a method for introducing basic sites into the materials, and nitrided zeolites have been shown to retain their structure, with good crystallinity [40, 43, 195, 196]. This method has advantages over ion exchange or impregnation of

alkali cations or salts to prepare basic zeolites [197, 198], as these procedures frequently yield materials with partially blocked pores [199].

Within the literature, high temperatures are typically used to "nitride" the zeolite materials, with Zhang *et al* reporting nitrogen content of ZSM-5 as high as 15 wt. % after treatment of the zeolite in flowing ammonia at 1100^{o}C for 10 hours [39]. However the structure of the zeolite was shown to be severely damaged at such extreme temperatures. In general, and regardless of the nature of the porous materials, there is always a risk of structural damage after prolonged ammonia treatment, hence methods have been sought which enable nitridation under milder conditions. Indeed studies by Xiong *et al*. have reported that Ru-modified silico-aluminophosphates can be nitrided at temperatures around 400^{o}C, since ammonia is decomposed in to more reactive species on the noble metal [200]. Studies by Ernst have also shown that small amounts of nitrogen are incorporated into the zeolite framework at low temperatures (300-500^{o}C) via the formation of Si-NH_2 species originating from silanol groups [201].

It is reasonable to suggest that the nitridation of zeolites could modify the surface acidity of the zeolites while maintaining the porous property of the parent zeolites at the same time. Indeed, BET surface area measurements conducted by Zhang and co-workers showed no significant change after nitridation of H-ZSM-5 in flowing ammonia at 800^{o}C for 10 hours, which confirms that no obvious structural damage occurred after such high temperature treatment [202].

As described in the introduction to H-ZSM-5 supported molybdenum catalysts in section 3.4.1, the incorporation of nitrogen in to the zeolite framework has shown these materials to be active for reactions such as the Knoevenagal condensation of benzaldehyde, and also the para-selective ethylation of ethylbenzene. Ernst has shown that zeolite materials with lower nitrogen content are more active in the Knoevenagal condensation of benzaldehyde, and reached the conclusion that at lower nitridation temperatures zeolites have both acidic and basic sites due to Si-OH and Si-NH_2 groups which are believed to be responsible for the high catalytic activity [201]. Nitrided zeolites are also believed to function as meso-microporous materials which provide bimodal pore systems, combining the benefits of each pore size regime, which could potentially improve the efficiency of zeolite catalysis [39].

The present interest in the catalytic activity of "nitrided" zeolite materials has a different origin to that which is described previously in the literature; introducing basic sites in to zeolites without blocking the pores. An isotopic nitrogen exchange reaction has been investigated using $^{15}N_2$ to investigate if it is possible to exchange the nitrogen present in the zeolite framework. This would verify the production and mobility of mono-atomic N species. Similar studies have been performed for isotopic oxygen exchange in transition metal supported zeolites, which is often used to characterise oxidation catalysts by investigating the reactivity of surface oxygen [203]. It was first documented by Winter that isotopic oxygen exchange can occur via two different pathways [204]. The first is by an $^{18}O_2$ molecule coming into contact with a solid containing ^{16}O atoms and exchanging only one atom so that the primary product is a $^{18}O^{16}O$ molecule. The second is when both atoms are exchanged during one interaction of the $^{18}O_2$ molecule with the solid i.e. $^{16}O_2$ is the primary exchange product. Most isotopic oxygen exchange reactions involving zeolites reported in the literature use supported transition metal oxides, and isotopic exchange occurs with oxygen atoms that are bonded to the supported metal oxide [203, 205, 206]. However a study by Novakov´a of Pt species in alkali faujasites has shown that activated oxygen species are able to be exchanged for zeolitic oxygens (heterolytic exchange) with a reasonable rate at about 400^{o}C [207]. This phenomenon was also observed in a study by Fejes and co-workers using ESR and Mössbauer spectroscopy on transition metal supported ZSM-5 materials [208].

Isotopic exchange reactions are usually followed by measuring the changing compositions of the gaseous phase with time using mass spectrometry, however in a study to identify the basic site on VAlON catalysts, Grange and co-workers have shown that the formation of different NH_x species on the surface of nitrided samples can be observed by FTIR spectroscopy [107].

3.4.7 FTIR Studies for $^{15}N_2$ exchange with ammonia treated H-ZSM-5 and MoO_3/H-ZSM-5

FTIR data is presented in Figures 3.4-10 to 3.4-14 of isotopic $^{15}N_2$ exchange with nitrogen incorporated in to the zeolite structure by ammonia treatment.

Figure 3.4-12 shows H-ZSM-5 after activation in vacuum and subsequent reaction with ammonia at 450°C for 11 hours together with the same sample that was in contact with 8 mbar $^{15}N_2$ for 13.5 hours.

Major bands at 3733 cm^{-1} (attributed to terminal SiOH), 3590 cm^{-1} (bridging OH), and 3 bands in the range between 2100 cm^{-1} and 1560 cm^{-1} (overtone lattice vibrations) can be observed in the spectra.

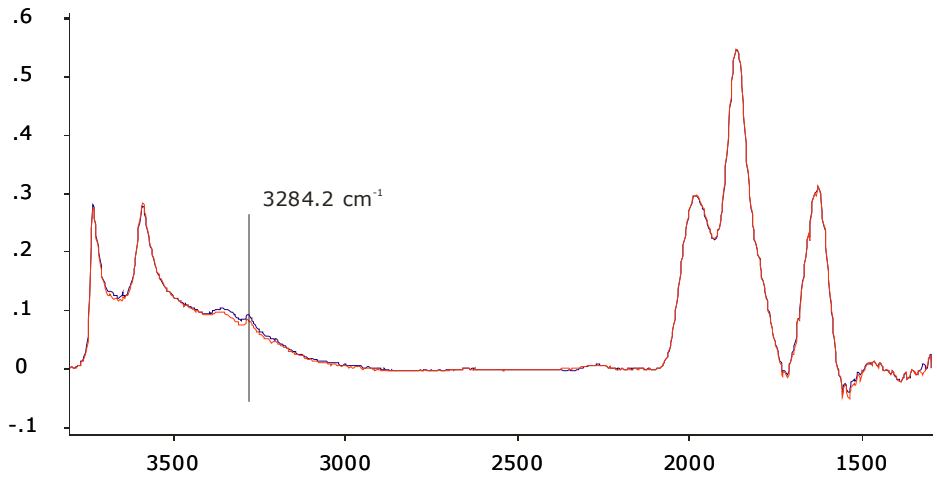

Figure 3.4-12. H-ZSM-5 after activation at 450°C in vacuum, reaction with 8 mbar ammonia at 450°C (red curve) and subsequent "exchange" with $^{15}N_2$ at 450°C (blue curve).

In addition, the reaction with ammonia led to a band at 1460 cm^{-1} (NH deformation vibration) and a broader band at 3359 cm^{-1} as well as a sharp band at 3284 cm^{-1}. This band can be attributed to NH stretching vibrations of surface -NH_2 groups. These surface -NH_2 groups have been reported to develop during high temperature treatment of zeolites by a surface reaction with OH groups as shown [201]:

$$Z\text{-}OH + NH_3 \longrightarrow Z\text{-}NH_2 + H_2O$$

Z = ZSM-5

The formation of framework bound -NH_2 groups was reported for the faujasite and mordenite structures with higher aluminium content to form basic zeolites some time ago, but only recently for H-ZSM-5 [201].

Contact of the material with 8 mbar $^{15}N_2$ at reaction temperature (450°C) did not lead to any isotopic exchange. A second experiment was conducted on the MoO_3/H-ZSM-5 material to investigate if the presence of molybdenum could facilitate isotopic nitrogen exchange. Figure 3.4-13 shows a comparison of H-ZSM-5 with 5 wt. % MoO_3/H-ZSM-5 at 30°C in vacuum and the same sample after activation at 650°C.

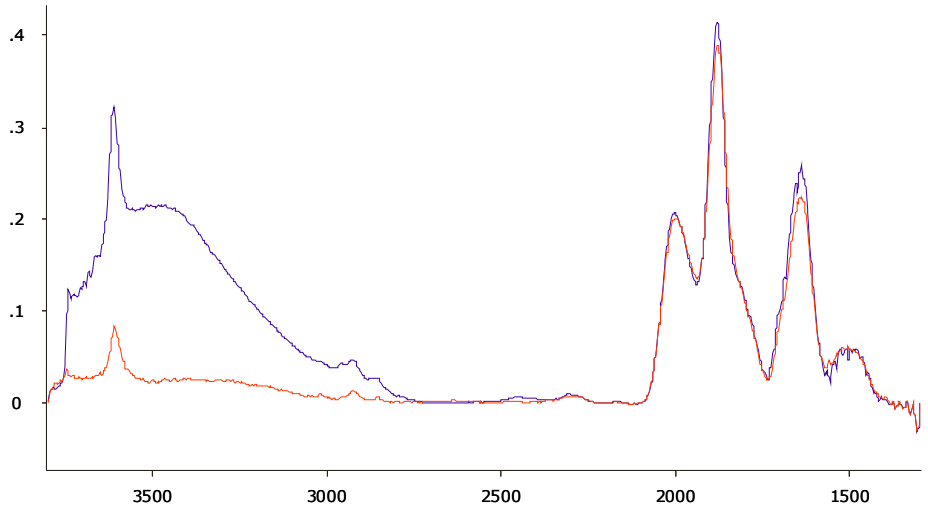

Figure 3.4-13. MoO_3/H-ZSM-5 in vacuum at 30°C (blue curve) and after activation at 650°C in vacuum.

In the sample before activation (blue), bands can again be observed at 3613 cm^{-1} (attributed to bridging OH), 3733 cm^{-1} (terminal SiOH), 2006 cm^{-1}, 1877 cm^{-1}, 1638 cm^{-1} (overtones) and a band at 1506 cm^{-1} (NH_4 deformation) is also observed. In addition, a broad band is observed at ca 3460 cm^{-1}, which can be attributed to hydrogen bonding OH stretching vibrations, or a very intense and hydrogen bonding NH stretching vibration. The slight decrease in the band at 1640 cm^{-1} (OH deformation vibration) however, suggests OH stretches.

After activation, the spectrum changes dramatically. The intensity of the bridging OH groups decrease significantly and the hydrogen bonding OH disappear completely. This suggests the

"exchange" of some of the bridging OH groups with cationic species, since no increase of hydrogen bonding OH could be observed. Figure 3.4-14 shows the FTIR data obtained from subjecting the activated MoO_3/H-ZSM-5 to ammonia treatment at 400°C, and exposing to $^{15}N_2$ at a temperature of 450°C.

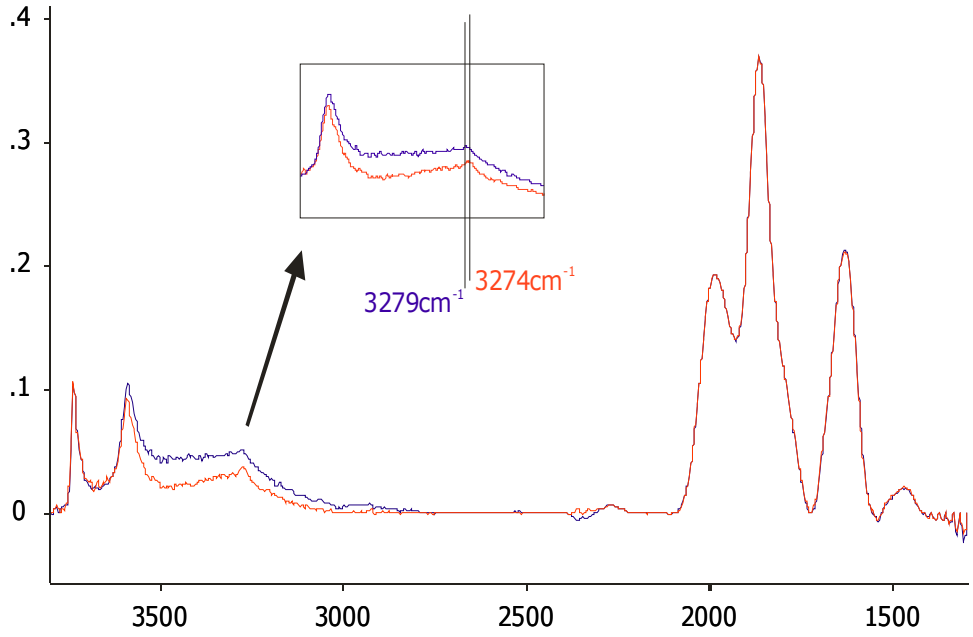

Figure 3.4-14. MoO_3/H-ZSM-5 after activation in vacuum, reaction with 8 mbar ammonia at 400°C (blue curve) and subsequent "exchange" with $^{15}N_2$ at 450°C (red curve). The inset corresponds to an expanded view.

Bands are again observed at 3359 cm^{-1} and 3279 cm^{-1}. This indicates that in both cases (H-ZSM-5 and Mo containing H-ZSM-5) the OH groups can be partially exchanged for $-NH_2$. For the MoO_3/H-ZSM-5, however, there is isotopic exchange with $^{15}N_2$. The enhanced image in Figure 3.4-14 shows the shift of the band at 3279 cm^{-1} to 3274 cm^{-1}. Calculation of the shift using a harmonic oscillator model suggests a shift of ca 7 cm^{-1}, which is well in line with the experimental finding of 5 cm^{-1}.

It would appear that the introduction of MoO_3 leads to the possibility of isotopic nitrogen exchange. This is similar to an observation by Novakova and Brabec during isotopic oxygen exchange with platinum supported zeolite materials [207]. In that case, oxygen molecules were

activated on the platinum metal, and were then exchanged for zeolitic oxygen, the spillover of activated oxygen species to zeolitic oxygen was assumed. In the case of mixed oxides, Delmon *et al.* have described this process as involving the activation of a small amount of molecular oxygen on some oxide phases (donors) which form mobile species (spillover oxygen) . These species then migrate to the other oxide phase (acceptor), react with its surface and in this way create or regenerate the sites necessary to form selectively the partially oxygenated products [209]. It is possible that an analogous nitrogen spillover mechanism is occurring in this case, however to the author's knowledge this not previously been reported in the literature and could open up new applications for zeolite dispersed nitrides.

3.5 Conclusions

In this chapter the ammonia synthesis activity of molybdenum containing nitride materials was determined, in order to establish which nitride materials would be suitable for lattice nitrogen reactivity studies in later chapters. It is clear from the data presented that the ternary nitride catalysts are more active for ammonia synthesis than the binary nitride catalysts with Co_3Mo_3N being the most active of the ternary nitrides. The ammonia synthesis activity of H-ZSM-5 supported β- and γ-molybdenum nitrides was also investigated and shown to be remarkably high when the amount of active molybdenum phase was considered. The introduction of iron as a dopant was also shown to have a promotional effect on the ammonia synthesis activity of H-ZSM-5 supported molybdenum nitrides.

Structure sensitivity in the ammonia synthesis reaction was investigated by comparing activities of powder and *nanorod* samples of bulk γ-Mo_2N and β-$Mo_2N_{0.78}$, and despite Volpe and Boudart reporting structure sensitivity on the basis of particle size [51], the change in catalyst morphology appears to have little effect on the reaction and, at least in this case, the influence of structure sensitivity is limited.

Following investigations by Wise and Markel into different preparation methods for molybdenum nitride i.e. temperature programmed reaction with ammonia or mixtures of H_2/N_2, studies in this chapter have shown that, in the case of binary nitrides, the highly specific temperature programmed ammonolysis method required to synthesise high surface

area nitrides produces an ammonia synthesis catalyst which has no advantage over catalysts which are directly nitrided in H_2/N_2. Furthermore, little influence of catalyst morphology upon reaction was observed.

By studying the XRD data of H-ZSM-5 supported nitrides tested for ammonia synthesis it was shown that the XRD pattern of the zeolite framework shifts to higher angles after introduction of MoO_3 and back upon ammonolysis of the MoO_3/H-ZSM-5 precursor. This is believed to be due to the nitridation of the MoO_3 and/ or the incorporation of nitrogen into the zeolite. An extra shoulder peak which is observed on the introduction of MoO_3 to the zeolite, and is still present after ammonolysis and subsequent ammonia synthesis was also observed in the XRD data and is believed to be indicative of a phase transition from an orthorhombic (H-ZSM-5) to monoclinic structure.

XPS measurements were carried out to confirm the presence of nitrided molybdenum species in the H-ZSM-5 supported molybdenum catalysts and although the data presented confirmed the presence of γ-Mo_2N. The zeolite supported molybdenum nitride species differed from the bulk γ-Mo_2N material, as it was impossible to fully remove the partially oxidised molybdenum component from the zeolite catalysts by argon ion etching, which suggests that the supported nitrides are best described as oxynitrides, which possibly interact strongly with the zeolite lattice.

FTIR was also used to conduct isotopic nitrogen exchange experiments over nitrided H-ZSM-5 and MoO_3/H-ZSM-5. It was shown that the presence of nitrided molybdenum was required for isotopic exchange, which shows that supported γ-Mo_2N species can be a source of reactive and mobile N species, which opens up possibilities for its application as a source of spill-over nitrogen.

4. Lattice Nitrogen Reactivity of Molybdenum Containing Nitride Materials

4.1 General Introduction

Interest in the catalytic chemistry of nitrides and oxynitrides in this project has a different origin to those described in the literature. One of the main aims of this research project was to investigate the possibility of applying metal nitrides as nitrogen transfer catalysts, in which nitrides could be viewed as "reservoirs" of activated nitrogen. This approach has its origins based upon the Mars-van Krevelen mechanism which is frequently encountered in oxidation reactions catalysed by oxides [1]. In this mechanism, oxidation occurs via the transfer of lattice oxygen to the substrate, generating the oxidised product and a transient lattice oxygen vacancy within the oxide catalyst, which is subsequently replenished by gas-phase oxygen containing species, usually O_2. A schematic of this general type of process is shown in Figure 4.4-1.

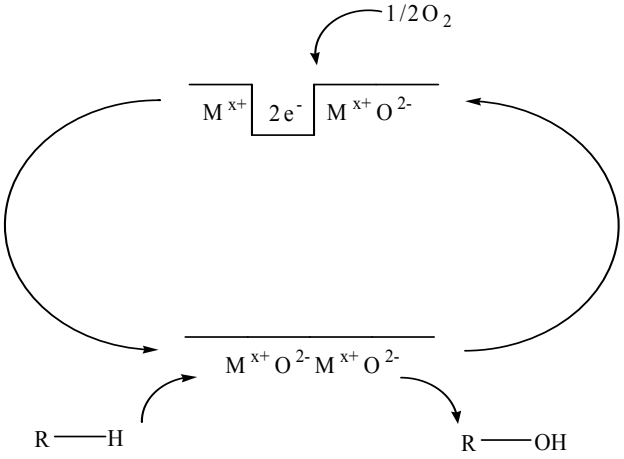

Figure 4.1-1. Schematic of Mars-van-Krevelen mechanism in oxidation catalysis

The lattice oxygen of the oxide is therefore reactive and reactions can also be observed even in the case of non-reducible oxides such as MgO [15], where it has been shown that isotopic oxygen exchange pathways can be strongly dependent upon the preparation route. In terms of process considerations for the occurrence of this mechanism, separation between substrate oxidation and catalyst re-oxidation can be beneficial in circumstances where there is the possibility of sequential gas-phase over-oxidation of a desired product [3]. The reactivity of

lattice oxygen applicable to a wide range of oxidation reactions for a large number of oxides has been established, for example the work of Winter [4] and Boreskov [5]. This general type of mechanism has also been observed for sulfur transfer reactions involving sulfide catalysts [2] and even with carbon in molybdenum carbide catalysts during methane partial oxidation. In the latter case, Green and co-workers have demonstrated direct lattice carbon transfer to the carbon monoxide produced in the partial oxidation of methane catalysed by molybdenum carbide [6].

The potential occurrence of nitrogen analogues of the Mars-van Krevelen mechanism occurring within metal nitride catalysts seems to have been largely ignored, despite early reports including those by Segal and Sebba centring upon uranium nitride catalysed ammonia synthesis, in which the importance of interstitial nitrogen was described [7, 8], and also studies by Panov and co-workers demonstrating isotopic nitrogen exchange and ammonia synthesis with uranium nitride [9]. However very recently, T.A.P. (Temporal Analysis of Products) reactor studies carried out by Olea *et al* have demonstrated the transfer of lattice nitrogen to the product in the direct ammoxidation of propane using a VAlON catalyst [10]. Furthermore, based upon the dramatic onset of ammonia decomposition activity of zirconium oxynitride associated with the β`- to β”- phase change, Soerijanto *et al.* have proposed a mechanism in which part of the product nitrogen originates from the lattice in a catalytic cycle wherein it is subsequently replenished from gas phase ammonia i.e. Figure 4.1-2 [11].

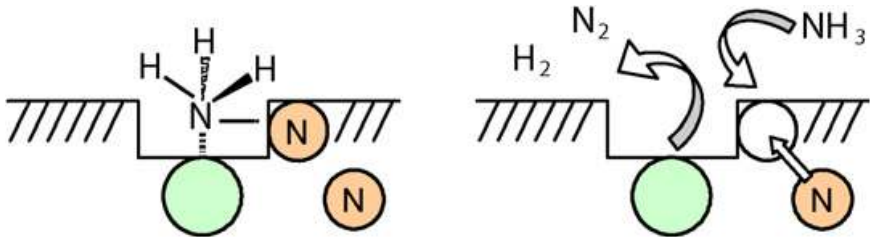

Figure 4.1-2. Schematic representation of ammonia decomposition in zirconium oxynitride catalyst [11].

In the present study the reactivity of lattice nitrogen within nitride materials is established via the comparison of ammonia synthesis activities using stoichiomteric H_2/N_2 mixtures (3:1 by volume) with H_2/Ar mixtures (3:1 by volume), as described in the experimental section. The

possibility of re-nitridation of materials is also investigated in a separate step. The separation of nitridation and de-nitridation steps may have potential merit in the development of novel nitrogen transfer pathways in which NH_3 is used as a nitrogen containing reagent where N_2 loss is thermodynamically limiting.

4.2 Results and Discussion: Co_3Mo_3N Lattice Nitrogen Reactivity

4.2.1 Reaction Data Co_3Mo_3N – Part 1

Co_3Mo_3N was the first catalyst to be studied in terms of terms of lattice nitrogen reactivity, due to its relatively high ammonia synthesis activity as described in Chapter 3. The ammonia synthesis rates were derived using the same method described previously and experiments were carried out closely following conditions employed by Aika and Kojima [16]. Comparing the ammonia synthesis activities using H_2/N_2 and H_2/Ar, completely different conductivity versus time plots are observed. The comparative conductivity versus time plot for the ammonia synthesis reaction over Co_3Mo_3N at 400°C using H_2/N_2 and H_2/Ar is given in Figure 4.2-1.

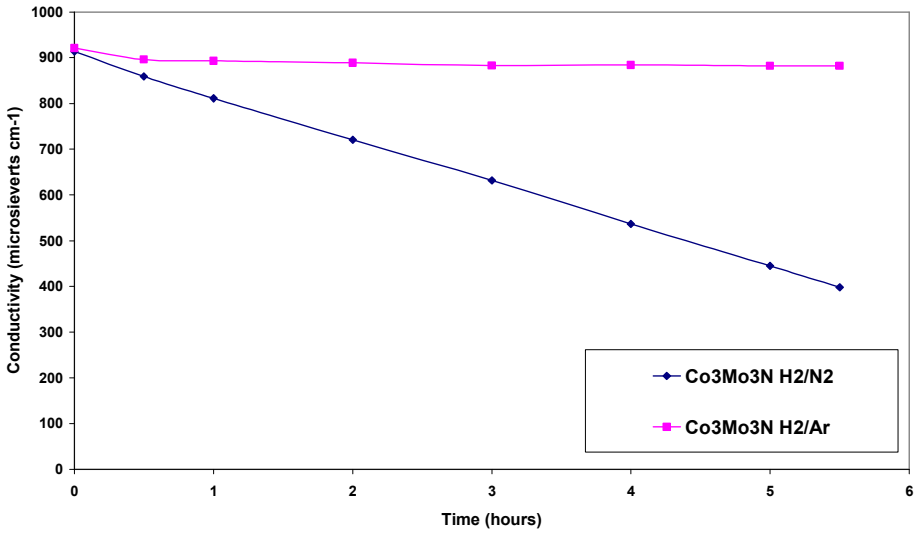

Figure 4.2-1 Comparison of conductivity H_2/N_2 vs. H_2/Ar at 400°C

Figure 4.2-1 highlights the steady state ammonia synthesis rate exhibited by Co_3Mo_3N in the standard reaction using H_2/N_2 at 400°C, and the analogous reaction which employs H_2/Ar at 400°C after the same initial pre-treatment step. In the reaction using H_2/Ar there is a sharp initial decrease in the conductivity of the solution, indicating ammonia production, during the first 30 mins on stream. This production of ammonia may occur via the hydrogenation of sorbed NH_x species, which are generated during the preparation of the catalyst by ammonolysis and the initial 2 hour pre-treatment in H_2/N_2 at 700°C, being swept off the surface of the catalyst when switching gasses after the pre-treatment. Another possibility is that a finite amount of lattice nitrogen is hydrogenated to form ammonia. The observed decrease in conductivity is short lived and thus ammonia production diminishes very quickly and the reaction eventually dies off where trace or no ammonia is produced. The observed diminution in the production of NH_3 is consistent with the consumption of nitrogen species which are not replenished.

The rate of ammonia synthesis for the first 30 minutes of reaction at 400°C for both H_2/N_2 and H_2/Ar are presented in Table 4.2-1.

Catalyst and Reaction Conditions	**NH_3 Synthesis Rate (μmol h^{-1} g^{-1}) within 0.5 hours on stream**
Co_3Mo_3N, 400°C (H_2/N_2)	200
Co_3Mo_3N, 400°C (H_2/Ar)	91

Table 4.2-1. Ammonia synthesis activity of Co_3Mo_3N at 400°C in both H_2/N_2 and H_2/Ar

The initial ammonia synthesis rate quoted in Table 4.2-1 for the reaction using H_2/N_2 is higher than the steady state rate for the standard ammonia synthesis reaction under the same conditions, as described in Chapter 3. This increased initial rate could again be attributed to the hydrogenation of sorbed NH_x species generated by the pre-treatment, indeed Aika and Kojima describe the first 30 minutes of reaction under the same conditions as a stabilisation period [16], suggesting that similar results were observed in early stages of reaction.

Since, when using H_2/Ar, the ammonia synthesis reaction ceases after 4 hours on stream at 400°C. The experiment was repeated; however the temperature was increased in 100°C increments up to 700°C. Whenever the ammonia synthesis reaction ceased (no further decrease in conductivity), the temperature was increased. The reaction profile is presented in Figure 4.2-2.

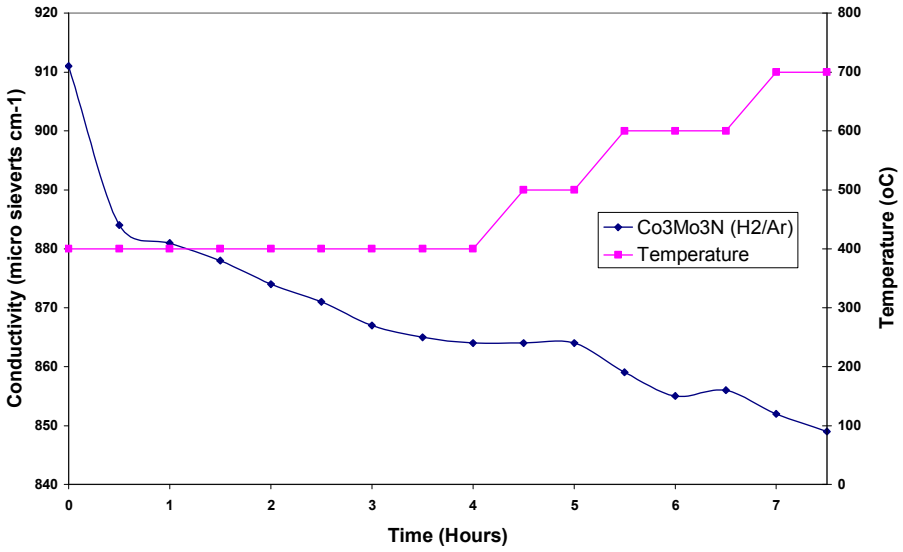

Figure 4.2-2. Conductivity data for NH_3 synthesis over Co_3Mo_3N with increasing temperature.

The ammonia synthesis rates of Co_3Mo_3N (under H_2/Ar) at temperatures between 400°C and 700°C are presented in Table 4.2-2.

Reaction Temperature/ Time	NH_3 Synthesis Rate (µmol h^{-1} g^{-1})
400°C (0 - 0.5 hr)	98
400°C (1 – 3.5 hr)	12
500°C (4 –5 hr)	0
600°C (5 – 6 hr)	16
700°C (6.5 – 7 hr)	12

Table 4.2-2. Ammonia synthesis activity of Co_3Mo_3N under H_2/Ar with increasing temperature.

Once again there is an initial burst of ammonia produced in the first 30 mins of reaction, with the rate being generally similar to that reported in Table 4.2-1, after which time the ammonia synthesis rate dramatically decreases with time on stream at 400°C. After 4 hours the reaction has plateaued and no further ammonia was produced. Increasing the reaction temperature further to 500°C, had no effect on the ammonia production and no reaction was observed, however by increasing the temperature again to 600°C it is clear that ammonia is produced from the reaction for a short period before ceasing and then the temperature was once again increased to 700°C at which point ammonia production was once again observed.

It appears that increasing the reaction temperature while flowing H_2/Ar over the catalyst appears to differentiate between lattice nitrogen species of varying reactivity present in the catalyst.

Analogous experiments were conducted employing H_2/N_2 as the feed gas in the experiment, and using the same temperature profile used in the H_2/Ar experiments. The conductivity data for this reaction is presented in Figure 4.2-3, as a comparison to the corresponding H_2/Ar profile shown in Figure 4.2-2

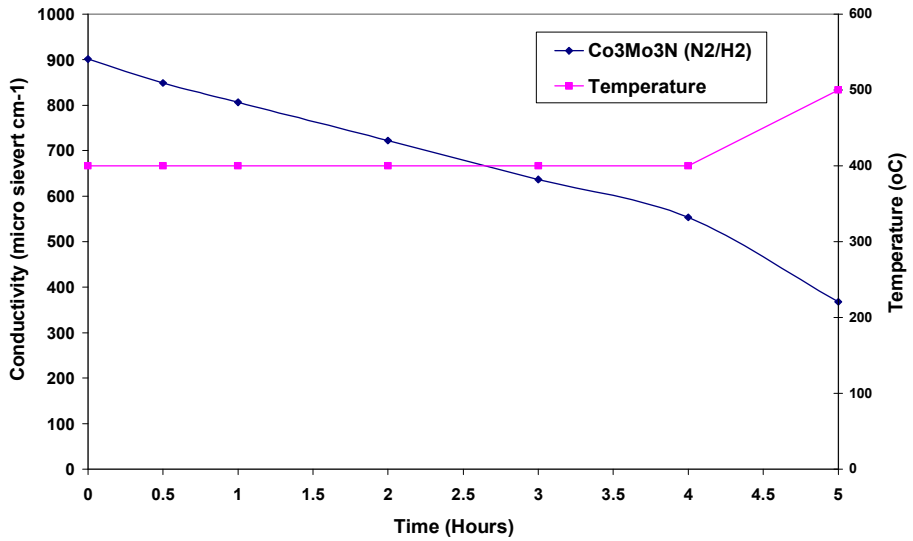

Figure 4.2-3. Conductivity data for the NH_3 synthesis using H_2/N_2 corresponds to NH_3 synthesis rate of 158 µmol $h^{-1}g^{-1}$ at 400°C and 369 µmol $h^{-1}g^{-1}$ at 500°C.

The reaction profile in Figure 4.2-3 shows similarities with the reaction conducted in H_2/Ar (Figure 4.2-2), both reactions exhibit steady state ammonia synthesis rates at 400^{o}C which increase when the temperature is increased to 500^{o}C. The data in Figure 4.2-3 is only shown for 5 hours on stream, after this point in the reaction, the sulfuric acid present in the bubbler has been completely consumed by the ammonia produced in the reaction. The sulfuric acid bubbler was changed for a fresh bubbler at this point, and the conductivity measurements continued as normal.

The ammonia synthesis rates of Co_3Mo_3N under H_2/N_2 at temperatures between 400-700^{o}C are presented in Table 4.2-3

Reaction Temperature/ Time	NH_3 Synthesis Rate (μmol h^{-1} g^{-1})
400^{o}C (0 – 0.5 hr)	189
400^{o}C (0.5 - 4 hr)	158
500^{o}C (4 – 5 hr)	369
600^{o}C (5 – 6 hr)	173
700^{o}C (6.5 – 7hr)	83

Table 4.2-3. Ammonia synthesis activity of Co_3Mo_3N under H_2/N_2 with increasing temperature.

As expected, when employing the same temperature profile, the ammonia synthesis activity of Co_3Mo_3N under H_2/N_2 is much higher than under H_2/Ar. When the temperature is increased to 500^{o}C there is a dramatic increase in the ammonia synthesis rate, this could be due to sorbed NH_x formed on the catalyst at 400^{o}C desorbing as the temperature is increased, or an added contribution to the ammonia synthesis rate by hydrogenated lattice nitrogen within the Co_3Mo_3N catalyst. Increasing the reaction temperature further shows the activity begin to decrease which is thought to be due the formation of ammonia being thermodynamically unfavourable at these high temperatures, as described in the experimental section.

4.2.2 Post-Reaction Nitrogen analysis

The results of the post-reaction nitrogen analysis of the Co_3Mo_3N samples studied in section 4.2.1, together with the calculated stoichiometric nitrogen content of the material, is given in Table 4.2-4.

Sample and testing conditions	Stoichiometric N Content (wt.%)	Observed N Content (wt.%)
Co_3Mo_3N (H_2/N_2) after 5.5 h at 400°C	2.93	2.8(3)
Co_3Mo_3N (H_2/Ar) after 5.5 h at 400°C	2.93	2.5(3)
Co_3Mo_3N (H_2/Ar) using temperature profile shown in Figure 4.2-2	2.93	1.5(3)
Co_3Mo_3N (H_2/N_2) using temperature profile shown in Figure 4.2-2	2.93	2.7(3)
Co_3Mo_3N (Ar) after 12 h at 700°C	2.93	2.3(3)
Co_3Mo_3N (H_2/Ar) after 12 h at 700°C	2.93	1.2(3)

Table 4.2-4. Nitrogen content Co_3Mo_3N samples after reactions in H_2/N_2, H_2/Ar, and Ar.

The post-reaction nitrogen content of the Co_3Mo_3N samples treated under standard ammonia synthesis conditions (H_2/N_2, 400°C) agrees reasonably well with the calculated stoichiometric amount for Co_3Mo_3N. In the case of the Co_3Mo_3N sample treated in H_2/Ar 400°C, a slightly lower nitrogen content than the calculated stoichiometric amount is observed. However, when the standard error in the technique used to determine the nitrogen content is considered, it can be said that both materials have comparable nitrogen content. Examination of the post-reaction nitrogen content of the material treated in H_2/Ar using the temperature profile shown in Figure 4.2-2 with a maximum temperature of 700°C, shows the nitrogen content of the Co_3Mo_3N sample has been dramatically reduced. Almost half (46%) of the observed nitrogen content of the standard Co_3Mo_3N sample has been lost from the material. Using calibration data and the conductivity versus time plots from the reaction profile, it can be calculated that the ammonia

produced from the reaction accounts for only 19% of the lost nitrogen content in this case, which is believed to be a consequence of the thermodynamics of the ammonia synthesis/ decomposition reaction, where N_2 formation is favoured over NH_3 production at higher temperatures.

Further experiments were undertaken in relation to the removal of nitrogen from the cobalt molybdenum nitride structure to determine the cause of the lost nitrogen. These reactions are comparable to experiments carried out by Grange and co-workers on the temperature programmed reduction of molybdenum nitride which documents the decomposition/ loss of nitrogen from γ-Mo_2N to form β-$Mo_2N_{0.78}$ under an inert atmosphere, and reduction to Mo metal under H_2, at high temperatures (1000^{o}C, 800^{o}C respectively) [12].

An experiment analogous with that which formed the nitrogen deficient sample (H_2/Ar, temperature profile to 700^{o}C) was carried out, however only H_2/N_2 was employed throughout the reaction to investigate the effect the H_2/Ar feed gas has on the loss of nitrogen from Co_3Mo_3N. Table 4.2-4 shows that the nitrogen content of this analogous reaction (H_2/N_2, temperature profile to 700^{o}C), has a nitrogen content which is comparable with the Co_3Mo_3N from the standard ammonia synthesis reaction (400^{o}C, H_2/N_2). It is evident that employing H_2/Ar at high temperatures is responsible for the removal of nitrogen from the material. The effect of high temperature was investigated by treating reduced Co_3Mo_3N material (H_2/N_2, 700^{o}C, 2 hours), in argon at a rate of 60 ml/min at 700^{o}C and dwelling at this temperature for 12 hours. Although diminished, the post-reaction nitrogen content of the material has not significantly decreased, and certainly not to the same extent observed when hydrogen is present. Thus it is believed that hydrogen is the key to removing nitrogen from the material at high temperatures, despite the fact that most nitrogen is lost in the form of N_2.

To investigate how much nitrogen could be removed from the Co_3Mo_3N material, experiments were conducted treating Co_3Mo_3N in 60 ml/min H_2/Ar at 700^{o}C for 12 hours. From the table it is clear that employing H_2/Ar at high temperatures for long periods, dramatically reduces the nitrogen content of the Co_3Mo_3N sample. However, it is surprising that the lengthy heating times involved in were not sufficient to completely remove nitrogen from the material to leave

only the constituent metals. Indeed there is no significant difference in the post-reaction nitrogen content of the Co_3Mo_3N sample which employed H_2/Ar and the temperature profile shown in Figure 4.2-2 with the Co_3Mo_3N sample which is held isothermally at 700°C under H_2/Ar for 12 hours, suggesting only a finite amount of nitrogen can be removed from the Co_3Mo_3N material at a maximum temperature of 700°C.

4.2.3 XRD Patterns

The post-reaction X-ray diffraction patterns of the cobalt molybdenum nitride samples studied under the conditions described in section 4.2.2 are shown in Figures 4.2-4 and 4.2-5.

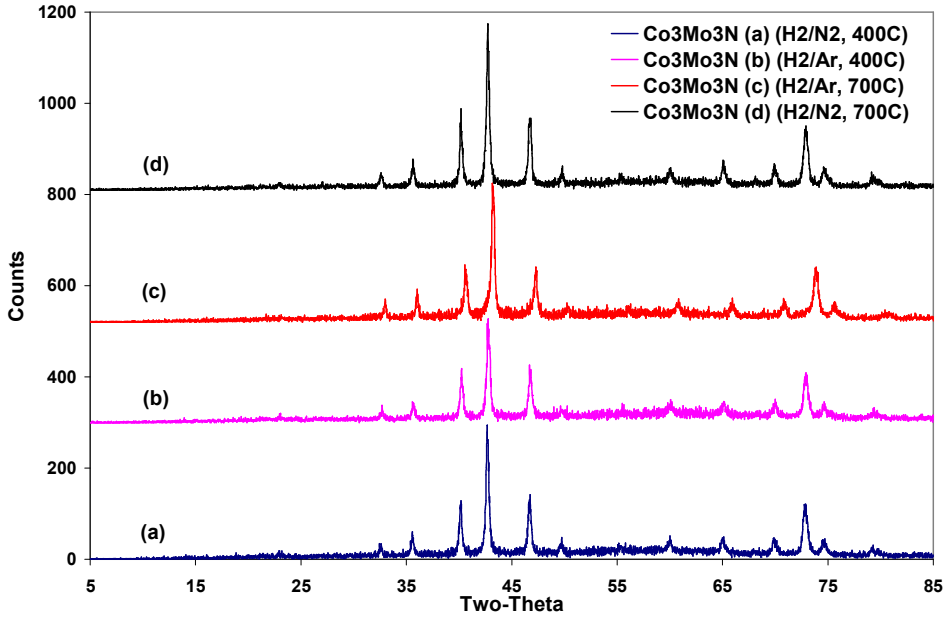

Figure 4.2-4. Post Reaction XRD patterns of Co_3Mo_3N with (a) 2.8(3) (b) 2.5(3) and (c) 1.5(3) (d) 2.7(3) wt. % nitrogen content.

The XRD data of all the post-reaction Co_3Mo_3N samples show the same characteristic reflections, however on closer inspection, the post-reaction X-ray diffraction patterns show more evidence of the loss of bulk nitrogen species. Comparison of the XRD data obtained for the Co_3Mo_3N sample treated under standard ammonia synthesis conditions (H_2/N_2, 400°C, (a))

with the Co_3Mo_3N sample treated in H_2/Ar at 400°C (b), shows that the patterns agree well, which is also reflected in the initial indexed unit cell parameters for both materials [(H_2/N_2) a = 11.032(1) Å, V = 1342.649 Å^3, (H_2/Ar) a = 11.04(8) Å, V = 1345.57 Å^3] and the post-reaction nitrogen analysis in Table 4.2-4.

When comparing the XRD patterns of the Co_3Mo_3N sample treated under standard ammonia synthesis conditions (H_2/N_2, 400°C, (a)) and the Co_3Mo_3N sample which is treated in H_2/Ar, using the temperature profile shown in Figure 4.2-2, (c), a considerable shift of the Bragg reflections to higher angles 2θ in the sample with the significantly lower nitrogen content is observed. This type of shift in the Bragg reflections is indicative of a significant reduction in the cubic cell volume, and therefore reflects the nitrogen deficient sample. The use of internal standards, NaCl (Fisher, 99.5 %), confirmed that these peaks shifts were intrinsic and not systematic and, comparing initial indexed unit cell parameters of a = 10.879(1) Å, V = 1287.53 Å^3 for the sample treated in H_2/Ar, using the temperature profile, (c), with those described by zur Loye *et al* for a standard Co_3Mo_3N sample [13], a = 11.0270(4) Å, V = 1340.8(1) Å^3, it is clear that the lattice parameters and therefore unit cell volume of the Co_3Mo_3N sample has decreased after reaction in H_2/Ar applying the temperature profile in Figure 4.2-2. The crystallographic data for the nitrogen deficient sample is included in Appendix 3.

Comparison of the XRD patterns show that this shift in Bragg reflections to higher angles 2θ is not observed when applying the same temperature profile (400-700°C) using H_2/N_2 throughout the reaction, and the X-ray diffraction pattern matches well with the post reaction XRD of the Co_3Mo_3N sample in which standard ammonia synthesis conditions were employed, suggesting no significant loss of nitrogen in this reaction. This is consistent with the post-reaction nitrogen analysis presented in Table 4.2-4. Indexing of the unit cell parameters of the Co_3Mo_3N sample subject to the temperature profile under H_2/N_2 (d), gives a = 11.016(2) Å and V = 1336.8(4) Å^3 which are in good agreement with values available in the literature as described previously [13].

The post-reaction XRD patterns of those Co_3Mo_3N samples used to determine the cause of nitrogen loss are given in Figure 4.2-5, and show the effect of longer heating times and reactant gas on the crystal structure of Co_3Mo_3N.

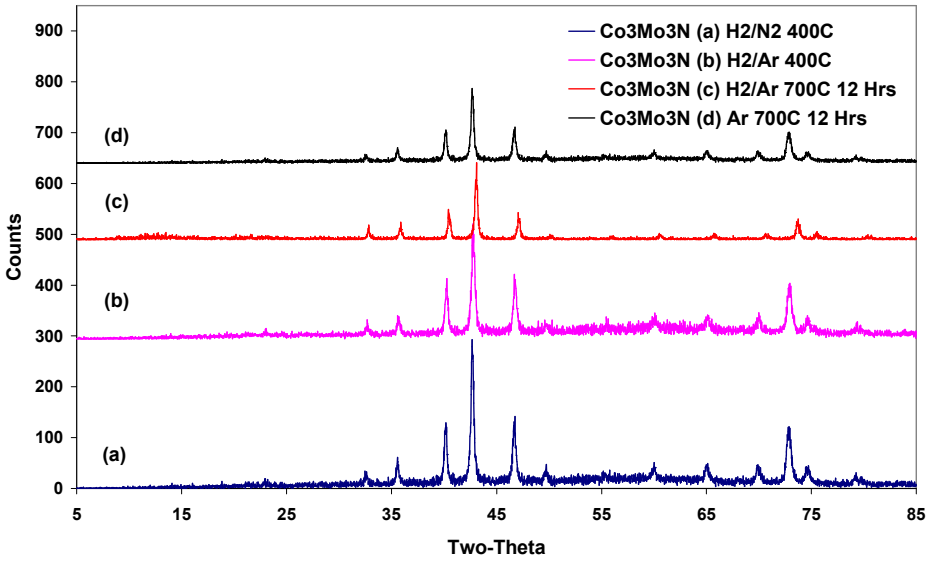

Figure 4.2-5. Post Reaction XRD patterns of Co_3Mo_3N with (a) 2.8(3) (b) 2.5(3) (c) 1.2(3) and (d) 2.3(3) wt. % nitrogen content.

There is no significant effect on the XRD pattern of Co_3Mo_3N after flowing argon over the material after at high temperature (700°C) for long periods (12 hours) after initial pre-treatment (H_2/N_2, 2 hours at 700°C), which is reflected in the post-reaction nitrogen content (within error of the analysis) and unit cell parameters when compared to standard Co_3Mo_3N [(H_2/N_2) a = 11.032(1) Å, (Ar) a = 11.019 Å]. When employing H_2/Ar in the reaction at 700°C for 12 hours, the same shift of the Bragg reflections to higher 2θ angles is observed as in the Co_3Mo_3N sample which was subject to the temperature profile in Figure 4.2-2 under H_2/Ar which is indicative of the unit cell volume decreasing i.e. lost nitrogen. The post-reaction nitrogen content of both samples is also very similar (Table 4.2-4). It is perhaps surprising however, that the material has not been completely reduced to the Co and Mo metals, or an alloy of both.

The shift in reflections observed in Co_3Mo_3N samples which are treated in H_2/Ar at 700^{o}C (for 12 hours or 1 hour) are identical, there is no increase in the shift to higher angles 2θ observed by increasing the length of time held at 700^{o}C under H_2/Ar.

It is clear from the XRD studies and nitrogen analysis that the presence of H_2 is essential to obtain the nitrogen deficient cobalt molybdenum nitride material. This implies that the hydrogenation of nitrogen species is a key requirement for N loss from the Co_3Mo_3N lattice and suggests that NH_x and/ or NH_3 species to be of importance in the process. Whilst the predominant from of lost nitrogen maybe lost as N_2, the possible transient formation of NH_3 or NH_x species allows the possibility of their entrapment by reacting species, this allows direct N transfer from the lattice to the substrate and new pathways to a host of nitrogen transfer reactions could become possible.

4.2.4 Rietveld Refinement

The post-reaction nitrogen analysis of the Co_3Mo_3N sample subject to the temperature profile in Figure 4.2-2 under H_2/Ar (Table 4.2-4) suggests a stoichiometry close to Co_6Mo_6N, and the substantial stoichiometric and structural changes after treatment of the Co_3Mo_3N sample in H_2/Ar with a maximum temperature of 700^{o}C, is reinforced by the Rietveld refinement of the XRD data. The XRD data for nitrogen deficient cobalt molybdenum nitride sample (N = 1.5(3) wt. %) could not convincingly be matched to the η-carbide structure of Co_3Mo_3N, in fact of all the models attempted, the best fit for this sample (with lowest indices and ESDs) was obtained for the so-called η-12 carbide structure adopted by Co_6Mo_6C (also cubic space group *Fd3m*) [14] which has never been reported as a nitride structure (Figure 4.4-4, overleaf).
In the η-12 structure, N atoms occupy uniquely the 8a (1/8,1/8,1/8) site and the 16c site previously occupied in Co_3Mo_3N (η-6 structure) is vacant.[14] In fact, after returning to the refinement for Co_3Mo_3N, the fit improved with a small N occupancy of the 8a (1/8,1/8,1/8) site as has been observed analogously for C in Co_3Mo_3C [14]. Hence, on treatment under H_2/Ar, half the lattice nitrogen is removed from the 16c site and the remainder migrates to the previously essentially vacant 8a position (giving a theoretical N content of 1.48 wt% for

Co_6Mo_6N and matching well with the nitrogen analysis for cobalt molybdenum nitride sample in Table 4.2-4 (N = 1.5(3) wt. %). All Rietveld refined patterns are included in the Appendix.

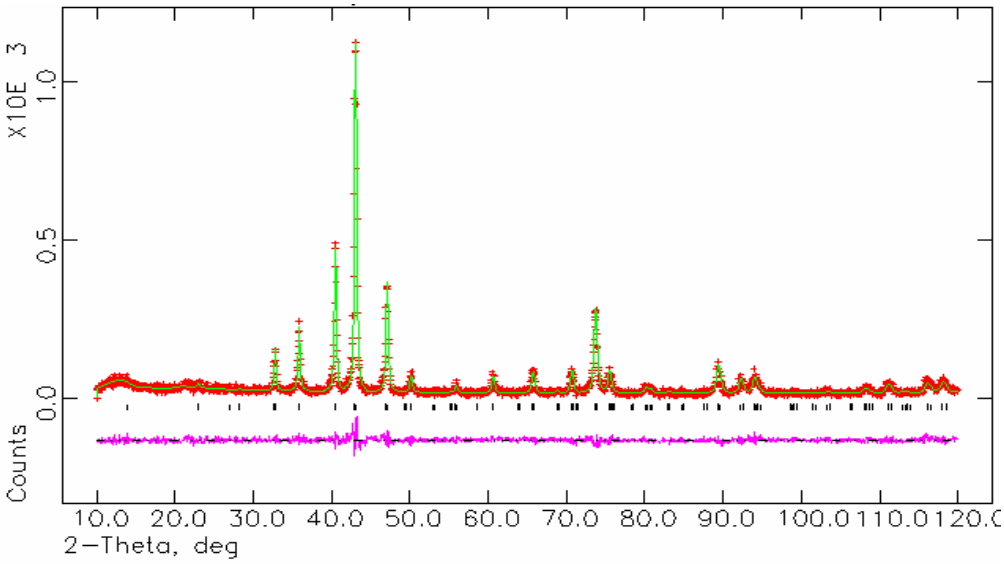

Figure 4.2-6. Profile plot for the refinement of nitrogen deficient cobalt molybdenum nitride sample (N = 1.5(3)) against XRD data. Observed data are signified by crosses, calculated data by the solid line. The difference profile is shown below and tick marks indicate the position of the nitride phase reflections.

Confirmation of the nitrogen deficient cobalt molybdenum nitride sample as the ordered N-deficient η-12 structure or a non-stoichiometric η-6 variant is only likely to be resolved incontrovertibly by neutron diffraction. However it is clear that high temperature treatment of the Co_3Mo_3N under H_2/Ar removes a substantial amount of the lattice nitrogen from the material, and consequently has profound effects on the η- carbide structure of Co_3Mo_3N.

Figure 4.2-7 emphasises the shift in Bragg reflections observed when removing and regenerating the nitrogen content of the cobalt molybdenum nitride samples. Comparison of the XRD patterns shows that the shift in Bragg reflections to higher angles 2θ (indicative of nitrogen loss) is not observed when applying the same temperature profile shown in Figure 4.2-2 under H_2/N_2 throughout the reaction, and the X-ray diffraction pattern agrees with the post reaction XRD of the standard sample Co_3Mo_3N, in which standard ammonia synthesis conditions were employed.

Indexing of the unit cell parameters of Co_3Mo_3N (H_2/N_2, temperature profile to 700°C) gives a = 11.016(2) Å and V = 1336.8(4) Å^3 which are in good agreement with values available in the literature [13] a = 11.0270(4) Å, V = 1340.8(1) Å^3 and the Rietveld refined structure also bears close resemblance to the literature models of Co_3Mo_3N unlike the nitrogen deficient sample shown in Figure 4.2-6.

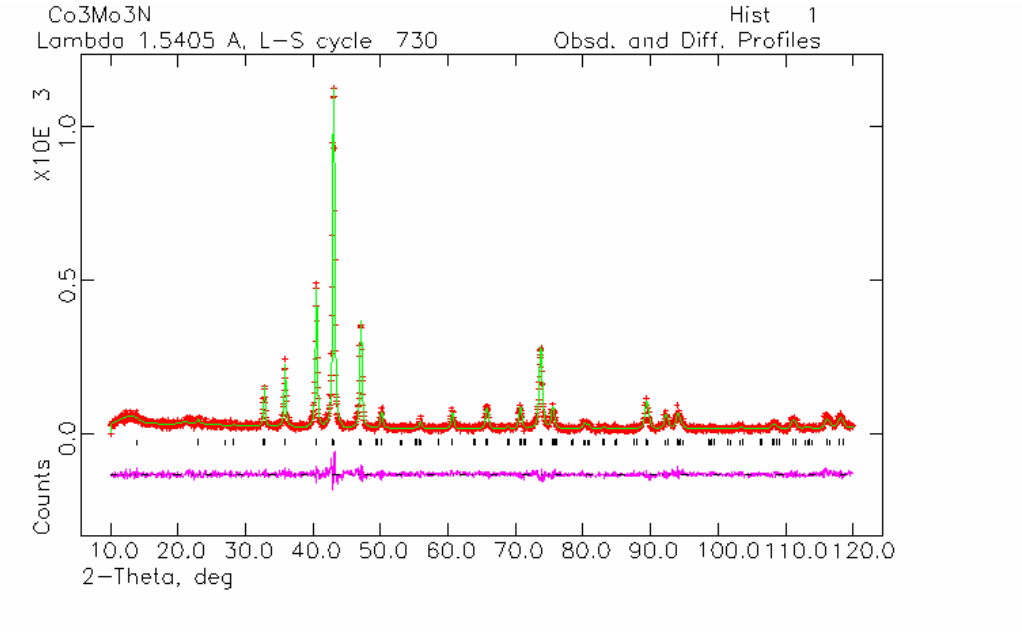

Figure 4.2-7. Profile plot for the refinement of Co_3Mo_3N sample (temperature profile under H_2/N_2 throughout the reaction, N = 2.7(3) wt. %) against XRD data. Observed data are signified by crosses, calculated data by the solid line. The difference profile is shown below and tick marks indicate the position of the nitride phase reflections.

Representations of both η-6 and η-12 structures are shown in Figures 4.2-8 and 4.2-9.

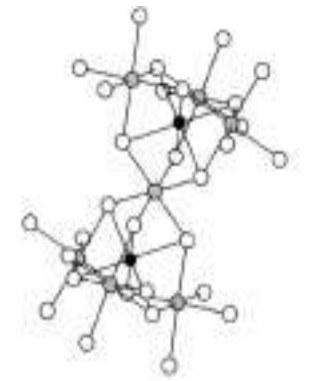

Figure 4.2-8. Interstitial positions of the η-carbide structure can be located on the 16c site (grey) or the 8a site (black). Both sites are octahedrally coordinated by the metal atoms that occupy the 48f site (white). The 32e and 16d site are not displayed for clarity [13].

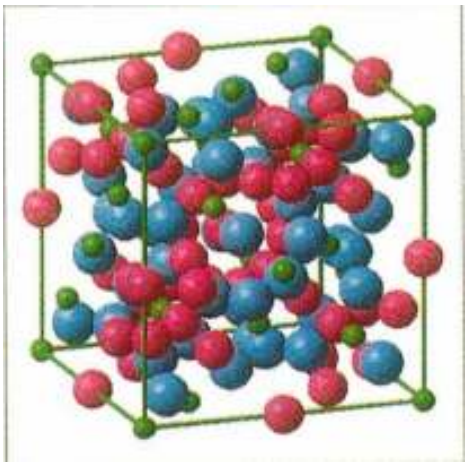

Figure 4.2-9. Representation of the η-6 structure

4.2.5 Reaction Data –Part 2

Following the synthesis of the nitrogen deficient cobalt molybdenum nitride sample, the ammonia synthesis activity of that material could be evaluated by cooling the material to reaction temperature, 400^{o}C, and switching the feed gas from H_2/Ar back to H_2/N_2, and conducting conductivity measurements as normal. The profile shows the steady state ammonia

synthesis activity of the nitrogen deficient sample is comparable with that of Co_3Mo_3N (175 and 167 µmol $h^{-1}g^{-1}$ respectively).

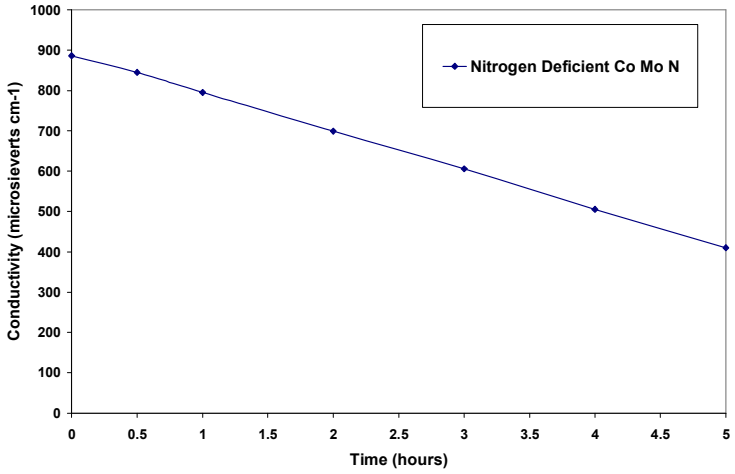

Figure 4.2.10. Reaction profile for ammonia synthesis of the nitrogen deficient cobalt molybdenum nitride, corresponding to 175 µmol $h^{-1}g^{-1}$

From the ammonia synthesis activity data presented here and in section 4.2.1, it is clear that employing H_2/N_2 in the reaction produces ammonia in much greater quantities. It could be suggested (Figure 4.2-11) that the nitrogen in the feed gas replaces the nitrogen which is lost from the material, akin to a re-nitriding step.

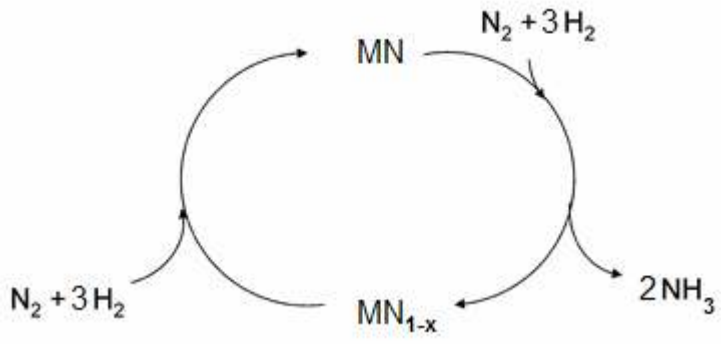

Figure 4.2-11. Cycle showing proposed loss and replenishment of nitrogen in metal nitride materials.

In an effort to regenerate the nitrogen content of the nitrogen deficient sample to restore the Co_3Mo_3N phase, the nitrogen deficient cobalt molybdenum nitride sample was "nitrided" *in-situ* using H_2/N_2, applying the same temperature profile shown in Figure 4.2-2, and dwelling at 700°C for 2 hours. This would therefore demonstrate the ability of cobalt molybdenum nitride to function as a nitrogen transfer catalyst, as described previously.

4.2.6 Post-Reaction Nitrogen Analysis and Lattice Parameters

Attempts were made to restore the nitrogen content of the N-deficient Co_3Mo_3N phase by treatment under H_2/N_2 using temperature profile shown in Figure 4.2-2 and then dwelling at 700°C for a further 2 for hours, and also at 400°C for 5.5 hours. The results of the post-reaction nitrogen analysis, and cubic lattice parameters of the cobalt molybdenum nitride samples studied under the conditions described in section 4.2.3 are presented and compared with the post-reaction nitrogen contents of those "restored" materials.

Sample and testing conditions	Stoichiometric N Content (wt%)	Observed N Content (wt%)	*a*/Å
Co_3Mo_3N (H_2/N_2) after 5.5 h at 400°C	2.93	2.8(3)	11.032(1)
Co_3Mo_3N (H_2/Ar) after 5.5 h at 400°C	2.93	2.5(3)	11.004(8)
Co_3Mo_3N (H_2/Ar) using temperature profile shown in Figure 4.2-2	2.93	1.5(3)	10.879(1)
Co_3Mo_3N (H_2/Ar) using temperature profile shown in Figure 4.2-2, then treated in H_2/N_2 at 700°C	2.93	2.8(3)	11.025(4)
Co_3Mo_3N (H_2/Ar) using temperature profile shown in Figure 4.2-2, then treated in H_2/N_2 at 400°C	2.93	2.0(3)	10.912(4)

Table 4.2-5. Nitrogen content and unit cell parameters of Co_3Mo_3N samples after reactions in H_2/N_2, H_2/Ar

The conditions used to probe the ammonia synthesis activity of the nitrogen deficient sample (H_2/N_2 400^{o}C) were initially applied to determine if these conditions were sufficient to regenerate the nitrogen content of the sample. The post-reaction nitrogen analysis of sample is slightly higher than that of the initial sample (N = 2.0(3) wt. % and N = 1.5(3) wt. %, respectively), and there is a small increase in the unit cell parameters presented in Table 4.2-5.

In order for cobalt molybdenum nitride to truly function as a nitrogen transfer agent, it must also be possible to replenish the depleted lattice nitrogen. The nitrogen content of the nitrogen deficient sample can be restored by applying the same heating rate applied to achieve the nitrogen deficient sample, but instead employing H_2/N_2 (Co_3Mo_3N N wt.% calculated = 2.93, observed = 2.8(3)), and the unit cell parameters are in good agreement with those calculated for standard Co_3Mo_3N (H_2/N_2, 400^{o}C). Hence the process of nitrogen loss / replenishment is fully reversible and the cobalt molybdenum nitride catalyst can be readily regenerated at elevated temperature.

4.2.7 XRD Patterns

The post-reaction XRD patterns of cobalt molybdenum nitride samples studied under those conditions described in section 4.2.5 are presented and compared with selected Co_3Mo_3N samples from section 4.2.1.

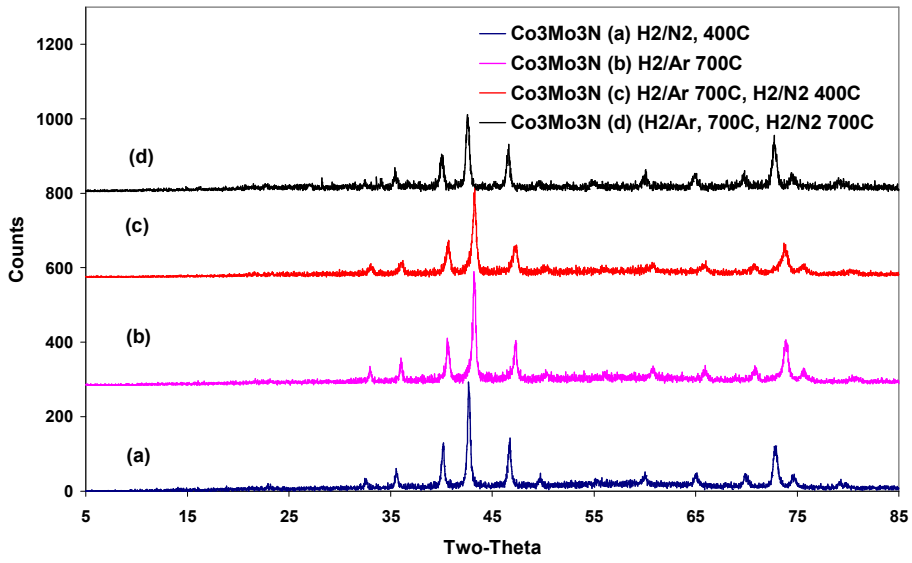

Figure 4.2-12. Post-reaction XRD of cobalt molybdenum nitride (a) 2.8(3) (b) 1.5(3) (c) 2.0(3) and (d) 2.8(3) wt% nitrogen content.

Comparing the XRD patterns presented in Figure 4.2-12 for the cobalt molybdenum nitride sample which has had nitrogen removed and subsequently replaced by switching back to H_2/N_2 and raising the temperature to 700°C (d), and the post-ammonia synthesis reaction of the nitrogen deficient material (H_2/N_2, 400°C (c)), with that of the nitrogen deficient sample (H_2/Ar, temperature profile to 700°C (b)), the shifted Bragg reflections observed in the nitrogen deficient have shifted back to lower angles 2θ in the case of sample which had nitrogen content fully restored and the pattern matches well with the patterns observed for standard Co_3Mo_3N (H_2/N_2, 400°C (a)). The Bragg reflections of the post-reaction XRD of the ammonia synthesis of the nitrogen deficient sample, (c), do not shift back to lower angles, and the pattern is still a good match with sample the original nitrogen deficient sample (b), although the nitrogen content has increased slightly.

Indexing the XRD pattern of regenerated Co_3Mo_3N sample shows that the lattice parameters are in good agreement with Co_3Mo_3N after standard ammonia synthesis (a) (sample (a), a = 11.032(1) Å, sample (d) a = 11.025(4) Å). These lattice parameters are significantly greater

than those observed for the nitrogen deficient samples shown in Table 4.2-5, suggesting that the nitrogen lost, has been replenished.

4.3 Results and Discussion: Fe_3Mo_3N, Ni_2Mo_3N, and γ-, β-, and δ-Molybdenum Nitride Lattice Nitrogen Reactivity

The results presented in section 4.2 exhibiting the reactivity of lattice nitrogen within Co_3Mo_3N, and the possibility of synthesising new materials, has been extended to include other binary and ternary bulk phase nitrides.

The reactions were carried out in exactly the same way as those conducted in section 4.2, the catalysts were subject to the standard pre-treatment at 700°C under H_2/N_2 for 2 hours before cooling to 400°C and switching to H_2/Ar and applying the temperature profile seen in Figure 4.2-2.

4.3.1 Reaction Data

The conductivity versus time plots for the reaction of ternary nitrides in H_2/Ar at a maximum temperature of 700°C are shown in Figure 4.3-1 (a)-(b).

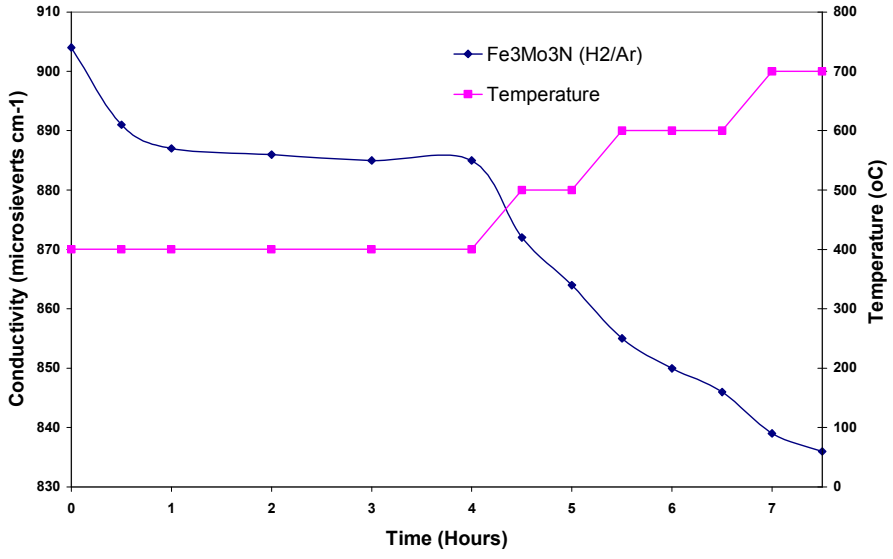

Figure 4.3-1 (a) Conductivity data for NH_3 synthesis over Fe_3Mo_3N with increasing temperature.

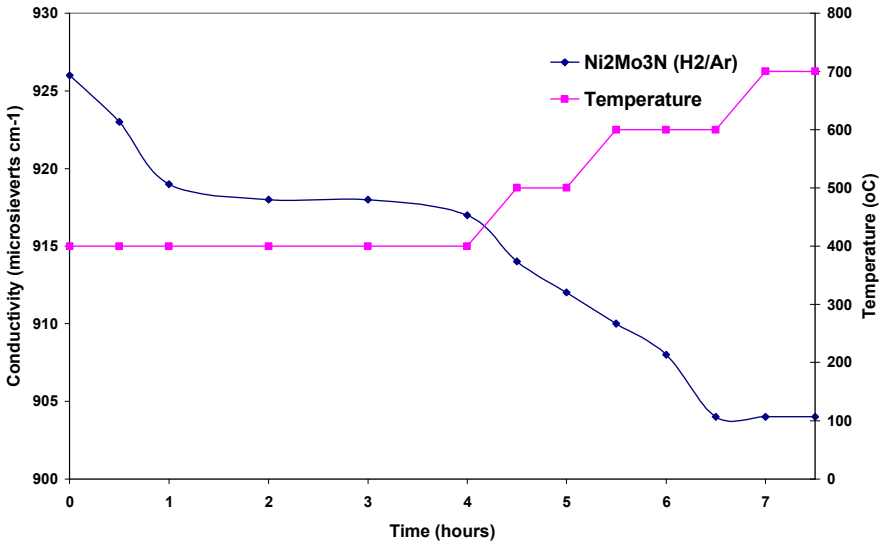

Figure 4.3-1 (b) Conductivity data for NH_3 synthesis over Ni_2Mo_3N with increasing temperature.

The conductivity plots provide information on the temperature dependence of ammonia formation via hydrogenation of the lattice nitrogen within the nitride materials. Considering first the ternary nitride catalysts, it can be seen from figures (a) and (b), Fe_3Mo_3N and Ni_2Mo_3N respectively, that these ternary nitrides exhibit behaviour analogous to that of the Co_3Mo_3N sample under the same conditions. There is an initial burst of ammonia which is attributable to an initial stabilisation period and after 4 hours on stream the reaction has reached steady state conditions and no further ammonia is produced. By increasing the temperature in 100^oC increments to a final temperature of 700^oC, more ammonia is produced from the reaction. The ammonia synthesis rates of the ternary nitride catalysts under H_2/Ar using the previously outlined temperature profile, including Co_3Mo_3N, are presented in Table 4.3-1.

Reaction Temperature/ Time	Co_3Mo_3N NH_3 Synthesis Rate ($\mu mol\ h^{-1}\ g^{-1}$)	Fe_3Mo_3N NH_3 Synthesis Rate ($\mu mol\ h^{-1}\ g^{-1}$)	Ni_2Mo_3N NH_3 Synthesis Rate ($\mu mol\ h^{-1}\ g^{-1}$)
400°C (0 - 0.5 hr)	98	47	11
400°C (1 – 3.5 hr)	12	1	1
500°C (4 –5 hr)	0	38	9
600°C (5 – 6 hr)	16	27	7
700°C (6.5 – 7.5 hr)	12	18	0

Table 4.3-1. Ammonia Synthesis Rates ternary nitride catalysts under H_2/Ar between 400-700°C.

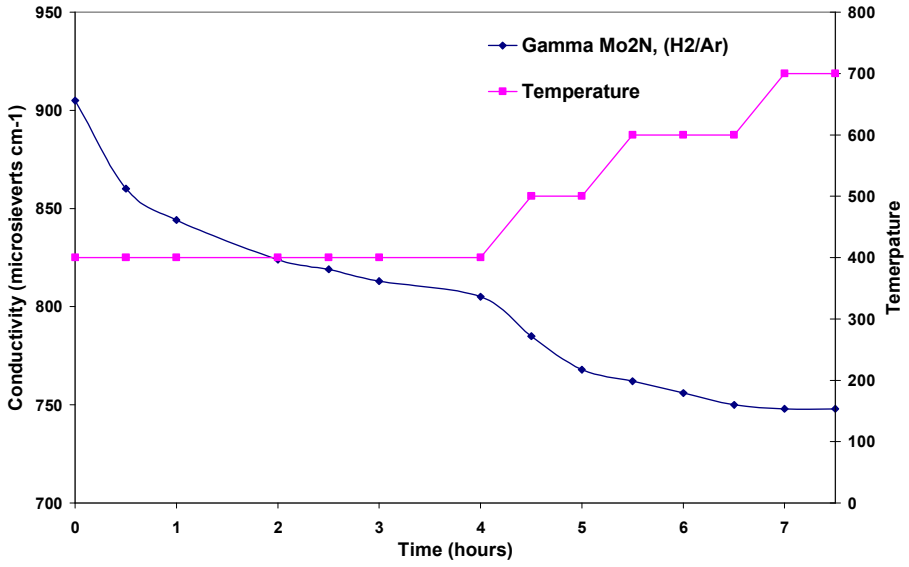

Figure 4.3-1 (c) Conductivity data for NH_3 synthesis over γ-Mo_2N with increasing temperature.

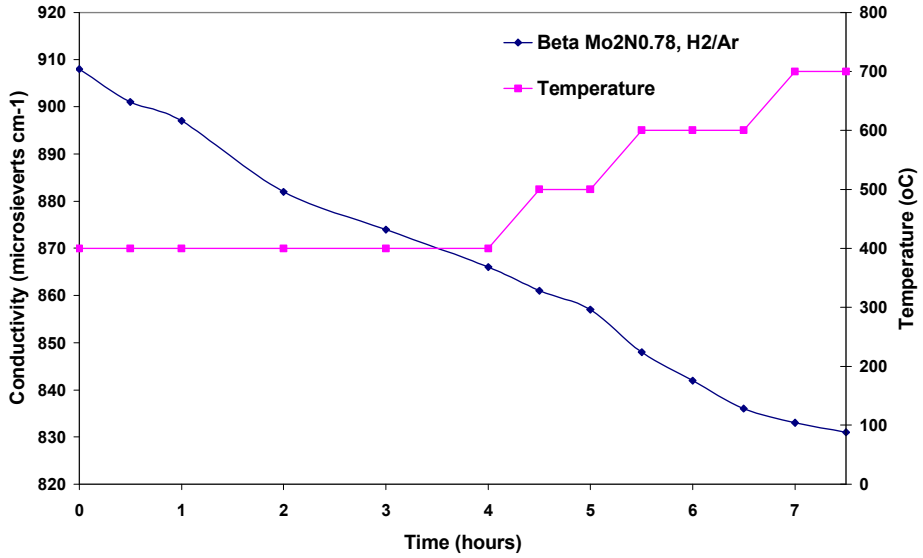

Figure 4.3-1 (d) Conductivity data for NH_3 synthesis over β-$Mo_2N_{0.78}$ with increasing temperature

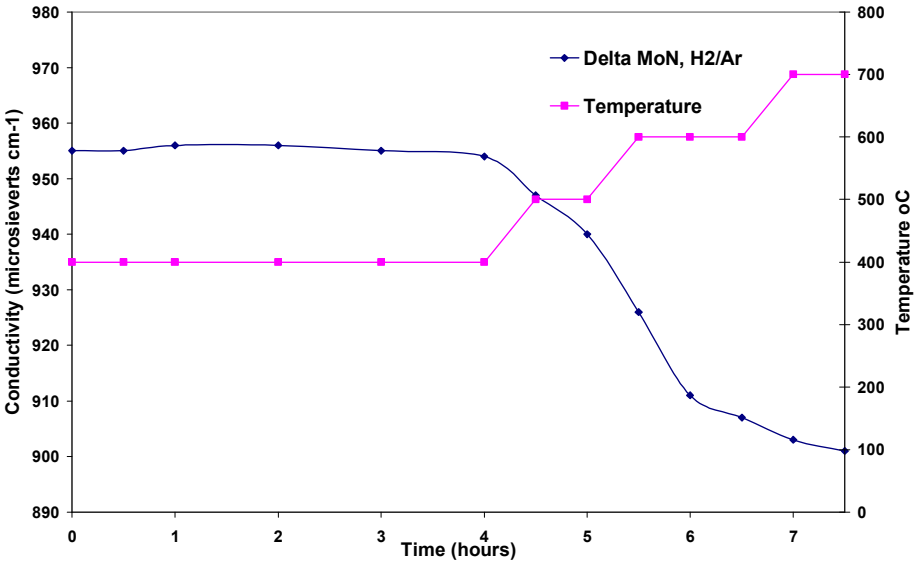

Figure 4.3-1 (e) Conductivity data for NH_3 synthesis over δ-MoN with increasing temperature.

The ammonia synthesis activity of the binary molybdenum nitride phases at temperatures between 400-700^{o}C under H_2/Ar are shown in Table 4.3-2.

Reaction Temperature/ Time	γ-Mo_2N	β-$Mo_2N_{0.78}$	δ-MoN
400°C (0 - 0.5 hr)	164	25	0
400°C (1 – 3.5 hr)	23	18	0
500°C (4 –5 hr)	67	16	25
600°C (5 – 6 hr)	22	27	53
700°C (6.5 – 7.5 hr)	3	9	11

Table 4.3-2. Ammonia Synthesis Rates ternary nitride catalysts under H_2/Ar between 400-700°C.

In Figure 4.3-1 (c) the γ-Mo_2N catalyst also exhibits similar behaviour; the rate of ammonia production slows down gradually after 4 hours on stream at 400°C, increasing the temperature increases the rate briefly, before it begins to slowly decrease again. However, in Figure 4.3-1 (d) the β-$Mo_2N_{0.78}$ sample slowly eliminates low levels of NH_3 over the entire temperature range investigated, whereas δ-MoN (e) only eliminates NH_3 at temperatures above 400°C. The diminution of NH_3 sometimes observed with increasing temperature can be indicative of the depletion of a finite pool of reactive nitrogen species, which are not replenished in the absence of a source of gas-phase nitrogen, or the increasing favourability of ammonia decomposition with temperature.

4.3-2 Post-Reaction Nitrogen Analysis

The post-reaction nitrogen contents of the binary and ternary nitride catalysts tested in section 4.2-1 are included in Table 4.3-1. Also included in the table, are calculated nitrogen contents based upon the stoichiometry of the various materials. It is apparent that significant deviations in post 400°C H_2/N_2 reactions from those expected on the basis of stoichiometry are apparent. It is probable that the origin of such deviations is the presence of sorbed NH_x species in those materials exhibiting greater quantities of nitrogen and surface oxidation on subsequent exposure to air for those with lower contents. It is again apparent, that despite the low levels of nitrogen loss as ammonia in the Ar/H_2 reduction sequences, as detailed in Table 4.3-1, substantial amount of lattice nitrogen is removed from the materials.

Sample	Stoichiometric nitrogen content (wt%)	Post H_2/N_2, 400°C reaction nitrogen (wt%)	Post H_2/Ar 700°C reaction nitrogen (wt%)	% of N lost attributed to NH_3
Fe_3Mo_3N	2.98	3.52(3)	1.97(3)	22.03
Ni_2Mo_3N	4.33	2.57(3)	2.33(3)	34.15
γ-Mo_2N	6.80	5.78(3)	2.93(3)	19.94
β-$Mo_2N_{0.78}$	5.39	5.71(3)	0	6.78
δ-MoN	12.74	13.33(3)	5.68(3)	3.16

Table 4.3-1. Nitrogen content of various nitrides following H_2/N_2 reaction at 400C and temperature programmed reaction with H_2/Ar at 700°C using the regimes shown in 4.3-1.

4.3-3 Post-Reaction XRD

The post-reaction X-ray diffraction patterns of the binary and ternary nitride samples are presented in Figure 4.3-2. The XRD data for the post reaction binary and ternary nitrides treated in N_2/H_2 at 400°C has already been shown in Chapter 3 but is included in the figures for ease of comparison. In Figure 4.3-2 comparison of the XRD patterns of pure phase Fe_3Mo_3N with the Fe_3Mo_3N sample treated in H_2/Ar at 700°C are similar in that the original phase is partly retained, with essentially no change in lattice parameter. However, there are additional reflections in the powder diffraction pattern at c.a. 40.6 and 74.1° 2θ which become apparent after reaction – in both cases these additional reflections correspond to the presence of Mo metal, due to the decomposition and partial reduction of the Fe_3Mo_3N structure.

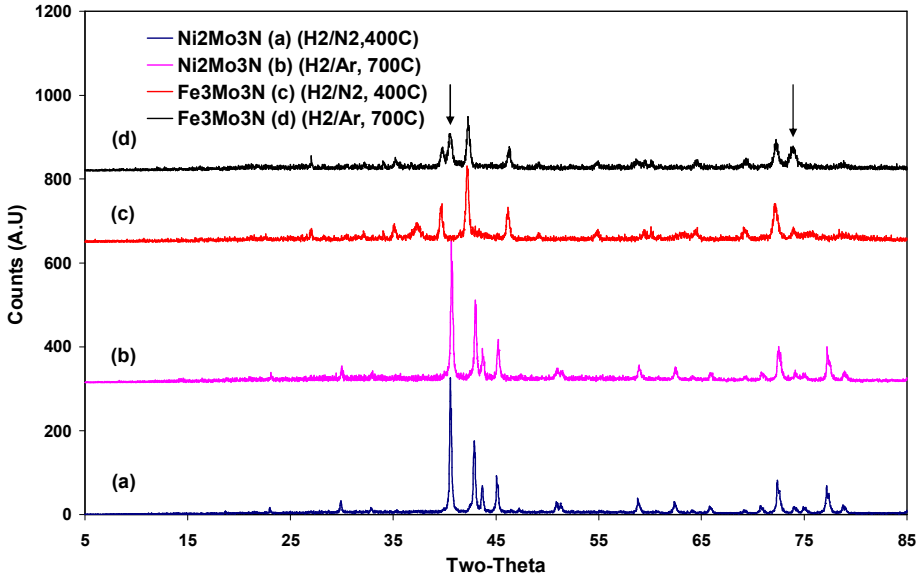

Figure 4.3-2. Post reaction XRD patterns of binary and ternary nitride samples

The behaviour of Ni_2Mo_3N upon nitrogen loss is more similar to, but much less pronounced than, Co_3Mo_3N, in that a shift of lattice parameter is observed, indicating the general maintenance of the phase but elimination of structural nitrogen (Figure 4.2-12)

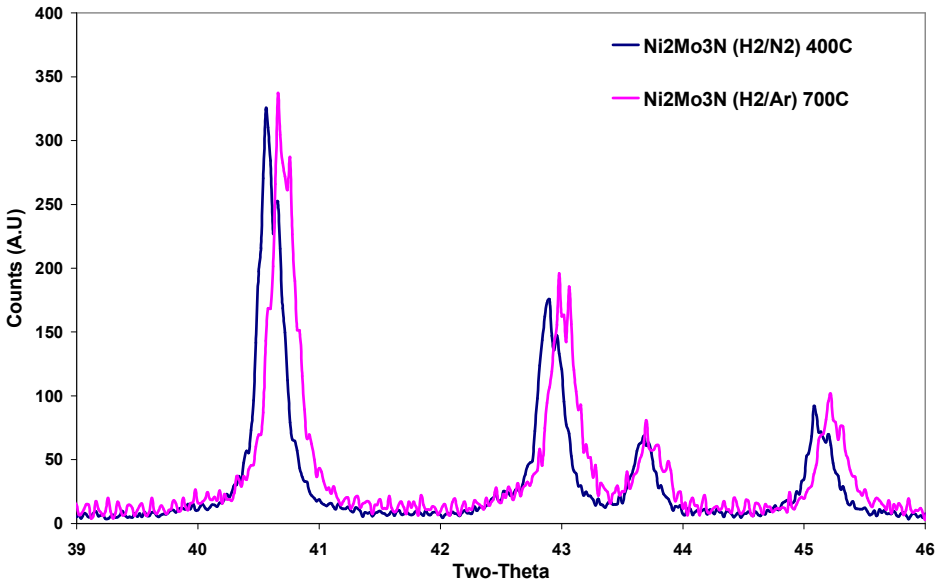

Figure 4.3-3. Post reaction XRD patterns of Ni_2Mo_3N after H_2/N_2 at 400°C and H2/Ar at 700°C.

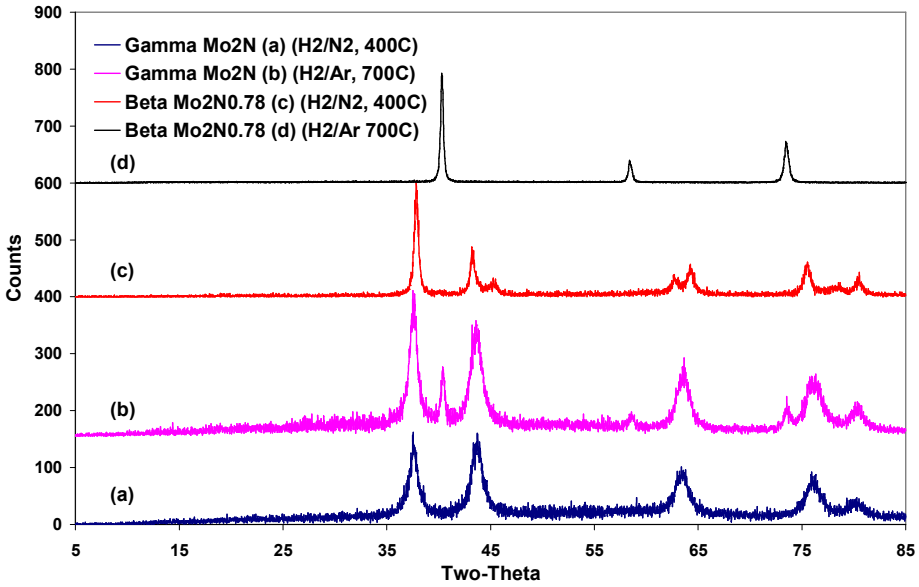

Figure 4.3-4. Post-reaction XRD patterns of molybdenum nitride samples under various conditions.

In the case of the γ-Mo_2N sample treated in H_2/Ar it is clear that the phase of the material has not dramatically changed. There are also similarities with the Fe_3Mo_3N sample as there are additional reflections that can be attributed to the partial reduction of the γ-Mo_2N to Mo metal. This general type of behaviour in that part of the sample is totally reduced whereas the remainder apparently has not reduced at all is intriguing. It is interesting to note there was no evidence the β- phase as an intermediate in the decomposition of γ-Mo_2N (Mo metal possesses a body centred unit cell as does β-$Mo_2N_{0.78}$). In all cases, the quantity of hydrogen passed over the nitride samples whilst they are held at 700°C, the highest temperature employed, is in large excess of that required to totally reduce the samples. Therefore, whilst only a fraction of the crystallites are reduced, it would appear that once reduction is initiated within a crystal it rapidly propagates throughout the crystallite resulting in total elimination of nitrogen from the structure, whilst reduction is not initiated in other crystallites. It is interesting to note that, in the case of γ-Mo_2N the resultant Mo metal formed has a comparatively narrow reflection width, which may indicate that it is derived from the larger crystals. However, inspection of the comparative widths of the Mo metal in the Fe_3Mo_3N (Figure 4.3-2) shows that this cannot be a general phenomenon. In comparison, the reaction of δ-MoN, which possesses the NiAs structure type and can therefore be described in terms of hexagonal close packing of Mo

atoms, at 700°C under H_2/Ar does not fully/ partially reduce to Mo metal as observed in the other molybdenum nitride phases. Instead over half of the structural nitrogen content of the material is lost (from nitrogen analysis Table 4.3-1) and the material transforms into the face centred cubic based γ-Mo_2N polymorph (Figure 4.3-5).

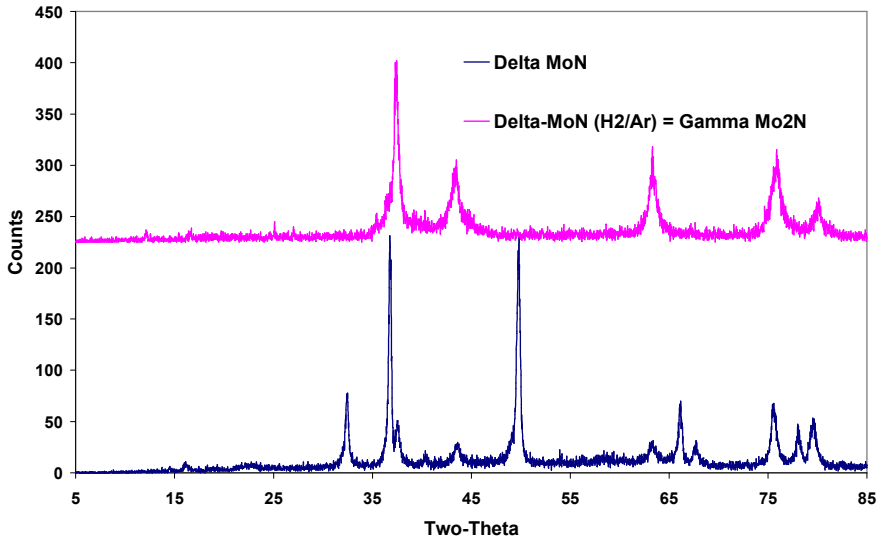

Figure 4.3-5. Post-reaction XRD showing transformation of δ-MoN to γ-Mo_2N under H_2/Ar at 700°C.

Experiments were conducted analogous to those which restored the nitrogen content in the nitrogen deficient Co_3Mo_3N/ Co_6Mo_6N sample, but applied to Mo metal. In initial studies attempting to reduce γ-Mo_2N to β-$Mo_2N_{0.78}$ it was found that heating the γ-Mo_2N in H_2/Ar at 700°C for 5 hours was sufficient to completely reduce the material to the Mo metal, removing all nitrogen. The experiment was carried out after 5 hours reduction in H_2/Ar, the temperature was held at 400°C, and the feed gas was switched to H_2/N_2 and held for 5.5 hours, the experiment was also repeated 700°C under H_2/N_2. The post-reaction XRD shown in Figure 4.3-6 shows partial nitridation of the Mo metal in H_2/N_2 at 400°C, with characteristic reflections of γ-Mo_2N occurring at 47.5, 43.9, 63.6 and 76.3° 2θ, however there is still a significant Mo presence ca. 41° 2θ . The reaction of Mo metal in H_2/N_2 at 700°C, shows a complete transformation to γ-Mo_2N. The presence of nitrogen was confirmed by combustion analysis, for the reaction at 400°C (N = 2.18(3) wt. %) and 700°C (N = 5.88(3) wt. %).

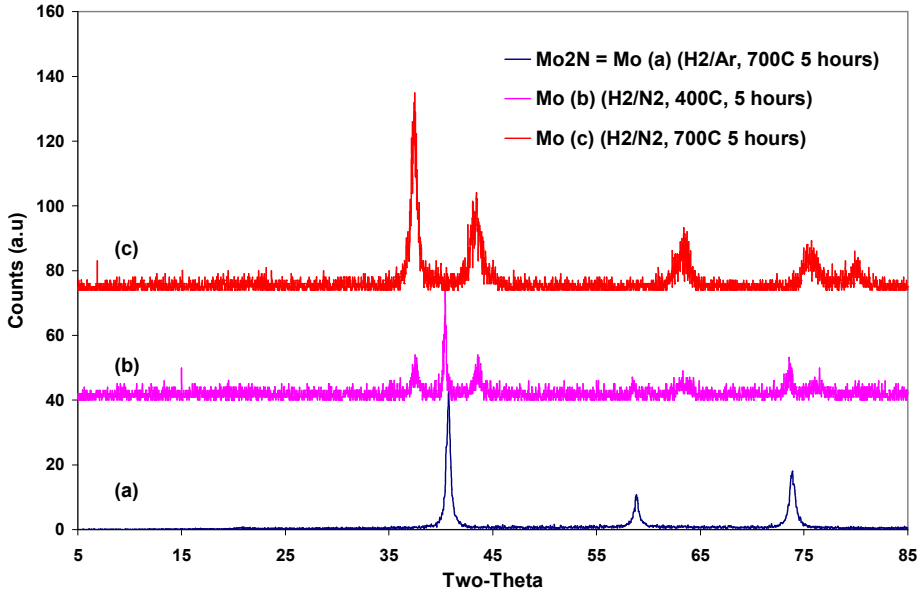

Figure 4.3-6. Post-reaction XRD data showing the regeneration of γ-Mo_2N from Mo metal.

4.4 Conclusions

In this chapter, the reactivity of lattice nitrogen present in binary and ternary bulk nitride materials was investigated using a series of gas switching experiments. It is clear from the data presented that nitrogen can be removed from these materials at high temperatures under hydrogen. It is interesting to note that using a specific temperature profile only β-$Mo_2N_{0.78}$ fully decomposed to the pure metal, all other post reaction materials retained nitrogen and XRD showed a mixture of constituent metal and nitrided species.

At present, the origins of the differences in the types of decomposition pathway, and their determining influences, are not clear. However the loss of nitrogen, and hence its potential for reaction, is evident. Despite the vast excess of hydrogen in the gas-phase, in all cases the predominant form of lost nitrogen is as N_2. This is believed to be a consequence of the favourable thermodynamics of ammonia decomposition at the higher reaction temperatures employed.

It has been shown that, in the case of nitrogen deficient cobalt molybdenum nitride and Mo metal, the nitrogen can be restored to the nitrogen deficient materials and regenerate the Co_3Mo_3N/ γ-Mo_2N phases in a series of H_2/Ar and H_2/N_2 switching experiments.

These experiments confirmed the function of cobalt molybdenum nitride as a nitrogen transfer catalyst. It is proposed that the evidence suggests that loss and subsequent regain of lattice nitrogen in the system reversibly cycles through the previously unknown nitride, Co_6Mo_6N, shown in Figure 4.4-1

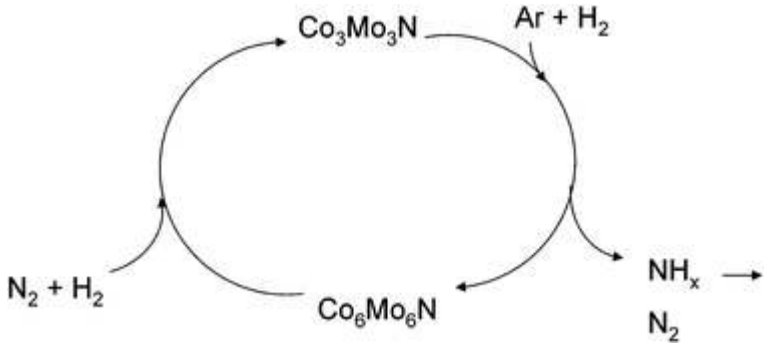

Figure 4.4-1. Cycle exhibited the loss and replenishment of lattice nitrogen in Co_3Mo_3N via Co_6Mo_6N, by H_2/Ar and H_2/N_2 switching experiments

5. Reactions of Benzene and Hydrogen over Bimetallic nitride Catalysts

5.1 General Introduction

Nitrogen is an essential element to all life as it is significant biologically as a constituent to both proteins and nucleotides. It is also the most abundant uncombined element available to man, as it comprises of around 79% of the earths atmosphere [1]. Nitrogen fixation – the process where dinitrogen gas is converted into more usable forms –occurs naturally, for example nitrogenases fix nitrogen into ammonium compounds, which can be utilised in biological systems for the production of amino acids or nucleic acids.

Nitrogen is not just important in a biological sense but also on an industrial level. Nitrogen is a major constituent of many high tonnage industrially produced products such as acrylamides (used in the polymer industry) and also to make ammonium nitrate, which is used to make fertiliser. Nitrogen fixation, which was previously mentioned as a process that occurs naturally in biological systems is also used for the production of ammonia. The Haber Bosch process is usually employed for the production of ammonia on an industrial scale [2]. In this process, the nitrogen is fixed using high pressure and medium temperature (350 bar and 450^{o}C respectively) with hydrogen over an promoted iron surface [2]. The Haber Bosch process has been in operation on an industrial scale for more than 80 years, although there have been steps forward in terms of the mechanistic understanding, there have only been minor improvements made to the process. However, BP Kellogg have recently developed a competing process, replacing the currently used iron catalyst with a more active Ru/C based formulation which saw the need for the harsh operating conditions of the Haber Bosch process resolved [3]. Bulk and supported transition metal nitrides have also been shown to be active ammonia synthesis catalysts (Chapter 3), and the possibility of lattice nitrogen reactivity in these materials has also studied (Chapter 4).

A great deal of the ammonia produced from the Haber Bosch process is used in large scale the preparation of nitrogen containing organic molecules. Preparation of such molecules can either

be by direct use of ammonia as a reactant, or indirectly where it is initially converted into another nitrogen containing precursor molecule. A good example of a process which can employ these two different routes is the large scale route to amines. Small aliphatic amines are generally manufactured by a process which employs ammonia directly, e.g. the direct amination of methanol to produce methylamines which are produced by the acid catalysed reaction of ammonia and methanol [4]:

$$CH_3OH + NH_3 \longrightarrow CH_3NH_2 + H_2O$$

Aromatic amines are, however, often produced by the hydrogenation of nitrogen precursors. For example, aniline is prepared by the catalytic reduction of nitrobenzene [5].

$$C_6H_5NO_2 + 3H_2 \longrightarrow C_6H_5NH_2 + 2H_2O$$

In the above process, the nitrobenzene is generally produced by nitration of benzene using a nitric acid- sulfuric acid mixture. The nitric acid employed is produced via a process involving ammonia oxidation at high temperatures. Nitrogen incorporation thus involves the production of amines via indirect processes involving a number of intermediate nitrogen inter-conversion stages, involving an acid intensive stage. The process can be described in the reaction scheme shown below.

$N_2 + 3H_2 \longleftrightarrow$	$2NH_3$	Ammonia Synthesis
$NH_3 + 2O_2 \longrightarrow$	$HNO_3 + H_2O$	Ammonia Oxidation
$2H_2SO_4 + HNO_3 \longrightarrow$	$NO_2^+ + H_3O^+ 2HSO_4^-$	Formation of Nitration Mixture
$C_6H_6 + NO_2^+ \longrightarrow$	$C_6H_5NO_2 + H^+$	Nitration
$C_6H_5NO_2 + 3H_2 \longrightarrow$	$C_6H_5NH_2 + H_2O$	Selective hydrogenation

When the scheme is studied, it is clear that a direct route to produce aniline, where the ammonia is reacted directly with the substrate, would be preferable [5-7]. A potential direct route is shown overleaf:

$$C_6H_6 + NH_3 \longrightarrow C_6H_5NH_2 + H_2$$

This potential route to aniline has an advantage over the traditionally used method as it avoids the use of acids on an industrial scale in the nitration step. However, the reaction has major disadvantages due to the co-production of hydrogen. This could be overcome by removing hydrogen via a reaction with gas phase O_2, although this would seriously affect the selectivity of the reaction. Due to these limitations - to the author's knowledge – there is no direct amination process for the synthesis of aniline, although a combinatorial approach conducted by Desrosiers *et al*. using cataloreactants has shown that selectivity to aniline is very high when using NiO and Co_3O_4 based sacrificial reagents [17].

5.2 The Proposed Route to Direct Aniline Synthesis

An alternative potential route to aniline that was investigated is shown below.

$$C_6H_6 + N(a) + 0.5H_2 \longrightarrow C_6H_5NH_2$$

N(a)= lattice or adsorbed nitrogen species

In this method the thermodynamic limitations would, potentially, be overcome as hydrogen is a reactant, rather than a product of the reaction.

This route shows the hydrogenation and direct insertion of the nitrogen species. Despite studies by Aika, Kojima and Jacobsen [8-10] demonstrating the high activity of some metal nitride catalyst for ammonia synthesis, there has been no previous study of the possibility of nitrogen insertion processes with nitrogen species as a reactant using metal nitrides. Other reactions can be envisaged including the e.g. the generation of HCN:

$$6Co_3Mo_3N + C_6H_6 \longrightarrow 6CoMo + 6HCN$$

The ammonia synthesis activity and lattice nitride reactivity of binary and ternary nitrides has been discussed in Chapters 3 and 4. Ternary nitrides are the most active ammonia synthesis

catalysts, Co_3Mo_3N in particular has demonstrated the ability to act as a possible nitrogen transfer source. The work of Green and co-workers has suggested the possibility of a Mars-van Krevelen reaction with transition metal carbides [11] (which have been shown to have analogous chemistry to nitrides) [12]. The materials tested in this chapter were the more active ternary nitride catalysts.

The aim of the work carried out in this chapter was to conduct preliminary investigations into the possibility of applying routes involving the direct activation of nitrogen to the synthesis of industrial products, this would reduce make the production of aniline, in particular, and is much more environmentally friendly as there are fewer steps involved in the synthesis (see aniline synthesis scheme) [1]. Once in the nitrided state, if direct nitrogen activation and incorporation of pathways become possible, there could be a reduction in the requirement for the use of ammonia, or its inter-conversion to derivatives, as reactants [1].

5.3 Reaction Data

The reactions of benzene and hydrogen over bimetallic nitride catalysts were conducted according to the procedure documented in the catalyst testing section in Chapter 2 (temperature raised from 400^{o}C to 700^{o}C). All products were condensed using an ice bath at the exit stream of the reactor, and analysed by GC-MS. The concentration of benzene flowed over the catalyst can be estimated using the Clausius-Clapeyron equation, and found to be 12% by volume.

5.3-1 GC-MS Data

Samples were dissolved in methanol in a 1:10 ratio to protect the filament inside the mass spectrometer. In all samples, only one peak at *ca.* 2.7 minutes was observed in the gas chromatograms, an example is shown overleaf in Figure 5.3-1. The expanded gas chromatograms and mass spectrometry analysis of all samples are also given in Figure 5.3-2 to 5.3-4.

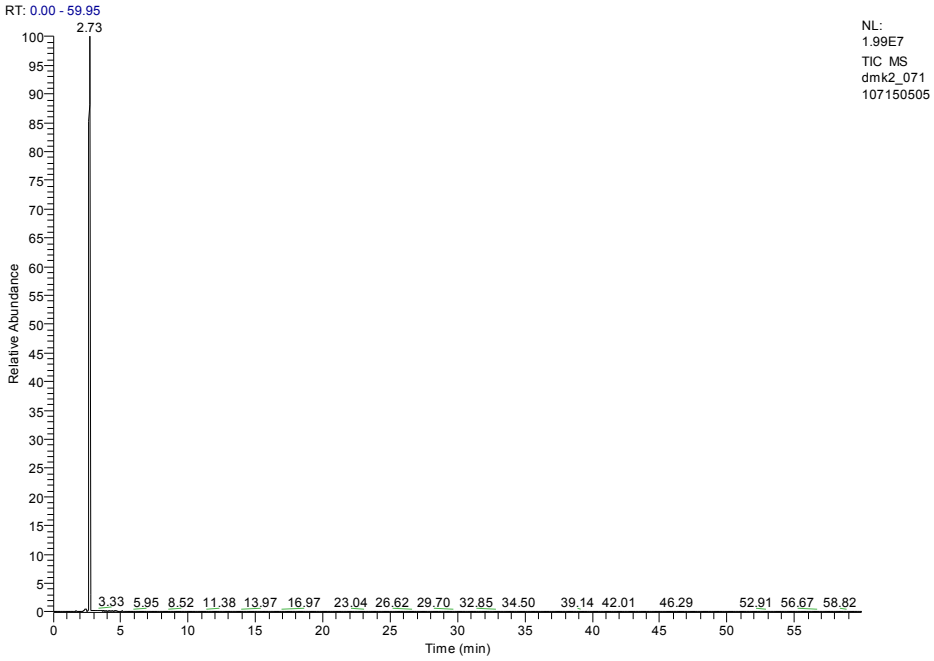

Figure 5.3-1. GCMS data showing single peak in chromatogram

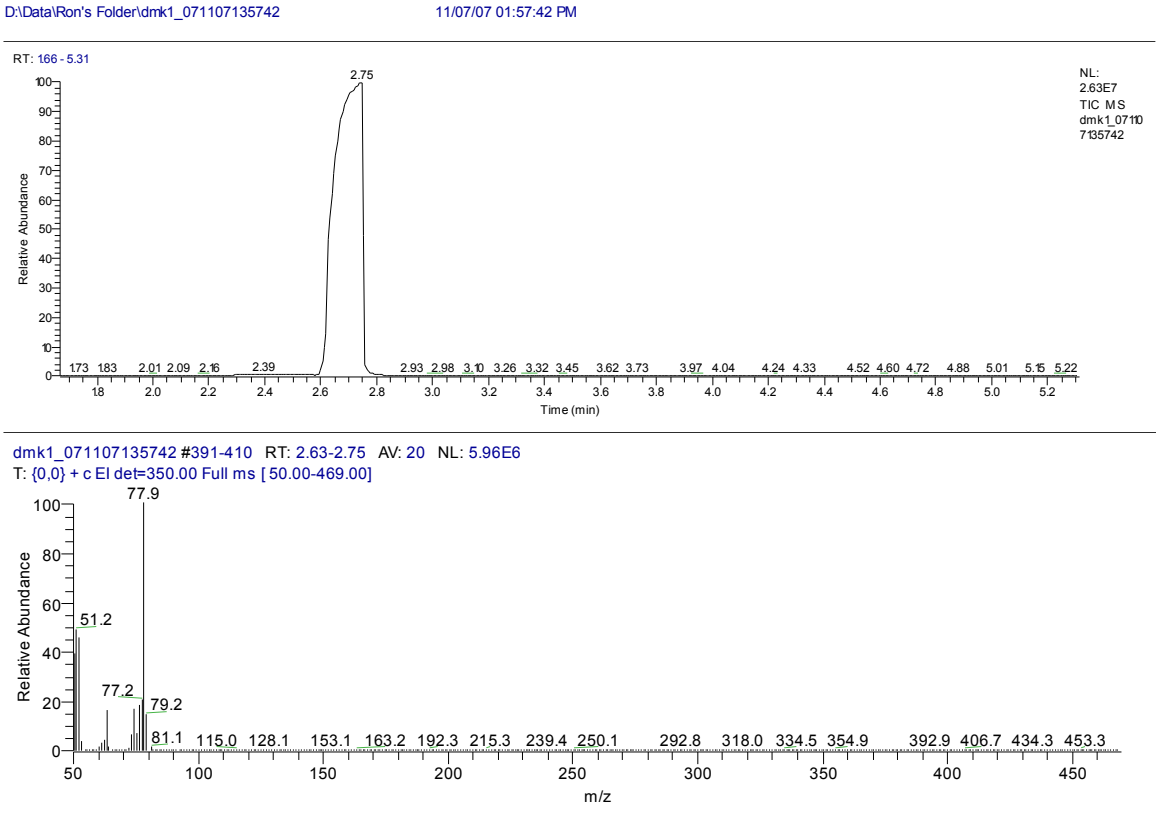

Figure 5.3-2. GC-MS data for reaction of benzene and H_2/N_2 over Co_3Mo_3N

In Figure 5.3-2, the peak in the gas chromatogram can be seen at 2.75 minutes, by highlighting this peak and analysing the mass spectrum for the peak, it is clear that dominant mass is 77.9 a.m.u which matches well with benzene (C_6H_6, 78 a.m.u) being the only component of the reactor exit condensate detected.

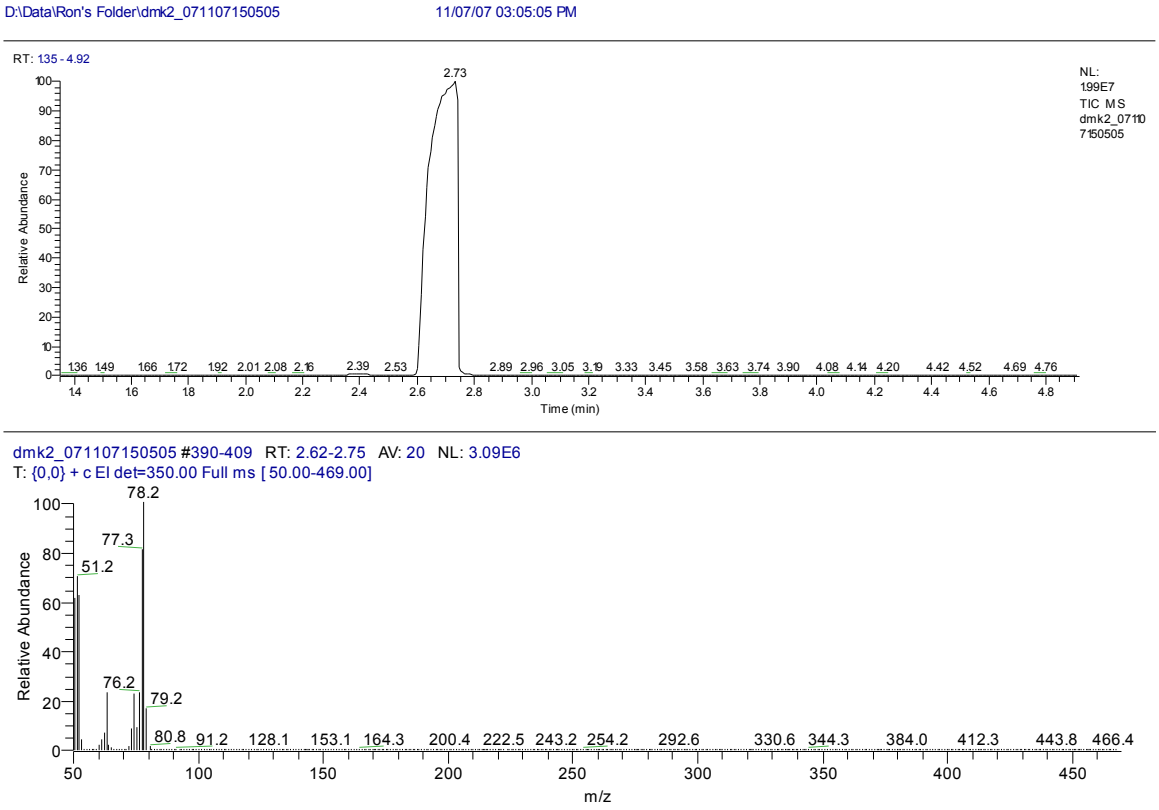

Figure 5.3-3. GC-MS data for reaction of benzene and H_2/N_2 over Fe_3Mo_3N

Post-reaction analysis of the liquid sample from the reaction of Fe_3Mo_3N again shows only a single peak in the gas chromatograph at 2.73 minutes and analysis of the mass spec data for the peak 78.2 a.m.u again agrees well with benzene, with no other significant products detected.

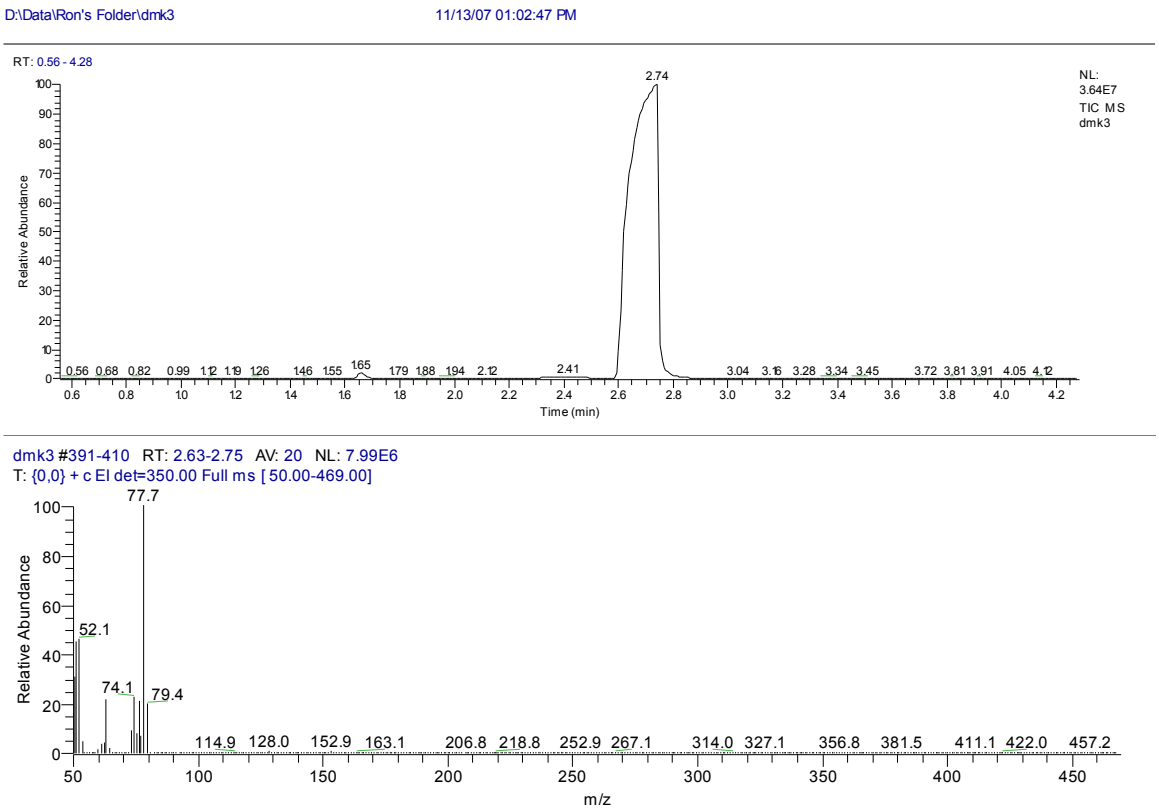

Figure 5.3-4. GC-MS data for reaction of benzene and H_2/N_2 over Ni_3Mo_3N

The Ni_2Mo_3N sample was similar to its iron and cobalt molybdenum nitride counterparts, only one peak was observed in the chromatogram at 2.74 minutes, mass spec data (77.7 a.m.u) showed that this peak could, again, be attributed to benzene (78 a.m.u)

5.3-2 Post-Reaction XRD Data

The post-reaction XRD patterns of the ternary nitrides are shown in Figure 5.3-5 to 5.3-7, the XRD patterns of these catalysts after a standard ammonia sythesis reaction are also included for comparison. In the case of Co_3Mo_3N and Fe_3Mo_3N, the XRD patterns of samples treated in H_2/N_2 + benzene using the temperature profile shown in Figure 4.2-2 have their reflections shifted to slightly lower angles $2\theta^o$. In the Co_3Mo_3N sample (Figure 5.3-5), in particular, this shift from 42.7^o to 42.4^o is exactly the shift reported by Bussell and co-workers [13] for the formation of Co_3Mo_3C from Co_3Mo_3N using mixtures of methane and hydrogen. There is also

an additional reflection in the XRD pattern at 26° (indicated with an arrow), this has been attributed to the formation of graphite, other arrows in Figure 5.3-1 indicate the positions of other graphite reflections, which may be masked by the dominant CoMo phase. The broad graphite reflection at 26° possibly indicates that the graphite present in the sample is very disordered or that there are very few layers of the material. Taking the interlayer spacing of graphite as 3.35Å , the number of layers present can be estimated by the Scherrer calculation, the crystallite size of the graphite reflection was calculated to be 219Å, therefore is 65 layers of graphite, suggesting the graphite is very disordered. Evidence of the reflection at 26° can also be seen in a paper by Wang and co-workers on the formation of Co_3Mo_3C [14], although no reference was made to its introduction to the Co_3Mo_3C phase. Tsuchida has also noted this additional reflection in the formation of Fe_3Mo_3C and attributed the reflection to a (002) carbon reflection [15].

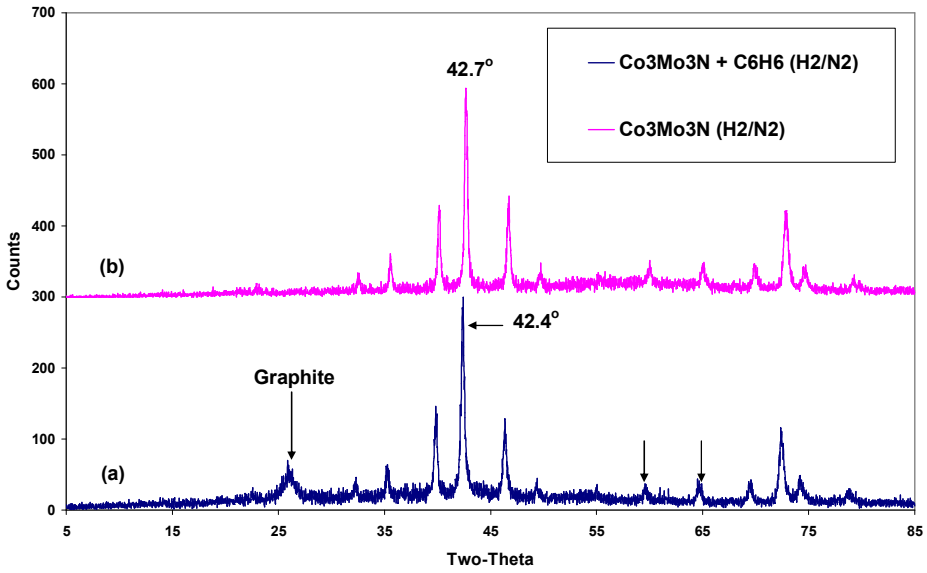

Figure 5.3-5. Powder X-ray diffraction patterns of Co_3Mo_3N samples (a) treated in H_2/N_2 and benzene, using temperature profile from Figure 4.2-2 and (b) Co_3Mo_3N treated in (H_2/N_2) at 400°C

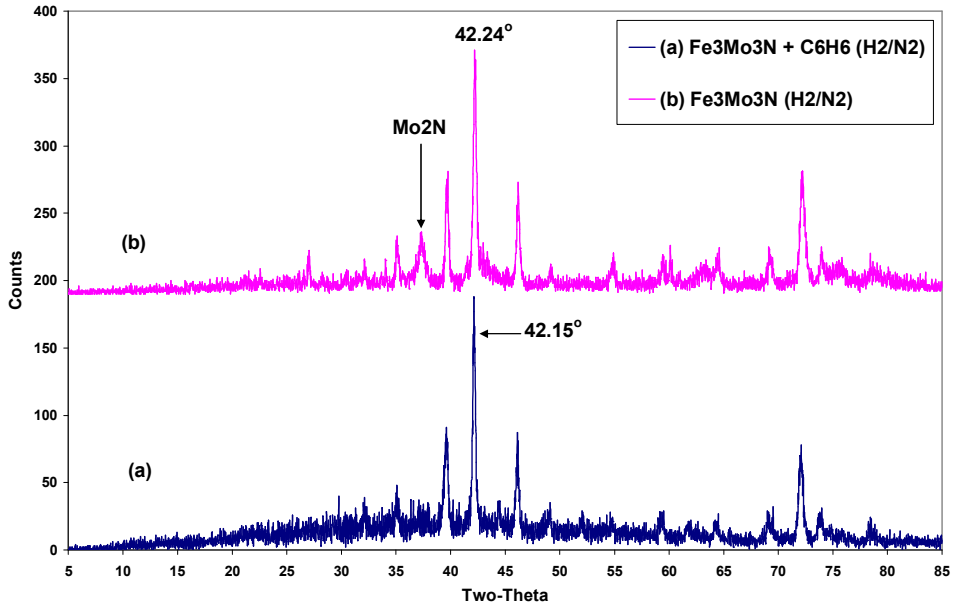

Figure 5.3-6. Powder X-ray diffraction patterns of Fe_3Mo_3N samples (a) treated in H_2/N_2 and benzene, using temperature profile from Figure 4.2-2 and (b) Fe_3Mo_3N treated in (H_2/N_2) at 400°C

In Figure 5.3-6, the Fe_3Mo_3N sample (H_2/N_2 + benzene, with temperature profile) has not shifted to lower angles of reflection to the same degree as the Co_3Mo_3N sample, however the carburization of Fe_3Mo_3N cannot be ruled out completely. The reflection indicated by an arrow in Figure 5.3-6(b) was previously attributed to γ-Mo_2N, however, there is no corresponding binary nitride or carbide reflection observed in the sample treated in benzene (Figure 5.3-6 (a)) and no Mo metal reflection.

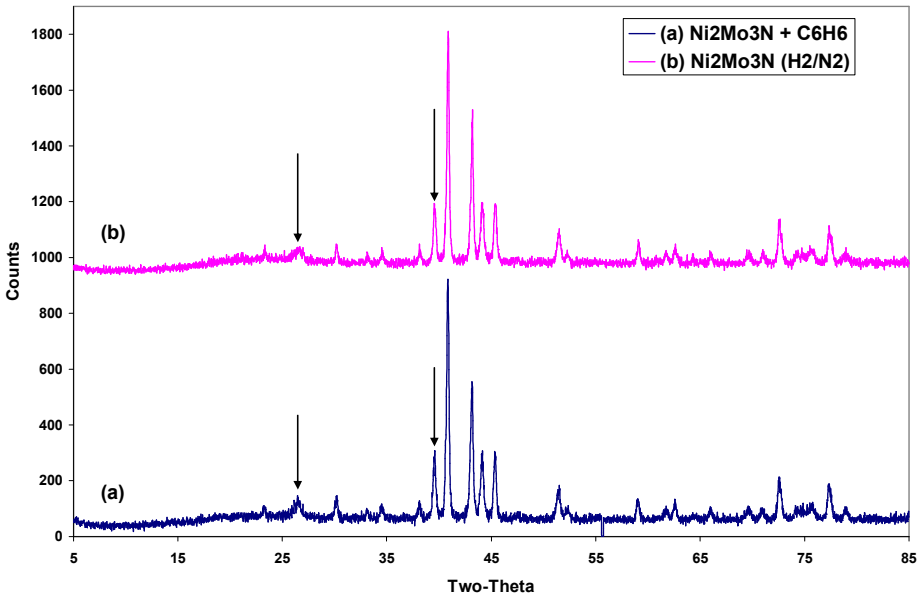

Figure 5.3-7. Powder X-ray diffraction patterns of Ni_2Mo_3N samples (a) treated in H_2/N_2 and benzene, using temperature profile from Figure 4.2-2 and (b) Ni_2Mo_3N treated in (H_2/N_2) at 400°C

Due to an unforeseen problem with the X-ray diffractometer at the Department of Chemistry, the powder XRD of the pre- and post-reaction Ni_2Mo_3N samples were carried out on a different diffractometer, kindly made available by the Department of Earth Sciences. Arrows in Figure 5.3-7 indicate reflections which were not present in previous XRD patterns of Ni_2Mo_3N. These extra reflections do not correspond to any previous impurities associated with Ni_2Mo_3N and may be an artefact of the instrument and will be investigated further.

There is no observed shift in reflections in the post-reaction XRD data for the Ni_2Mo_3N + benzene sample (Figure 5.3-7) and there is no significant change in the pre- or post-reaction XRD pattern.

The shift in the Bragg angle for the Fe_3Mo_3N was indicative of an increase in unit cell volume (and possibly the presence of carbon in the lattice, as shown by the reaction of Co_3Mo_3N), however there is no significant difference in the Ni_2Mo_3N XRD data. The post-reaction C and N analysis can be used to accurately determine if these materials are in fact carbonitrides, which have been isolated as intermediates during the carburization of ternary nitrides usually in the form $Co_3Mo_3C_xN_{1-x}$ [13, 14, 16].

5.3-3 Post-Reaction Carbon and Nitrogen Analysis

The post-reaction carbon, nitrogen and hydrogen contents of the ternary nitride materials were determined by combustion analysis, and are shown below in Table 5.3-1.

Sample	Observed N Content Wt. %	Observed C Content Wt. %	Observed H Content Wt. %
Co_3Mo_3N	0	28.96(3)	0
Fe_3Mo_3N	0	3.63(3)	0.50(3)
Ni_2Mo_3N	1.06/ 0.94(3)	25.54(3)	0

Table 5.3-1 Post-reaction nitrogen and carbon content of ternary nitride material tested after reaction with benzene and hydrogen

The post-reaction carbon/ nitrogen content of the Co_3Mo_3N sample confirm the complete removal of nitrogen from the material to the equivalent carbide. The post-reaction carbon content of the material is much greater than that of stoichiometric Co_3Mo_3C (2.52 wt. %). This could be explained by the reflection attributed to graphite in the post-reaction XRD pattern shown in Figure 5.3-5, and possible carbonaceous deposits formed on the surface of the material. The Ni_2Mo_3N sample still contains some nitrogen; however carbon is the dominant species present in the material and, as in the cobalt molybdenum sample, the carbon content exceeds that expected of Ni_2Mo_3C. The excess carbon in the case cannot be precisely attributed to the presence of graphite, as the erroneous peak present in the post-reaction XRD (Figure 5.3-7) is also present in the pre-reaction material as explained in section 5.3-2. From the XRD data and combustion analysis, the post-reaction Ni_2Mo_3N sample cannot then, be confidently assigned to the carbide structure and may be best described as a carbo-nitride.

Despite having zero nitrogen content, the post-reaction Fe_3Mo_3N sample exhibits much lower carbon content than the other ternary nitride materials tested and is closer to the stoichiometric carbon content of Fe_3Mo_3C (2.56%). The lower carbon content of the iron molybdenum sample could due to fewer carbonaceous deposits (coke) present on the the catalyst surface when compared with the cobalt/ nickel molybdenum materials, and also the absence of any

extra reflections which could be attributed to carbon e.g. graphite. There is also hydrogen present in the iron molybdenum sample, which could also be asscociated with the carbon, possibly a CH_x species.

5.3-4 Conclusions

The work carried out in this brief chapter was undertaken to investigate the possibility of direct synthesis of aniline from benzene by trapping reactive NH_x species produced from the hydrogenation of ternary nitride catalysts. These initial results appear to suggest that no reaction occurs during the experiment as the GCMS data indicates the presence of benzene with no other products detected. It is believed that the hydrogenation of lattice nitrogen occurs at too high a temperature for the insertion of reactive nitrogen species.

Shifts to lower angles $2\theta^o$ in the post-reaction XRD patterns for Co_3Mo_3N and Fe_3Mo_3N indicate carbiding of the materials by the hydrocarbon flowing over the catalyst. This is most evident in the case of Co_3Mo_3N, as the shift observed matches exactly with that recorded by Bussell and co-workers [13] for the formation of Co_3Mo_3C from Co_3Mo_3N using mixtures of methane and hydrogen. The results from combustion analysis agree well with the carburization of Co_3Mo_3N. Furthermore, the extra reflection present in the post-reaction Co_3Mo_3N sample, which has been documented by Wang and co-workers on the formation of Co_3Mo_3C [14], is attributed to graphite and provides an explanation for the excess carbon present in the post-reaction sample. Combustion analysis of the post-reaction Fe_3Mo_3N shows the presence of carbon and hydrogen, and the presence of CH_x species cannot be discounted. Although the post-reaction Ni_2Mo_3N sample contains significant amounts of carbon, there is no observed shift in the angle of reflection in the post-reaction XRD pattern of compared with standard Ni_2Mo_3N.

References

1. N.N Greenwood, A. Earnshaw, "Chemistry of the Elements", Pergamon Press, Oxford, (1984).
2. M. V. Twigg (ed.), "Catalyst Handbook" 2nd Edn., Wolfe Publishing Frome (1989).
3. M. Bielawa, T. Kurtz, Genger, O. Hinrichsen, Ind. Eng. Chem. Res. 40, 2793, (2001)
4. D. R. Corbin, S. Schwartz, G. C. Sonnichsen, Catal. Today, 37, 71, (1997).
5. J. Becker, W. F. Holderich, Catal. Lett. 54, 125 (1997).
6. P. Desrosiers, S. Guan, A. Hagemeyer, D. M. Lowe, C. Lugmair, D. M. Poojary, H. turner, H. Weinberg, X. Zhou, R. Armbrust, G. Fengler and U. Notheis, Catal, Today 81, 319, (2003).
7. S. A. Axon, S. D. Jackson, P. R. R Claes, WO patent 99/10311, (1999).
8. C. J. H. Jacobsen, Chem Comm. 1057, (2000).
9. R. Kojima, K-I. Aika, Appl. Catal. A: Gen, 215, 149, (2001).
10. A. Boisen, S. Dahl, C. J. H. Jacobsen, J. Catal. 208, 180 (2002).
11. T. Xiao, A. Hamif, A. P. E. York, Y, Nishizaka, M. L. H. Green, Phys. 4, 4549, (2002).
12. "The Chemistry of Transition Metal carbides and Nitrides", Ed. S. T. Oyama, Chapman & Hall, London, (1996).
13. S. Korlann, B. Diaz, M. E. Bussell, Chem. Mater. 14, 4049, (2002).
14. X-H. Wang, M-H. Zhang, W. Lia, K-Y. Taoa, Dalton Trans., 5165, (2007).
15. T. Tsuchida, J. Mater. Sci. 1735, 36, (2001).
16. S. Alconchel, F. Sapiñab, E. Martínezb, Dalton Trans., 2463-2468, (2004).
17. P. Desrosiers, S. Guana, A. Hagemeyer, D. M. Lowea, C. Lugmair, D. M. Poojary, H. Turner, H. Weinberg, X. Zhoua, R. Armbrust, G. Fengler , U. Notheis., Catal. Today, 319, 81, (2003).

6. Conclusions

In this thesis, the reactivity/ mobility of lattice nitrogen present in nitride based catalysts was investigated. Throughout the project, the experimental work undertaken has been split into three discrete sections. The first section sought to determine the most active molybdenum nitride based ammonia synthesis catalyst, and the effect of preparation and the possibility of structure sensitivity within these materials was considered. The effect of nitriding molybdenum supported on H-ZSM-5 and the introduction of dopants was also studied.

The second section dealt with the hydrogenation of lattice nitrogen within bulk binary and ternary nitride materials to investigate the possibility of producing reactive NH_x species. From the data presented, the removal of nitrogen from these materials and its potential for reaction was evident.

The third section investigated the reaction of benzene and hydrogen over bulk ternary nitride catalysts in an attempt to trap the reactive NH_x species, for the production of aniline.

Beneficial insights into all three of these objectives were obtained and are summarised below:

- After comparing the ammonia synthesis activities of binary γ-, β- and δ-molybdenum nitrides it has been shown that the ammonia synthesis activities of the β- and γ- molybdenum nitride phases are comparable on a mass normalised basis, with δ- phase exhibiting a comparatively low activity. Furthermore, when the influence of surface area is taken into account, the β-phase is by far the most active catalyst. This implies that the lengthy, highly specific temperature programmed ammonolysis reaction required to prepare the high surface area γ-phase, produces an ammonia synthesis catalyst which, at best, has no advantage to one prepared by the direct reaction of the oxide precursor with H_2/N_2 at high temperatures.

- On comparing the ammonia synthesis activities of cobalt, iron and nickel molybdenum nitrides and their precursors, it is apparent that in the case of CoMo and FeMo oxide, the ammonia synthesis activities exhibited after nitridation in H_2/N_2 are lower than those observed when the catalysts are prepared by ammonolysis (much lower in the case of iron molybdenum oxide oxide). The opposite effect is observed in the case Ni_2Mo_3N, with preparation in H_2/N_2 being favoured over ammonolysis due to higher ammonia synthesis activity. Unlike the

binary nitrides, the effect of preparing the cobalt and iron molybdenum nitride catalysts in mixtures of H_2/N_2 has been shown to significantly affect the ammonia synthesis activities, implying that the temperature programmed ammonolysis route produces a more active ammonia synthesis catalyst. The exception is Ni_2Mo_3N, which is significantly more active after preparation in H_2/N_2.

- By preparing and nitriding MoO_3/H-ZSM-5 and looking more closely at the XRD patterns of the fresh and nitrided materials, the diffraction patterns show that the relative intensities of selected reflections, indicative of the H-ZSM-5 structure (23-25^o 2θ), have increased for all nitrided materials relative fresh H-ZSM-5 / MoO_3/H-ZSM-5. It was also shown that the diffraction peaks shift to higher angles 2θ^o after impregnation of the Mo species on to the zeolite support, and shift back to lower angles after ammonolysis and subsequent ammonia synthesis when compared to the fresh H-ZSM-5 support material. This change in the relative intensities of the three strongest peaks, and also the peaks shifting to lower diffraction angles indicate an increase in lattice, and therefore the nitridation of the Mo species and/ or the incorporation of nitrogen in to the zeolite. An extra shoulder peak is observed in the XRD patterns of those H-ZSM-5 materials in which molybdenum is present, and also after the fresh H-ZSM-5 is nitrided). These shoulder peaks are indicative of a phase transition of the zeolite from orthorhombic (fresh H-ZSM-5) to monoclinic forms (MoO_3/H-ZSM-5, γ-Mo_2N/H-ZSM-5, β-Mo_2N/H-ZSM-5 and nitrided H-ZSM-5).

- XPS measurements conducted on bulk and H-ZSM-5 supported molybdenum nitride have suggested that there is an analogy between zeolite dispersed molybdenum carbide catalysts and preparing zeolite dispersed molybdenum nitride or oxy-nitride species. The zeolite supported molybdenum nitride species showed some differences from the bulk γ-Mo_2N material, for example it was impossible to fully remove the partially oxidised molybdenum component from the zeolite catalysts by argon ion etching, which suggests that the supported nitrides are best described as oxynitrides, which possibly interact strongly with the zeolite lattice.

- Ammonia synthesis activity measurements of nitrided MoO_3/H-ZSM-5 were conducted, and when considering the amount of active catalyst that is present on the support, the activity of the supported molybdenum nitride catalysts is remarkably high. The supported nitride materials exhibit the same trend for both the γ-Mo_2N and β-$Mo_2N_{0.78}$ supported materials, and the use of Fe has been shown to have a promotional effect on both materials. XPS measurements have shown the presence of Fe^0 in the nitrided material. Using gallium as a dopant shown to have no effect on the γ-Mo_2N/H-ZSM-5 material and a negative effect on the catalytic activity of the β-$Mo_2N_{0.78}$/H-ZSM-5 material.

- Isotopic nitrogen exchange experiments conducted using FTIR spectroscopy on nitrided H-ZSM-5 and MoO_3/H-ZSM-5 have shown that the presence of nitrided molybdenum was required for isotopic exchange. This demonstrates that supported γ-Mo_2N species can be a source of reactive and mobile N species, opening up possibilities for its application as a source of spill-over nitrogen.

- Hydrogenation of lattice nitrogen in bulk nitride materials has shown to be a function of temperature. Increasing temperature according to the temperature profile shown in Figure 4.2-2 appears to differentiate between weakly and strongly bound nitrogen species. Although some ammonia is produced, most of the lattice nitrogen is lost as dinitrogen.

- In the case of Co_3Mo_3N, only a finite amount of lattice nitrogen can be removed at 700^oC. By removing ca. 50% of the structural nitrogen present in Co_3Mo_3N, and refinement of XRD data, it is apparent that a previously unknown nitride structure, the η-12 Co_6Mo_6N, has been prepared. The nitrogen removed from the Co_3Mo_3N structure has been restored by nitridation of the material at 700^oC in H_2/N_2, confirming the function of cobalt molybdenum nitride as a nitrogen transfer catalyst.

- Similar experiments conducted using Fe_3Mo_3N and Ni_2Mo_3N demonstrated the loss of nitrogen from the materials, although not to the same extent as Co_3Mo_3N. The post-reaction XRD data was not significantly different from the initial materials, and it is concluded that these materials did not demonstrate the same nitrogen transfer capabilities as Co_3Mo_3N.

- Gas switching experiments conducted with binary γ-, β- and δ-molybdenum nitrides has shown that nitrogen can be removed from these materials at high temperatures under hydrogen. In the case of γ- and δ-molybdenum nitride, >50% of the nitrogen content of the starting material is removed. The post-reaction XRD data for these materials shows the decomposition of γ-Mo_2N to a mixture of γ-Mo_2N and Mo metal and the decomposition of δ-MoN to γ-Mo_2N, interestingly β-$Mo_2N_{0.78}$ completely decomposes to Mo metal, and not a sub-stoichiometric molybdenum nitride polymorph. As in the nitrogen deficient Co_3Mo_3N sample, it was demonstrated that the nitrogen content of reduced molybdenum nitride can be restored by treatment at 700^oC in H_2/N_2.

- At present, the origin of the differences in the types of decomposition pathway, and their determining influences, are not clear. However the loss of nitrogen, and hence its potential for reaction, is evident

- Reactions investigating the direct conversion of benzene to aniline were undertaken over ternary nitride catalysts. It was proposed that the reaction would occur by trapping reactive NH_x species produced from the hydrogenation of ternary nitride catalysts. GCMS data indicates the presence of benzene only in the products. It is believed that the hydrogenation of lattice nitrogen occurs at too high a temperature for the insertion of reactive nitrogen species. XRD data of post-reaction materials demonstrate carbiding of the Co_3Mo_3N and Fe_3Mo_3N materials by the hydrocarbon flowing over the catalyst. The results from combustion analysis agree well with the carburization of Co_3Mo_3N, Ni_2Mo_3N and Fe_3Mo_3N, the extra reflection present in the post-reaction Co_3Mo_3N sample, attributed to graphite, provides an explanation for the excess carbon present in the post-reaction sample.

References

1. R. Niewa and H. Jacobs, Chem. Rev., 96, 2053, (1996).
2 R. Niewa and F. J. DiSalvo, Chem. Mater., 2733, 10, (1998).
3 E Kroke and M. Schwarz, Co-ord. Chem. Rev.,493, 248, (2004)
4 A. Simon, Co-ord. Chem. Rev., 253, 163, (1997).
5 "The chemistry of transition metal carbides and nitrides", S. T. Oyama (ed.), Blackie Academic and Professional, Glasgow, (1996).
6 A. Zerr, G. Miehe, G. Serghiou, M. Schwarz, E. Kroke, R. Riedel, H. Fuess, P. Kroll and R. Boehler, Nature, 340, 400, (1999)
7 K. Leinenweber, M. O'Keffee, M. Somayazulu, H. Hubert, P. F. McMillan and G. W. Wolf, Chem.-Eur. J., 3076, 5, (1999)
8 N. Scotti, W. Kockelmann, J. Senker, S. Trassel and H. Jacobs, Z. Anorg. Allg. Chem., 1435, 625, (1999).
9 G. Serghiou, G. Miehe, O. Tschauner, A. Zerr and R. Boehler, J. Chem. Phys., 4659, 111, (1999)
10 J. W. McCauley and N. D. Corbyn, J. Am. Ceram. Soc., 476, 62, (1979)
11 J. Grins, P-O. Koll and G. Svensson, J. Solid State Chem., 48, 117, (1995)
12. S. T. Oyama and G. L. Haller, Catalysis, Spec. Per. Rep., Vol. 5, RSC London, 333, (1982)
13 P. W. Lednor (ed), Catal. Today, 15, (1992)
14 E. Furimsky, Appl. Catal. A,1, 240, (2003)
15. D. H. Gregory, *J. Chem. Soc., Dalton Trans.*, 259, (1999).
16 F. A. Cotton and G. Wilkinson, "*Advanced inorganic chemistry*", 5th Edn., Wiley, New York, (1988).
17 S. T. Oyama, "*The chemistry of transition metal carbides and nitrides*", S. T. Oyama (ed.), Blackie Academic and Professional, Glasgow, Chapter 1, 1, (1996)
18 R. Marchand, X. Gouin, F. Tessier and Y. Laurent, "*The chemistry of transition metal carbides and nitrides*", S. T. Oyama (ed.), Blackie Academic and Professional, Glasgow, Chapter 13, 252, (1996)
19. Zhaobin W, Qin, X, P. Grange, B. Delmon, J. Catal. 176, 168, (1997).

20 M. Vettraino, X. He, M. Trudeau, J. E. Drake and D. M. Antonelli, *Adv. Funct. Mater.*, 174, 12, (2002)

21 M. Vettraino, X. He, M. Trudeau and D. Anotnelli, *Stud. Surf. Sci. and Catal.*, 661, 141, (2002)

22 M. Vettraino, M. Trudeau, A. Y. H. Lo, R. W. Schurko and D. Antonelli*, J. Am. Chem. Soc.*, 9567, 124, (2002)

23 Volpe and M. Boudart, *J. Solid State Chem*., 332, 59, (1985)

24 J-G. Choi, R. L. Curl and L. V. Thompson, *J. Catal*., 218, 146, (1994)

25 G. W. Haddix, D. H. Jones, J. A. Reimer and A. T. Bell, *J. Catal*., 556, 112, (1988)

26 Z. Wei, Q. Xin, P. Grange and B. Delmon, *J. Catal*., 176, 168, (1997)

27 E. J. Markel and J. W. van Zee, *J. Catal*., 643, 126, (1990)

28 C. W. Colling, J-G. Choi and L. T. Thompson, *J. Catal*., , 35, 160, (1996)

29 B. G. Demczyk, J-G. Choi and L. T. Thompson, *Appl. Surf. Sci*., 63, 78 (1994)

30 C. H. Jaggers, J. N. Michaels and A. M. Stacy, *Chem. Mater*., 150, 2, (1990)

31 C. W. Colling and L. T. Thompson, *J. Catal*., 193, 146, (1994).

32. M. Nagai, A. Miyata, T. Kusagaya and S. Omi, "*The chemistry of transition metal carbides and nitrides*", S. T. Oyama (ed.), Blackie Academic and Professional, London, Chapter 17, 372, (1996)

33 Z. Wu, C. Li, Z. Wei, P. Ying and Q. Xin, *J. Phys. Chem. B*, 979, 106, (2002)

34 R. S. Wise and E. J. Markel, *J. Catal*., 335, 145, (1994)

35 M. K. Neylon, S. K. Bej, C. A. Bennett and L. T. Thompson, *Appl. Catal. A: Gen*., 13, 232, (2002)

36 Y. Zhang, Y. Li, R. Raval, C. Li, R. Zhai and Q. Xin, *J. Mol. Catal. A: Chem*., 241, 132, (1998)

37 S. Korlann, B. Diaz and M. E. Bussel, *Chem. Mater*., 4049, 14, (2002)

38 C. C. Yu, S. Ramanathan and S. T. Oyama, *J. Catal*., 1, 173, (1998)

39 C. Zhang, Z, Xu, K. Wan and Q. Liu, *Appl. Catal. A: Gen*., 55, 258, (2004)

40 S. Ernst, M. Hartmann, S. Sauerbeck and T. Bongers, *Appl. Catal. A: Ge*n, 117, 200, (2000)

41 N. Fripiat and P. Grange, *J. Mater. Sci*., 2057, 34, (1999)

42 S. Delsarte, A. Aroux and P. Grange, *Phys. Chem. Chem. Phys*., 2821, 2, (2000)

43 A. Massinon, E. Gueguen, R. Conanec, R. Marchand, Y. Laurent and P. Grange, *Stud. Surf. Sci. and Catal*., 77, 101, (1996)

44 R. L. Puurunen, S. M. K. Airaksinen and A. O. I. Krause, *J. Catal*., 281, 213, (2003)

45 R. L. Puurunen, A. Root, P. Sarv, M. M. Viitanen, H. H. Brongersma, M. Lindblad and A. O. I. Krause, *Chem. Mater*., **14**, 720, (2002)

46. D. A. King and F. Sebba, *J. Catal*., 253, 4, (1965)

47 D. A. King and F. Sebba, *J. Catal*., 430, 4, (1965)

48. J-G. Choi, J. Ha and J-W. Hong, *Appl. Catal. A: Gen*., 47, 168, (1998)

49 M. R. Hillis, C. Kemball and M. W. Roberts, *Trans. Faraday Soc*., 3570, 62, (1966)

50 K-I. Aika and A. Ozaki, *J. Catal*., 311, 14, (1969)

51 L. Volpe and M. Boudart, *J. Phys. Chem*., 4874, 90, (1986)

52 R. Kojima and K-I. Aika, *Appl. Catal A:Gen*., 141, 219, (2001)

53 R. Kojima and K-I. Aika, *Chem. Lett*., 514, (2000)

54 R. Kojima and K-I. Aika, *Appl. Catal. A: Gen*., 149, 215, (2001)

55 R. Kojima and K-I. Aika, *Appl. Catal. A: Gen*., 121, 218, (2001)

56 R. Kojima and K-I. Aika, *Appl. Catal. A: Gen*., 157, 219, (2001)

57 C. J. H. Jacobsen, M. Brorson, T. Sehested, H. Teunissen and E. Turnqvist, US Patent 6, 235, 676, (1999).

58 C. J. H. Jacobsen, *Chem. Commun*., 1057, (2000)

59 C. J. H. Jacobsen, S. Dahl, B. S. Clausen, S, Bahn, A. Logadottir and J. K. Norskov, *J. Am. Chem. Soc*., 8405, 123, (2001)

60 A. Boisen, S. Dahl and C. J. H. Jacobsen, *J. Catal*., 180, 208, (2002)

61 M. Vettraino, M. Trudeau, A. Y. H. Lo, R. W. Schurko and D. Antonelli*, J. Am. Chem. Soc.*, 9567, 124, (2002)

62 W. J. McGill and F. Sebba, *J. Catal*., 104, 2, (1963)

63 S. T. Oyama, *J. Catal*., 35, 133, (1992)

64 R. Bafrali and A. T. Bell, *Surf. Sci*., 353, 278, (1992)

65 H. J. Lee, J-G. Choi, C. W. Colling , M. Mudholkar and L. T. Thompson, *Appl. Surf. Sci*., 12, 89, (1995)

66 J. A. J. Rodriguez, G. M. da Cruz, G. Bugli, M. Boudart and G. Djega-Mariadassou, *Catal. Lett.*,1, 45, (1997)

67 X. Chen, T. Zhang, L. Xia, T. Li, M. Zheng, Z. Wu, X. Wang, Z. Wei, Q. Xiu and C. Li, *Catal. Lett*., 21, 79, (2002)

68 R. Brayner, G. Djega-Mariadassou, G. M. da Cruz and J. A. J. Rodrigues, *Catal. Today*, 225, 57, (2000)

69 M. K. Neylon, S. K. Bej, C. A. Bennett and L. T. Thompson, *Appl. Catal. A:Gen*., 13, 232, (2002)

70 R. C. Bowman, M. H. Tegen and G. E. Hartwell, US Patent 4,922,024, (1990)

71 M. Florea, R. Prada-Silvy and P. Grange, *Catal. Lett*., 63, 87, (2003)

72 M. Florea, R. Prada-Silvy and P. Grange, *Appl. Catal. A: Gen*., 289, 255, (2003)

73 R. Prada-Silvy, M. Florea, N. Blangenois and P. Grange, *AIChE Journal*, 2228, 49, (2003)

74 M. Olea, M. Florea, I. Sack, R. Prada Silvy, E. M. Gaigneaux, G. B. Marin and P. Grange, *J. Catal.*, 152, 232, (2005)

75 C. Shi, A. M. Zhu, X. F. Yang and C. T Au, *Catal. Lett*., 9, 97, (2004)

76 C. Shi, A. M. Zhu, X. F. Yang and C. T. Au, *Appl. Catal. A: Gen*., 223, 276, (2004)

77 H. He, H. X. Dai, K. Y. Ngan and C. T. Au, *Catal. Lett*., 147, 71, (2001)

78 C. Shi, X. F. Yang and C. T. Au, *Catal. Today*, 819, 93-95, (2004)

79 Y. Egashira and H. Komiyama, *Ind. Eng. Chem. Res*., 1583, 29, (1990)

80 G. S. Rhantora, A. T. Bell and J. A. Reimer, *J. Catal*., 40, 108, (1987)

81 A. Guerrero-Ruiz, Y. Zhang, B. Bachiller-Baeza and I. Rodriguez-Ramos, *Catal. Lett*., 165, 55, (1998).

82. Z. Wu, Z. Hao, P. Ying, C. Li and Q. Xin, *J. Phys. Chem. B*, , 12275, 104, (2000).

83 Y. Li, Y. Fan and Y. Chen, *Catal. Lett*., 111, 82, (2002)

84 P. Rodriguez, J. l. Brito, A. Albornorz, M. Labadi, C. Pfaff, S. Marrero, D. Moronta and P. Betancourt, *Catal. Commun*, 79, 5, (2004)

85 H. A. Al-Megren, T. Xiao, S. L. Gonzalez-Cortes, S. H. Al-Khowaiter and M. L. H. Green, J. *Mol. Catal. A: Chem*., 143, 225 (2005)

86 H. Imamura, T. Nuruyu, T. Kawasaki, T. Teranishi and Y. Sakata, *Catal. Lett*., 185, 96, (2004)

87 P. Perez-Romo, C. Potvin, J-M. Manoli, M. M. Chehimi and G. Djega-Maraidassou, *J. Catal*, 187, 208, (2002)

88 P. Perez-Romo, C. Potvin, J. M. Manoli, R. Contant and G. Djega-Mariadassou, *J. Catal*., 191, 205, (2002)

89 H. A. Al-Megren, T. Xiao, S. L. Gonzalez-Cortes, S. H. Al-Khowaiter and M. L. H. Green, J. *Mol. Catal. A: Chem*., 143, 225, (2005)

90 Y. Laurent, P. Bastians, R. Conanec, R. Marchand, Y. Laurent, L. Gandia, M. Montes, J. Fernandez and A. Odriozola, *Stud. Surf. Sci. and Catal*., 381, 91, (1995)

91 S. Delsarte, V. Serin, A-M. Flank, F. Villain and P. Grange, *J. Solid State Chem.*, 163, 163, (2002)

92 T. Blasco, A. Corma, K. Fernandez, V. Fornes and R. Guil-Lopez, *Phys. Chem. Chem. Phys.*, 4493, 1, (1999)

93 M. J. Climent, A. Corma, V. Fornes, A. Frau, R. Guil-Lopez, S. Ibarra and J. Prino, *J. Catal*., 392, 163 (1996)

94 N . Fripiat, V. Parvulescu, V. I. Parvulescu and P. Grange, *Appl. Catal. A: Gen*., 331, 181, (1999)

95 N. Fripiat, R. Conanec, A. Auroux, Y. Laurent and P. Grange, *J. Catal*., 543, 167 (1997)

96 N. Fripiat, R. Conanec, R. Marchand, Y. Laurent and P. Grange, *J. Eur. Ceram. Soc*., 2011, 17 (1997)

97 S. Delsarte, A. Aroux and P. Grange, *Phys. Chem. Chem. Phys*., 2821, 2, (2000)

98 S. Delsarte and P. Grange*, Stud. Surf. Sci. and Catal*., 3237, 130 (2000)

99 S. Delsarte, V. Peltier, Y. Laurent and P. Grange, Stud. *Surf. Sci. and Catal*., 869, 118, (1997)

100 S. Delsarte, V. Serin, A-M. Flank, F. Villain and P. Grange, *J. Solid State Chem.*, 163, 163, (2002)

101 Delsarte, F. Mause, J-C. Lavalley and P. Grange, *Catal. Lett*.,79, 68, (2000)

102 S. Delsarte, V. Serin, A. M. Flank, F. Villain and P. Grange, *J. Synchroton Rad*., 433, 6, (1999)

103 H. Wiame, L. Bois, P. L'haridon, Y. Laurent and P. Grange*, J. Eur. Ceram. Soc*., 2017, 17, (1997)

104 H. M. Wiame, C. M. Cellier and P. Grange, *J. Phys. Chem. B*, 591, 104, (2000)

105 H. M. Wiame, M. A. Centeno, L. Legendre and P. Grange, Stud. *Surf. Sci. and Catal.*, 879, 117, (1998)

106 H. Wiame, L. Bois, P. Lharidon, Y. Laurent and P. Grange, *Solid State Ionics*, 755, 101-103, (1997)

107 H. Wiame, C. Cellier and P. Grange, *J. Catal*., 406, 190, (2000)

108 S. K. Bej and L. T. Thompson, *Appl. Catal. A: Gen*., 141, 264, (2004)

109 P. W. Lednor and R. de Ruiter, *J. Chem. Soc., Chem. Commun*., 1625, (1991)

110 S. Kaskel and K. Schlichte, *J. Catal*., 270, 201, (2001)

111 H. Irie, Y. Watanabe and K. Hashimoto, *J. Phys. Chem. B*, 5483, 107, (2003)

112 M. Miyauchi, A. Ikezawa, H. Tobimatsu, H. Irie, K. Hashimoto, *Phys. Chem. Chem. Phys.*, 865, 6, (2004)

113 S. Yiu, H. Yamaki, M. Komatsu, Q. Zhang, J. Wang, Q. Tang, F. Saito and T. Sato, *J. Mater. Chem*., 2996, 13, (2003)

114 T. Sano, N. Negishi, K. Koike, K. Takeuchi and S. Matsuzawa, *J. Mater. Chem.*, 380, 14, (2004)

115 S. Sakthivel and H. Kisch, *Chem. Phys. Chem*., 487, 4, (2003)

116 T. Ihara, M. Miyoshi, Y. Iriyama, O. Matsumoto and S. Sugihara, *Appl. Catal. B: Env*., 403, 42, (2003)

117 O. Diwald, L. Thompson, E. G. Goralski, S. D. Walck and J. T. Yates, Jr, *J. Phys. Chem. B*, 52, 108, (2004)

118 T. Morikawa, R. Asahi, T. Ohwaki, K. Aoki and Y. Taga*, Jap. J. Appl. Phys.,* L561, 40 (2001)

119. Hitoki, T. Taneka, J. N. Kondo, M. Hara, H. Kobayashi and K. Domen, *Chem. Commun*.. 1698, (2002)

120 M. Hara, T. Takata, J. N. Kondo and K. Domen, *Catal. T*oday, 313, 90, (2004)

121 G. Garcia Cervantes, F. J. Cadete Santos Aires and J. C. Bertolini, *J. Catal*., 26l, 214, (2003)

122 C. Methivier, J. Massardier and J. C. Bertolini, *Appl. Catal. A:Gen*., 337, 182, (1999)

123 F. J. Cadete Santos Aires, S. Ramierz, G. Garcia Cervantes, E. Rogemond and J. C. Bertolini, *Appl. Catal. A: Gen*., 289, 238 (2003)

124 F. Monnet, Y. Schuurmann, F. Cadete Santos Aires, J. C. Bertolini and C. Mirodatos, *Catal. Today*, 51, 64, (2001)

125 J-C. Wu, Z-A. Lin, J-W. Pan and M-H. Rei, *Appl. Catal. A: Gen*., 117, 219, (2001)

126 C. J. H. Jacobsen, *J. Catal*., ,1, 200, (2001)

127 C-A. Lin, J. C. S. Wu, J-W. Pan and C-T. Yeh, *J. Catal*., 39, 210, (2002)

128 M. A. Centeno, M. Debois and P. Grange, *J. Catal*., 296, 192, (2000)

129 E. Gueguen, S. Delsarte, V. Peltier, R. Conanec, R. Marchand, Y. Laurent and P. Grange, *J. Eur. Ceram. Soc*., 2007, 17, (1997)

130 S. Delsarte, F. Mauge and P. Grange, *J. Catal*.,1, 202, (2001)

131 N. Fripiat and P. Grange, *Catal. Lett*., 53, 62, (1999)

132 T. Becue, J-M. Manoli, C. Potvin, R. J. Davis and G. Djega-Mariadassou*, J. Catal*., 110, 186, (1999)

133 M. Ito, K. Machida, K. Hirose, T. Sakata, H. Mori and G. Adachi, *J. Phys. Chem. B*, 9498, 103, (1999)

134 N. Segal and F. Sebba, *J. Catal*., 105, 8, (1967)

135 N. Segal and F. Sebba, *J. Catal*., 113, 8, (1967)

136 T. Xiao, A. Hanif, A. P. E. York, Y. Nishizaka and M. L. H. Green, *Phys. Chem. Chem. Phys*., 4549, 4, (2002)

137 M. Olea, M. Florea, I. Sack, R. Prada Silvy, E. M. Gaigneaux, G. B. Marin and P. Grange, *J. Catal.*, 152, 232, (2005)

138 M. Kilo, M. A. Taylor, C. Argirusis, G. Borchardt, M. Lerch, O. Kaitasov and B. Lesage, *Phys. Chem. Chem. Phys*.,3645, 6, (2004)

139. Zeitschrift für anorganische und allgemeine Chemie, H. Soerijanto , C. Rödel, U. Wild, M. Lerch, R. Schomäcker, R. Schlögl, T. Ressler, 632, 12-13, 2157 (2006).

140. S. T. Oyama, J. C Schlatter, Ind. Eng. Chem. Res,1639-1648, 27, (1988).

141. M. A. Albiter, R. Huirache-Acuna, F. Paraguay-Delgad, *et al*. Nanotechnology, 3473-3481, 17, (2006).

142. X. W. Lou, H. C. Zeng, Chem. Mater., 4781-4789, 14, (2002).

143. D. S. Bem., C. P. Gibson., H. C. Zur-Loye. Chem. Mater 5 (4): 397-399 Apr (1993).

144. L. Bois, P. L' Haridon, H. Wiame, P. Grange, Materials Research Bulletin, 9-19, Vol. 33, No. 1, (1998).

145. H. Wiame, L. Bois, P. L' Haridon, Y. Laurent, P. Grange, Solid State Ionics 101-103, 755-759, (1997).

146. M. Itoh, K-I. Machida, K. Hirose, T. Sakata, H. Mori, G-Y. Adachi. J. Phys. Chem. B. 103, 9498, (1999).

147. J. S. J. Hargreaves and D. Mckay, Catalysis Specialist Periodic Report 19, 83 (2006).

148. M. Nagai, Appl. Catal. A: Gen. 322, 178 (2007).

149. M. Nagai. Y. Yamamoto. R. Aono., Coll. and Sur. A: Physiochem. Eng. Aspects 241, 257-263. (2004).

150. S. W Gong, H. K. Chen, W. Li, *et al*. Energy and Fuels 20 (4): 1372-1376, (2006).

151. R. Karam, R. Ward, Inorg. Chem. 9(6)1385 – 1387 (1970).

152. J. G. Choi, H. J. Lee, L. T. Thompson. App. Sur. Sci., 78, 299-307, (1994).

153. K. Inamaru, K. Baba, S. Yamanaka, Chem. Mater., 17 (24), 5935-5940, (2005).

154. A. Y. Ganin, L. Kienle, G. V Vajenine, J. Solid State Chem. 179, 2339-2348, (2006)

155. B. R. Sahu, L. Kleinman, Physical Review B, 70, (2004).

156. C. L. Bull, T. Kawashima, P. F. McMillan, D. Machon, O. Shebanova, D. Dalsenberger, E. Soignard, E. Takayama-Muromachi and L. C. Chapan, J. Solid State Chem. 179, 1762 (2006).

157. R. Marchand, F. Tessier and F. J. Di Salvo, J. Mater. Chem. 9, 297 (1999).

158. K. Hada, J. Tanabe, S. Omi, M. Nagai, J. Catal. 207, 10, (2002).

159. J. G. Choi, J. R. Brenner, C. W. Coiling, B. G. Demczyk, J. L. Dunning and L. T. Thompson, Catal. Today 15, 201 (1992).

160. M. A. Albiter, R. Huirache-Acuna, F. Paraguay-Delgado, J. L. Rico and G. Alonso-Nunez, Nanotechnology 17, 3473 (2006).

161. A. Mittasch, Z. *Elektorchem*., 36, 567, (1930).

162. P. E Rauch, F. J DiSalvo, J. Solid State Chem 11, 162-166, (1994).

163. S. Alconchel, F. Sapina, D. Beltran, A. Beltran, J. Mater. Chem., 8, 1901-1909, (1998).

164. K. S. Weil and P. N. Kumta, Mater, Sci. Eng. B, 38, 109-117, (1996).

165. P. Subramanya Herle, M. S. Hegde,. Sooryanarayana, T. N. Guru Row, G. N. Subbanna, Inorg. Chem., 37, 4128-4130, (1998).

166. H. Zhang, Z. Zhao, C. Xu, A. Duan, W. Lin. H. Tian, I. E. Wachs, Materials Research Bulletin 41, 2334-2340, (2006).

167. B.C Gates, Catalytic Chemistry, Wiley, (1992).

168. Y. Wang, W. Li, M. Zhang, N. Guan, K. Tao. Appl. Catal. A: Gen. 215, 39, (2001).

169. C. Shi, A. M. Zhu, X. F. Yang, C. T. Au, Appl. Catal. A: Gen 293, 83-90, (2005).

170. M. Nagai, T. Miyao, T. Tuboi, Catal. Lett. 18, 9, (1993).

171. M. Nagai, Y. Goto, O. Uchino, S. Omi, Catal. Today. 43, 249, (1998).

172. S. Burns, J. S. J. Hargreaves, P. Pal *et al*. Catal. Today 114 (4): 383-387, (2006).

173. M. Guisnet, N.S. Gnep, Appl. Catal. A: Gen. 146 33, (1996).

174. D. Mckay, J. S. J. Hargreaves and R. F. Howe, Catalysis Letters, 112, 109-113 (2006).

175. Z. L. Liu , M. Meng, Y. L. Fu *et al*. Mater. Lett. 54 (5-6): 364-371, (2002).

176. G. L. Bull, P. F. McMillan, E. Soignard, K. Leinenweber, J. Solid. State. Chem. 1488-1492, 177, (2004)

177. Sir. C. Goodeve, K. H. Jack, Discuss. Faraday. Soc. 4, (1948).

178. E. L. Wu, S. L. Lawson, D. H. Olsen, A. C. Rohrman, G. T. Kokotailo., J. Phys. Chem., 2777, (1979).

179. C. A. Fyfe, G. J. Kennedy, C. T. De Schutter, G. T. Kokotailo, J. Chem. Soc. Chem. Comm., 541, (1984).

180. D. G. Hay, H. Jaeger, J. Chem. Soc. Chem. Comm., 1433, (1984).

181. D. G. Hay, H. Jaeger, G. W. West., J. Phys. Chem., 89, 1070, (1985).

182. D. M. bibby, N. B. Milestone, J. e. Paterson, L. P. Aldridge., J. Catal., 97, 493, (1986).

183. J.-Z. Zhang, M.A. Long, R.F. Howe, Catal. Today 44, 293, (1998).

184. D. Wang, J.H. Lunsford, M.P. Rosynek, J. Catal. 169, 347 (1997).

185. W. Li, D. Meitzner, R.L. Borry III, E. Iglesia, J. Catal. 191, 373 (2000).

186. R.W. Borry, Y.-H. Kim, A. Huffsmith, J.A. Reimer, E. Iglesia, J. Phys. Chem. B 103, 5787 (1999).

187. H.S. Lacheen, E. Iglesia, Phys. Chem. Chem. Phys. 7, 538 (2005).

188. V.T.T. Ha, L.V. Tiep, P. Meriaudeau, C. Naccache, J. Mol. Catal. A: Chem. 181, 283 (2002).

189. B. Li, S. Li, N. Li, H. Chen, W. Zhang, X. Bao, B. Lin, Micropor. Mesopor. Mater. 88, 244 (2006).

190. S. Burns, J.S.J. Hargreaves, M. Stockenhuber, R.P.K. Wells, Micropor. Mesopor. Mater. 104, 97, (2007).

191. W. Liu, Y. Xu, S.-T. Wong, L. Wang, J. Qiu, N. Yang, J. Mol. Catal. A: Chem. 120, 257 (1997).

192. T. Becue, J.M. Manoli, C. Potvin, G. Djega-Mariadassou and M. Delamar, J. Phys. Chem. B 101, 6429, (1997).

193. T. Kadono, T. Kubota and Y. Okamoto, Catal. Today 87, 107, (2003).

194. C. Shi, A.M. Zhu, X.F. Yang and C.T. Au, Appl. Catal: A. 276, 233, (2004)

195. P. Grange, P. Bastains, R. Conanec, R. Marchand, Y. Laurent,. Appl. Catal. A. 114, L191, (1994).

196. A. Stein, B. Wehrle, M. Jansen, Zeolites, 13, 291, (1993).

197. D. Barthomeuf, Catal. Rev. –Sci. Eng, 521, (1996).

198. A. Corma, S. Iborra, S. Miguel, J. Primo, J. Catal. 173, 315, (1998).

199. D Desplantier-Giscard, C. Danumah, S. Kaliaguine, Appl. Catal. A, 222, 299, (2001).

200. J. Xiong, Y. Ding, H. Zhu, L. Yan, S. Liu, J. Phys. Chem. B, 107, 1366, (2003).

201. K. Narasimharao, M. Hartmann, H. H. Thiel, S. Ernst, Micropor. Mesopor. Mater. 90, 377, (2006).

202. X. Guan, N. Li, Guangjun,Wu, J. Chen, F. Zhang, N. Guan, J. Mol. Catal. A. 248, 220, (2006).

203. T. V. Voskoboinikov, H.-Y. Chen, W. M. H. Sachtler, J. Molec. Catal. A. 155, 155, (2000).

204. R. S Winter, J. Chem. Soc. London, 2889, (2000).

205. J. Valyon, W. K. Hall, J. Catal. 143, 520, (1993).

206. L. Brabec, M. Jeschke, R. Klik, J. Novakova, L. Kubelkova, J. Meusinger, Appl. Catal. A. 170, 105, (1998).

207. J. Novakova, L. Brabec, J. Catal. 166, 186, (1997).

208. P. Fejes, J. B. Nagy, K. Lazar, J. Halasz, Appl. Catal. A. 190, 117, (2000).

209. S. Hoornaerts, D. VandePutte, F.C. Thyrion, P. Ruiz, B. Delmon, Catalysis Today 33, 139-150, (1997).

210. M. Nagai, Y. Goto, A. Miyata, M. Kiyoshi, K. Hada, K. Oshikawa, S. Omi, J. Catal 182, 292-301 (1999).

211. Gong SW, Chen HK, Li W, et al. Appl. Catal. A: Gen 279, 1-2, 257-261 (2005).

212. Gong SW, Chen HK, Li W, et al. Chin. J. Catal 24 687-690 (2003).

213. Gong SW, Chen HK, Li W, et al. Catal. Comm. 5, 10, 621-624 (2004).

214. J.Z .Zhang, M.A Long and R.F. Howe, Catal. Today 44, 293, (1998).

215.P. Mars and D. W. van Krevelen, *Chem. Eng. Sci. Spec. Sup*pl. 41, 263, (1954).

216. P. Tetenyi, Chapter 4 in "Isotopes in heterogeneous catalysis", eds J. S. J. Hargreaves, S. D. Jackson and G. Webb, Imperial College Press, London. (2006).

217. G. E. Keller and M. Bhasin, J. Catal. 73, 9 (1982).

218.G. K. Boreskov, Disc. Faraday. Soc. 263, 41, (1966).

219.T. Xiao, A. Hanif, A. P. E. York, Y. Nishizaka and M. L. H. Green, Phys. Chem. Chem. Phys. 4, 4549 (2002).

220 .G. I. Panov , G. K. Boreskov, A. S. Kharitonov, E. M Moroz, V.I Sobolev, Kinetics and Catalysis, 25 (1): 101-106, (1984).

221. H. Soerijanto, C. Rodel, U. Wild, M. Lerch, R. Schomacker, R. Schlogl and T. Ressler, J. Catal. 250, 19 (2007).

222. S.K. Jackson, R. C. Layland, H.C. zur Loye, J. Alloys Compd., 94, 291, (1999).

223. M. Newsam, A. J. Jacobsen, L. E. McCandlish, R. S. Polizzotti, J. Solid. State. Chem., 75, 296, (1988).

224. A. Burrows, S. Coluccia, J. S. J. Hargreaves, R. W. Joyner, C. J. Kiely, G. Marta, I. M. Mellor, and M. Stockenhuber, J. Catal. 234, 14, (2005).

225. "Practical Surface Analysis: Second edition, D. Briggs, M.P. Seah. Thompson press (1983).

Appendix 1. Ammonia Synthesis Calibration/ Calculations

The mean conductivity of seven different 0.00108 mol L^{-1} solutions of H_2SO_4 and $(NH_4)_2SO_4$ was determined. The table below shows the conductivities observed

Conductivity H_2SO_4 ($\mu S\ cm^{-1}$)	Conductivity $(NH_4)_2SO_4$ ($\mu S\ cm^{-1}$)
923	330
918	329
913	327
913	319
918	323
923	330
917	326
Mean ~ 918	Mean ~ 326

The calculation shown below demonstrates how the ammonia synthesis rates were calculated with respect to the conductivity versus time plot for every ammonia synthesis experiment.

Moles of H_2SO_4 = Concentration (H_2SO_4) x Volume (H_2SO_4)

= 0.00108 x 0.2

= 2.16 x 10^{-4} moles of H_2SO_4

Multiply by 2 for equivalent H^+ in NH_3 = 4.32 x 10^{-4} moles of ammonia required to completely react with H_2SO_4.

Change in conductivity for reaction $H_2SO_4 + NH_3 \longrightarrow (NH_4)_2SO_4$

= 918 – 326

= 592 $\mu S\ cm^{-1}$

Number of moles of ammonia required / Total change in conductivity

= 4.32 x 10^{-4} / 592 = 7.3 x 10^{-7} mol/ $\mu S\ cm^{-1}$

Gradient of conductivity versus time plot, m, multiplied by 7.3 x 10^{-7} mol/ $\mu S\ cm^{-1}$ = χ

χ / 0.4 g of catalyst = y mol h^{-1} g^{-1}

The maximum partial pressure achievable by the ammonia synthesis reactions presented in this thesis (i.e. at ambient pressure and 400^{o}C) can be calculated by the following expression

$$N_2 + H_2 \qquad 2NH_3$$

Let χ = mole fraction of NH_3 at equilibrium. The sum of the mole fractions of N_2 and H_2 must then be (1- χ) . Since these gases have the ratio 23.3% N_2 and 76.7% H_2, as determined by GC analysis, it follows that

$$\chi N_2 = 0.233 (1- \chi) \text{ and } \chi H_2 = 0.767 (1- \chi)$$

And if p = total pressure, the following equation can be applied

$$K\rho = \rho^2 NH_3 / \rho N_2 \, X \, \rho^3 H_2$$

the maximum partial pressure of NH_3 quoted by Aika is 0.0262. 0.7%

Appendix 2. FTIR Spectra of Gas-phase NH_3 from Standard Reaction

An FTIR spectrum of the exit stream of the ammonia synthesis reactor was taken from a standard reaction using Co_3Mo_3N to confirm the presence of ammonia in the product stream.

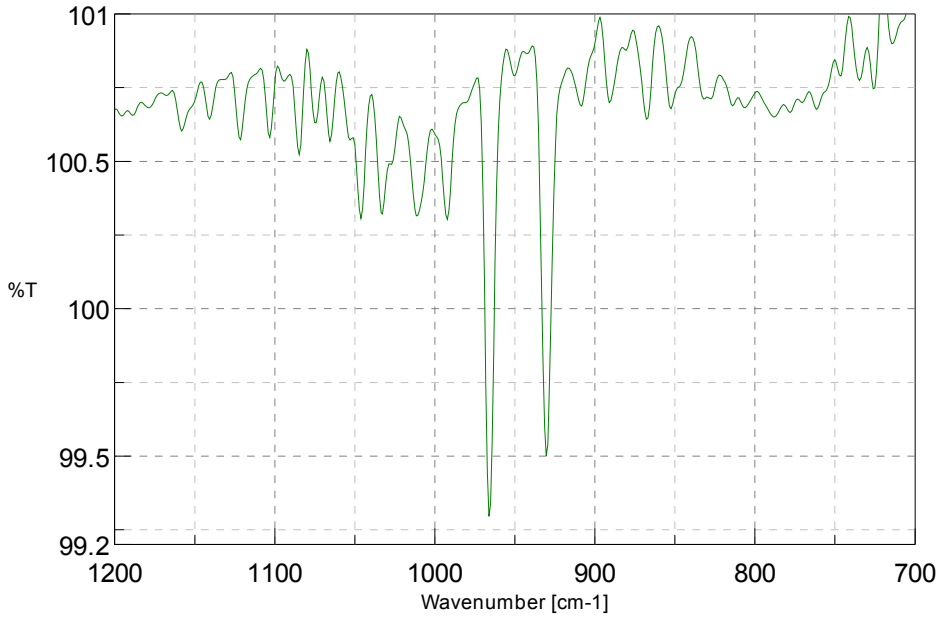

Appendix 3. Rietveld/ Crystallographic Data for Co_3Mo_3N Samples

The crystallographic/ Rietveld data for the Co_3Mo_3N samples described in Chapter 4 are included here.

Crystallographic data for Co_3Mo_3N (H_2/N_2) using temperature profile shown in Figure 4.2-2 at 298 K:

```
                |----------------------------------------|
                |     Program PUBTABLES Version Win32    |
                |  Generate crystal structure data tables |
                | Distributed on Wed Dec 25 11:38:28 2002 |
                |----------------------------------------|

       |-----------------------------------------------------------|
       |            Allen C. Larson and Robert B. Von Dreele       |
       |      Manuel Lujan, Jr. Neutron Scattering Center, MS-H805  |
       |      Los Alamos National Laboratory, Los Alamos, NM  87545|
       |                                                           |
       | Copyright, 2000, The Regents of the University of California. |
       |-----------------------------------------------------------|

GENLES was run on May 09 23:18:38 2007    Total cycles run1151

The Current Least-Squares controls are

Maximum number of cycles is   12
I/SigI cut-off is  1.00


Anisotropic thermal factors are defined by
  T = exp(h**2*astr**2*u11+... +2*h*k*astr*bstr*u12+... )


Space group F d -3 m
The lattice is centric  F-centered cubic         Laue symmetry m3m
 Multiplicity of a general site is 192
 The symmetry of the point 0,0,0 contains 1bar

The equivalent positions are:

( 1)     X      Y      Z  ( 2)     Z      X      Y  ( 3)     Y      Z      X
( 4) 1/4+X  1/4+Y     -Z  ( 5)    -Z  1/4+X  1/4+Y  ( 6) 1/4+Y     -Z  1/4+X
( 7) 1/4-Z  1/2+X  3/4-Y  ( 8) 3/4-Y  1/4-Z  1/2+X  ( 9) 1/2+Y  1/4-Z  3/4-X
(10) 3/4-X  1/2+Y  1/4-Z  (11) 1/4-Z  3/4-X  1/2+Y  (12) 1/2+X  3/4-Y  1/4-Z
(13)     Y      X      Z  (14)     Z      Y      X  (15)     X      Z      Y
(16) 1/4+Y  1/4+X     -Z  (17)    -Z  1/4+Y  1/4+X  (18) 1/4+X     -Z  1/4+Y
(19) 1/4-Z  1/2+Y  3/4-X  (20) 3/4-X  1/4-Z  1/2+Y  (21) 1/2+X  1/4-Z  3/4-Y
(22) 3/4-Y  1/2+X  1/4-Z  (23) 1/4-Z  3/4-Y  1/2+X  (24) 1/2+Y  3/4-X  1/4-Z


Lattice constants are
 a =  11.0157(7)  b = A  c = A
 Alpha =  90     Beta =  90    Gamma =  90
Cell volume = 1336.72(14)
```

Name	X	Y	Z	Ui/Ue*100	Site sym	Mult	Type	Seq	Fractn
CO1	0.29192(29)	0.29192(29)	0.29192(29)	1.69*	3M(111)	32	CO	1	1.0000
CO2	0.500000	0.500000	0.500000	1.52*	-3M(111)	16	CO	2	1.0000
MO3	0.92611(25)	0.125000	0.125000	0.38*	MM2d100	48	MO	3	1.0000
N4	0.125000	0.125000	0.125000	2.50	-43M	8	N	4	0.16(10)
N5	0.000000	0.000000	0.000000	2.50	-3M(111)	16	N	5	0.87(9)

Thermal parameters multiplied by 100.0 are

Name	U11	U22	U33	U12	U13	U23
CO1	1.69(15)	1.69(15)	1.69(15)	0.18(16)	0.18(16)	0.18(16)
CO2	1.52(24)	1.52(24)	1.52(24)	-0.08(23)	-0.08(23)	-0.08(23)
MO3	0.89(18)	0.13(10)	0.13(10)	0.00	0.00	-0.07(16)
N4	2.50	2.50	2.50	0.00	0.00	0.00
N5	2.50	2.50	2.50	0.00	0.00	0.00

Crystallographic data for Co_3Mo_3N (H_2/Ar) using temperature profile shown in Figure 4.2-2 (believed to be Co_6Mo_6N) at 298 K:

```
                |----------------------------------------|
                |     Program PUBTABLES Version Win32    |
                |  Generate crystal structure data tables |
                | Distributed on Wed Dec 25 11:38:28 2002 |
                |----------------------------------------|

        |-------------------------------------------------------------|
        |            Allen C. Larson and Robert B. Von Dreele         |
        |      Manuel Lujan, Jr. Neutron Scattering Center, MS-H805    |
        |      Los Alamos National Laboratory, Los Alamos, NM  87545  |
        |                                                             |
        | Copyright, 2000, The Regents of the University of California. |
        |-------------------------------------------------------------|

 GENLES was run on May 09 22:31:33 2007    Total cycles run 729

 The Current Least-Squares controls are

 Maximum number of cycles is   12
 I/SigI cut-off is  1.00


 Anisotropic thermal factors are defined by
   T = exp(h**2*astr**2*u11+... +2*h*k*astr*bstr*u12+... )


 Space group F d -3 m
 The lattice is centric  F-centered cubic         Laue symmetry m3m
  Multiplicity of a general site is 192
  The symmetry of the point 0,0,0 contains 1bar

 The equivalent positions are:

 ( 1)     X      Y      Z  ( 2)     Z      X      Y  ( 3)     Y      Z      X
 ( 4) 1/4+X  1/4+Y     -Z  ( 5)    -Z  1/4+X  1/4+Y  ( 6) 1/4+Y     -Z  1/4+X
 ( 7) 1/4-Z  1/2+X  3/4-Y  ( 8) 3/4-Y  1/4-Z  1/2+X  ( 9) 1/2+Y  1/4-Z  3/4-X
 (10) 3/4-X  1/2+Y  1/4-Z  (11) 1/4-Z  3/4-X  1/2+Y  (12) 1/2+X  3/4-Y  1/4-Z
 (13)     Y      X      Z  (14)     Z      Y      X  (15)     X      Z      Y
 (16) 1/4+Y  1/4+X     -Z  (17)    -Z  1/4+Y  1/4+X  (18) 1/4+X     -Z  1/4+Y
 (19) 1/4-Z  1/2+Y  3/4-X  (20) 3/4-X  1/4-Z  1/2+Y  (21) 1/2+X  1/4-Z  3/4-Y
 (22) 3/4-Y  1/2+X  1/4-Z  (23) 1/4-Z  3/4-Y  1/2+X  (24) 1/2+Y  3/4-X  1/4-Z
```

Lattice constants are
a = 10.8803(11) b = A c = A
Alpha = 90 Beta = 90 Gamma = 90
Cell volume = 1288.01(23)

Name	X	Y	Z	Ui/Ue*100	Site sym	Mult	Type	Seq	Fractn
CO1	0.29222(24)	0.29222(24)	0.29222(24)	1.94*	3M(111)	32	CO	1	1.0000
CO2	0.500000	0.500000	0.500000	2.52*	-3M(111)	16	CO	2	1.0000
MO3	0.92838(21)	0.125000	0.125000	0.62*	MM2d100	48	MO	3	1.0000
N4	0.125000	0.125000	0.125000	2.50	-43M	8	N	4	0.85(9)

Thermal parameters multiplied by 100.0 are

Name	U11	U22	U33	U12	U13	U23
CO1	1.94(12)	1.94(12)	1.94(12)	0.04(14)	0.04(14)	0.04(14)
CO2	2.52(22)	2.52(22)	2.52(22)	0.77(23)	0.77(23)	0.77(23)
MO3	0.80(15)	0.53(8)	0.53(8)	0.00	0.00	-0.29(13)
N4	2.50	2.50	2.50	0.00	0.00	0.00

Profile difference plots for Co_3Mo_3N sample [(H_2/Ar) using temperature profile shown in Figure 4.2-2]= **A** and Co_3Mo_3N sample [(H_2/Ar) using temperature profile shown in Figure 4.2-2, and then treated in H_2/N_2 at 700°C] = **B**, at 298 K.

(I) **A** with both anion site occupancies freely refined **(best fit)**

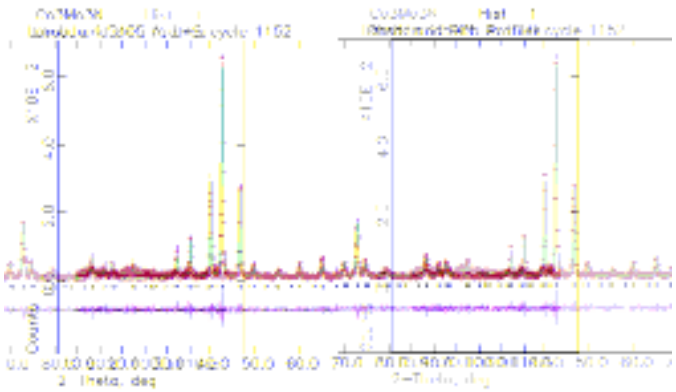

(I) **B** with both anion site occupancies freely refined

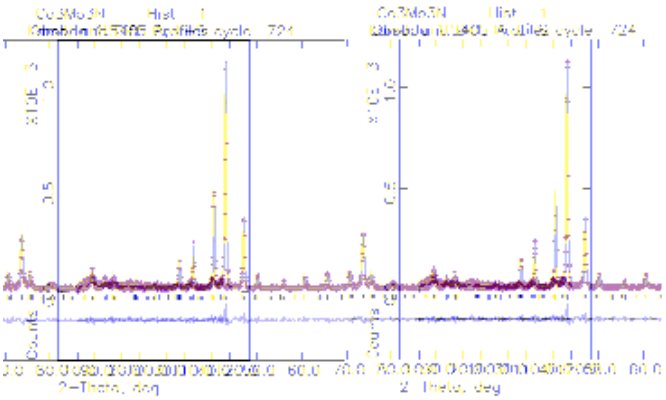

(II) **A** with the 8a site fixed as vacant

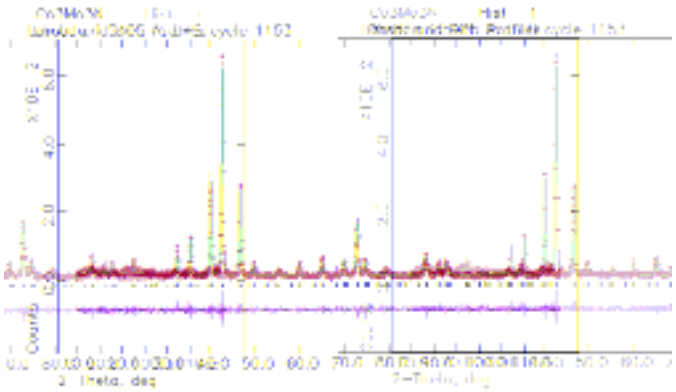

(II) **B** with the 8a site fixed as vacant

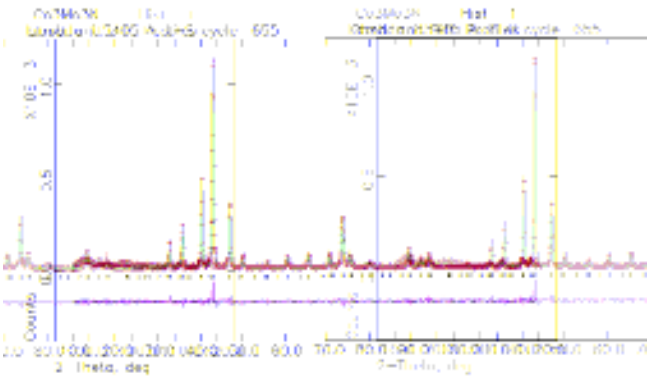

(III) **A** with the 16c site fixed as vacant

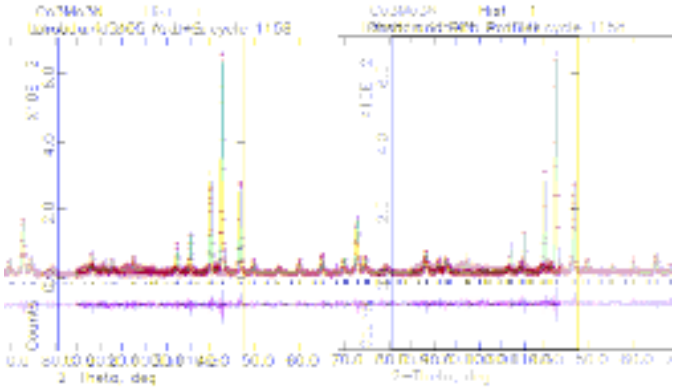

(III) **B** with the 16c site fixed as vacant **(best fit)**

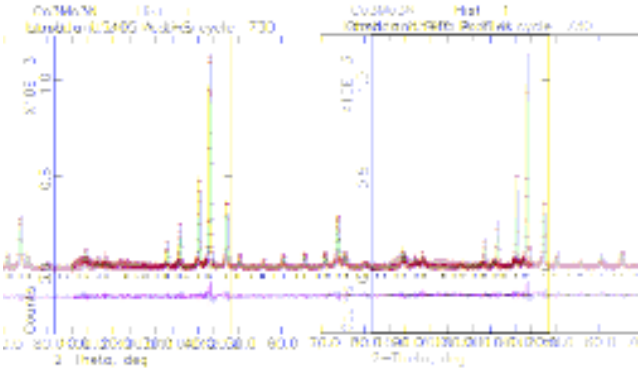

Each of the sample data were fitted to three models; (I) where both anion sites (*8a*, *16c*) were freely varied without constraint, (II) a model where the *8a* site was fixed as vacant (i.e. not refined) and (III) a model where the *16c* site was fixed as vacant (i.e. not refined).

For the Co_3Mo_3N sample **A** [(H_2/Ar) using temperature profile shown in Figure 4.2-2], model (I) gave the best fit, model (II) gave a marginally worse fit (increased R indices) while (III) gave notably higher R factors and errors and yielded an occupancy for the *8a* site that produced a markedly lower N stoichiometry than the analytical data.

For the Co_3Mo_3N sample **B** [(H_2/Ar) using temperature profile shown in Figure 4.2-2, and then treated in H_2/N_2 at 700^oC], model (III) gave the best fit, model (II) gave much higher R factors and errors and yielded an occupancy for the *16c* site that produced a markedly lower N stoichiometry than the analytical data while model (I) produced a physically meaningless negative site occupancy for the *16c* site and higher indices.

Tables of bond lengths and angles for Co_3Mo_3N sample [(H_2/N_2) using temperature profile shown in Figure 4.2-2] and Co_3Mo_3N sample [(H_2/Ar) using temperature profile shown in Figure 4.2-2 (believed to be Co_6Mo_6N)] at 298 K.

(i) Co_3Mo_3N (H_2/N_2) using temperature profile shown in Figure 4.2-2

Vector	Length	Optr Cell	Neighbor atom coordinates		
CO1_CO1	2.589(9)	-4 1 1 0	0.45808	0.45808	0.29192
CO1_CO1	2.589(9)	-5 0 1 1	0.29192	0.45808	0.45808
CO1_CO1	2.589(9)	-6 1 0 1	0.45808	0.29192	0.45808
CO1_CO2	2.3834(19)	-4 1 1 0	0.25000	0.25000	0.50000
CO1_CO2	2.3834(19)	-5 0 1 1	0.50000	0.25000	0.25000
CO1_CO2	2.3834(19)	-6 1 0 1	0.25000	0.50000	0.25000
CO1_MO3	2.624(4)	111 0 0-1	0.12500	0.32389	0.12500
CO1_MO3	2.624(4)	119 0-1 0	0.12500	0.12500	0.32389
CO1_MO3	2.7283(22)	-101 1 0 0	0.07389	0.37500	0.37500
CO1_MO3	2.7283(22)	-108 1 0 1	0.37500	0.37500	0.07389
CO1_MO3	2.7283(22)	-122 1 1 0	0.37500	0.07389	0.37500
CO1_MO3	2.624(4)	220 0 0-1	0.32389	0.12500	0.12500

Angle	Degrees	atom 1 loc	atom 3 loc
CO2_CO1_CO2	109.58(13)	-4 1 1 0	-5 0 1 1
CO2_CO1_CO2	109.58(13)	-4 1 1 0	-6 1 0 1
CO2_CO1_MO3	124.34(10)	-4 1 1 0	111 0 0-1
CO2_CO1_MO3	66.39(9)	-4 1 1 0	119 0-1 0
CO2_CO1_MO3	124.34(10)	-4 1 1 0	220 0 0-1
CO2_CO1_CO2	109.58(13)	-5 0 1 1	-6 1 0 1
CO2_CO1_MO3	124.34(10)	-5 0 1 1	111 0 0-1
CO2_CO1_MO3	124.34(10)	-5 0 1 1	119 0-1 0
CO2_CO1_MO3	66.39(9)	-5 0 1 1	220 0 0-1
CO2_CO1_MO3	66.39(9)	-6 1 0 1	111 0 0-1
CO2_CO1_MO3	124.34(10)	-6 1 0 1	119 0-1 0
CO2_CO1_MO3	124.34(10)	-6 1 0 1	220 0 0-1
MO3_CO1_MO3	72.37(12)	111 0 0-1	119 0-1 0
MO3_CO1_MO3	72.37(12)	111 0 0-1	220 0 0-1
MO3_CO1_MO3	72.37(12)	119 0-1 0	220 0 0-1

Vector	Length	Optr Cell	Neighbor atom coordinates		
CO2_CO1	2.3834(19)	4 0 0 1	0.54192	0.54192	0.70808
CO2_CO1	2.3834(19)	5 1 0 0	0.70808	0.54192	0.54192
CO2_CO1	2.3834(19)	6 0 1 0	0.54192	0.70808	0.54192
CO2_CO1	2.3834(19)	-4 1 1 0	0.45808	0.45808	0.29192
CO2_CO1	2.3834(19)	-5 0 1 1	0.29192	0.45808	0.45808
CO2_CO1	2.3834(19)	-6 1 0 1	0.45808	0.29192	0.45808
CO2_MO3	2.7488(20)	106 0 0-1	0.37500	0.37500	0.67611
CO2_MO3	2.7488(20)	109 0 0 0	0.62500	0.62500	0.32389
CO2_MO3	2.7488(20)	116 0-1 0	0.37500	0.67611	0.37500
CO2_MO3	2.7488(20)	124 0 0 0	0.62500	0.32389	0.62500
CO2_MO3	2.7488(20)	204-1 0 0	0.67611	0.37500	0.37500
CO2_MO3	2.7488(20)	210 0 0 0	0.32389	0.62500	0.62500

Angle	Degrees	atom 1 loc	atom 3 loc
CO1_CO2_CO1	65.78(20)	4 0 0 1	5 1 0 0
CO1_CO2_CO1	65.78(20)	4 0 0 1	6 0 1 0
CO1_CO2_CO1	180.000(0)	4 0 0 1	-4 1 1 0
CO1_CO2_CO1	114.22(20)	4 0 0 1	-5 0 1 1
CO1_CO2_CO1	114.22(20)	4 0 0 1	-6 1 0 1
CO1_CO2_CO1	65.78(20)	5 1 0 0	6 0 1 0
CO1_CO2_CO1	114.22(20)	5 1 0 0	-4 1 1 0
CO1_CO2_CO1	180.000(0)	5 1 0 0	-5 0 1 1
CO1_CO2_CO1	114.22(20)	5 1 0 0	-6 1 0 1
CO1_CO2_CO1	114.22(20)	6 0 1 0	-4 1 1 0
CO1_CO2_CO1	114.22(20)	6 0 1 0	-5 0 1 1
CO1_CO2_CO1	180.000(0)	6 0 1 0	-6 1 0 1
CO1_CO2_CO1	65.78(20)	-4 1 1 0	-5 0 1 1

CO1_CO2_CO1	65.78(20)	-4 1 1 0	-6 1 0 1
CO1_CO2_CO1	65.78(20)	-5 0 1 1	-6 1 0 1

Vector	Length	Optr Cell	Neighbor atom coordinates		
MO3_CO1	2.7283(22)	105 1-1-1	0.70808	0.04192	0.04192
MO3_CO1	2.624(4)	107 1-1-1	0.95808	0.29192	-0.04192
MO3_CO1	2.624(4)	111 1-1-1	0.95808	-0.04192	0.29192
MO3_CO1	2.7283(22)	-101 1 0 0	0.70808	0.20808	0.20808
MO3_CO2	2.7488(20)	7 1-1 0	0.75000	0.00000	0.25000
MO3_CO2	2.7488(20)	11 1 0-1	0.75000	0.25000	0.00000
MO3_MO3	3.098(4)	2 1-1 0	1.12500	-0.07389	0.12500
MO3_MO3	3.098(4)	3 1 0-1	1.12500	0.12500	-0.07389
MO3_MO3	2.8667(11)	5 1-1 0	0.87500	0.17611	0.37500
MO3_MO3	2.8667(11)	17 1 0-1	0.87500	0.37500	0.17611
MO3_MO3	2.8667(11)	-2 1 1 0	0.87500	0.07389	-0.12500
MO3_MO3	2.8667(11)	-3 1 0 1	0.87500	-0.12500	0.07389
MO3_MO3	3.098(4)	111 1 0-1	1.12500	0.32389	0.12500
MO3_MO3	3.098(4)	119 1-1 0	1.12500	0.12500	0.32389
MO3_N4	2.1909(28)	1 1 0 0	1.12500	0.12500	0.12500
MO3_N5	2.1106(11)	1 1 0 0	1.00000	0.00000	0.00000
MO3_N5	2.1106(11)	5 1 0 0	1.00000	0.25000	0.25000

Angle	Degrees	atom 1 loc	atom 3 loc
CO1_MO3_CO1	164.57(15)	107 1-1-1	111 1-1-1
CO1_MO3_N4	82.29(8)	107 1-1-1	1 1 0 0
CO1_MO3_N5	87.033(33)	107 1-1-1	1 1 0 0
CO1_MO3_N5	87.033(34)	107 1-1-1	5 1 0 0
CO1_MO3_N4	82.29(8)	111 1-1-1	1 1 0 0
CO1_MO3_N5	87.033(34)	111 1-1-1	1 1 0 0
CO1_MO3_N5	87.033(33)	111 1-1-1	5 1 0 0
N4_MO3_N5	67.32(7)	1 1 0 0	1 1 0 0
N4_MO3_N5	67.32(7)	1 1 0 0	5 1 0 0
N5_MO3_N5	134.63(14)	1 1 0 0	5 1 0 0

Vector	Length	Optr Cell	Neighbor atom coordinates		
N4_MO3	2.1909(28)	1-1 0 0	-0.07389	0.12500	0.12500
N4_MO3	2.1909(28)	2 0-1 0	0.12500	-0.07389	0.12500
N4_MO3	2.1909(28)	3 0 0-1	0.12500	0.12500	-0.07389
N4_MO3	2.1909(28)	111 0 0-1	0.12500	0.32389	0.12500
N4_MO3	2.1909(28)	119 0-1 0	0.12500	0.12500	0.32389
N4_MO3	2.1909(28)	220 0 0-1	0.32389	0.12500	0.12500

Angle	Degrees	atom 1 loc	atom 3 loc
MO3_N4_MO3	90.000(0)	1-1 0 0	2 0-1 0
MO3_N4_MO3	90.000(0)	1-1 0 0	3 0 0-1
MO3_N4_MO3	90.000(0)	1-1 0 0	111 0 0-1
MO3_N4_MO3	90.000(0)	1-1 0 0	119 0-1 0
MO3_N4_MO3	180.000(0)	1-1 0 0	220 0 0-1
MO3_N4_MO3	90.000(0)	2 0-1 0	3 0 0-1
MO3_N4_MO3	180.000(0)	2 0-1 0	111 0 0-1
MO3_N4_MO3	90.000(0)	2 0-1 0	119 0-1 0
MO3_N4_MO3	90.000(0)	2 0-1 0	220 0 0-1
MO3_N4_MO3	90.000(0)	3 0 0-1	111 0 0-1
MO3_N4_MO3	180.000(0)	3 0 0-1	119 0-1 0
MO3_N4_MO3	90.000(0)	3 0 0-1	220 0 0-1
MO3_N4_MO3	90.000(0)	111 0 0-1	119 0-1 0
MO3_N4_MO3	90.000(0)	111 0 0-1	220 0 0-1
MO3_N4_MO3	90.000(0)	119 0-1 0	220 0 0-1

Vector	Length	Optr Cell	Neighbor atom coordinates		
N5_MO3	2.1106(11)	1-1 0 0	-0.07389	0.12500	0.12500
N5_MO3	2.1106(11)	2 0-1 0	0.12500	-0.07389	0.12500
N5_MO3	2.1106(11)	3 0 0-1	0.12500	0.12500	-0.07389
N5_MO3	2.1106(11)	-1 1 0 0	0.07389	-0.12500	-0.12500
N5_MO3	2.1106(11)	-2 0 1 0	-0.12500	0.07389	-0.12500
N5_MO3	2.1106(11)	-3 0 0 1	-0.12500	-0.12500	0.07389

Angle	Degrees	atom 1 loc	atom 3 loc
MO3_N5_MO3	94.45(9)	1-1 0 0	2 0-1 0
MO3_N5_MO3	94.45(9)	1-1 0 0	3 0 0-1

MO3_N5_MO3	180.000(0)	1-1 0 0	-1 1 0 0
MO3_N5_MO3	85.55(9)	1-1 0 0	-2 0 1 0
MO3_N5_MO3	85.55(9)	1-1 0 0	-3 0 0 1
MO3_N5_MO3	94.45(9)	2 0-1 0	3 0 0-1
MO3_N5_MO3	85.55(9)	2 0-1 0	-1 1 0 0
MO3_N5_MO3	180.000(0)	2 0-1 0	-2 0 1 0
MO3_N5_MO3	85.55(9)	2 0-1 0	-3 0 0 1
MO3_N5_MO3	85.55(9)	3 0 0-1	-1 1 0 0
MO3_N5_MO3	85.55(9)	3 0 0-1	-2 0 1 0
MO3_N5_MO3	180.000(0)	3 0 0-1	-3 0 0 1
MO3_N5_MO3	94.45(9)	-1 1 0 0	-2 0 1 0
MO3_N5_MO3	94.45(9)	-1 1 0 0	-3 0 0 1
MO3_N5_MO3	94.45(9)	-2 0 1 0	-3 0 0 1

(ii) Co_3Mo_3N sample (H_2/Ar) using temperature profile shown in Figure 4.2-2 (believed to be Co_6Mo_6N)

Vector	Length	Optr Cell	Neighbor atom coordinates		
CO1_CO1	2.548(7)	-4 1 1 0	0.45778	0.45778	0.29222
CO1_CO1	2.548(7)	-5 0 1 1	0.29222	0.45778	0.45778
CO1_CO1	2.548(7)	-6 1 0 1	0.45778	0.29222	0.45778
CO1_CO2	2.3522(15)	-4 1 1 0	0.25000	0.25000	0.50000
CO1_CO2	2.3522(15)	-5 0 1 1	0.50000	0.25000	0.25000
CO1_CO2	2.3522(15)	-6 1 0 1	0.25000	0.50000	0.25000
CO1_MO3	2.5928(35)	111 0 0-1	0.12500	0.32162	0.12500
CO1_MO3	2.5928(35)	119 0-1 0	0.12500	0.12500	0.32162
CO1_MO3	2.7173(18)	-101 1 0 0	0.07162	0.37500	0.37500
CO1_MO3	2.7173(18)	-108 1 0 1	0.37500	0.37500	0.07162
CO1_MO3	2.7173(18)	-122 1 1 0	0.37500	0.07162	0.37500
CO1_MO3	2.5928(35)	220 0 0-1	0.32162	0.12500	0.12500

Angle	Degrees	atom 1 loc	atom 3 loc
CO2_CO1_CO2	109.71(10)	-4 1 1 0	-5 0 1 1
CO2_CO1_CO2	109.71(10)	-4 1 1 0	-6 1 0 1
CO2_CO1_MO3	124.16(8)	-4 1 1 0	111 0 0-1
CO2_CO1_MO3	66.88(8)	-4 1 1 0	119 0-1 0
CO2_CO1_MO3	124.16(8)	-4 1 1 0	220 0 0-1
CO2_CO1_CO2	109.71(10)	-5 0 1 1	-6 1 0 1
CO2_CO1_MO3	124.16(8)	-5 0 1 1	111 0 0-1
CO2_CO1_MO3	124.16(8)	-5 0 1 1	119 0-1 0
CO2_CO1_MO3	66.88(8)	-5 0 1 1	220 0 0-1
CO2_CO1_MO3	66.88(8)	-6 1 0 1	111 0 0-1
CO2_CO1_MO3	124.16(8)	-6 1 0 1	119 0-1 0
CO2_CO1_MO3	124.16(8)	-6 1 0 1	220 0 0-1
MO3_CO1_MO3	71.38(10)	111 0 0-1	119 0-1 0
MO3_CO1_MO3	71.38(10)	111 0 0-1	220 0 0-1
MO3_CO1_MO3	71.38(10)	119 0-1 0	220 0 0-1

Vector	Length	Optr Cell	Neighbor atom coordinates		
CO2_CO1	2.3522(15)	4 0 0 1	0.54222	0.54222	0.70778
CO2_CO1	2.3522(15)	5 1 0 0	0.70778	0.54222	0.54222
CO2_CO1	2.3522(15)	6 0 1 0	0.54222	0.70778	0.54222
CO2_CO1	2.3522(15)	-4 1 1 0	0.45778	0.45778	0.29222
CO2_CO1	2.3522(15)	-5 0 1 1	0.29222	0.45778	0.45778
CO2_CO1	2.3522(15)	-6 1 0 1	0.45778	0.29222	0.45778
CO2_MO3	2.7325(17)	106 0 0-1	0.37500	0.37500	0.67838
CO2_MO3	2.7325(17)	109 0 0 0	0.62500	0.62500	0.32162
CO2_MO3	2.7325(17)	116 0-1 0	0.37500	0.67838	0.37500
CO2_MO3	2.7325(17)	124 0 0 0	0.62500	0.32162	0.62500
CO2_MO3	2.7325(17)	204-1 0 0	0.67838	0.37500	0.37500
CO2_MO3	2.7325(17)	210 0 0 0	0.32162	0.62500	0.62500

Angle	Degrees	atom 1 loc	atom 3 loc
CO1_CO2_CO1	65.57(17)	4 0 0 1	5 1 0 0
CO1_CO2_CO1	65.57(17)	4 0 0 1	6 0 1 0
CO1_CO2_CO1	179.941(0)	4 0 0 1	-4 1 1 0
CO1_CO2_CO1	114.43(17)	4 0 0 1	-5 0 1 1
CO1_CO2_CO1	114.43(17)	4 0 0 1	-6 1 0 1
CO1_CO2_CO1	65.57(17)	5 1 0 0	6 0 1 0
CO1_CO2_CO1	114.43(17)	5 1 0 0	-4 1 1 0
CO1_CO2_CO1	179.972(0)	5 1 0 0	-5 0 1 1
CO1_CO2_CO1	114.43(17)	5 1 0 0	-6 1 0 1
CO1_CO2_CO1	114.43(17)	6 0 1 0	-4 1 1 0
CO1_CO2_CO1	114.43(17)	6 0 1 0	-5 0 1 1
CO1_CO2_CO1	179.941(0)	6 0 1 0	-6 1 0 1
CO1_CO2_CO1	65.57(17)	-4 1 1 0	-5 0 1 1
CO1_CO2_CO1	65.57(17)	-4 1 1 0	-6 1 0 1
CO1_CO2_CO1	65.57(17)	-5 0 1 1	-6 1 0 1

Vector	Length	Optr Cell	Neighbor atom coordinates		
MO3_CO1	2.7173(18)	105 1-1-1	0.70778	0.04222	0.04222
MO3_CO1	2.5928(35)	107 1-1-1	0.95778	0.29222	-0.04222
MO3_CO1	2.5928(35)	111 1-1-1	0.95778	-0.04222	0.29222

MO3_CO1	2.7173(18)	-101 1 0 0	0.70778	0.20778	0.20778
MO3_CO2	2.7325(17)	7 1-1 0	0.75000	0.00000	0.25000
MO3_CO2	2.7325(17)	11 1 0-1	0.75000	0.25000	0.00000
MO3_MO3	3.0253(33)	2 1-1 0	1.12500	-0.07162	0.12500
MO3_MO3	3.0253(33)	3 1 0-1	1.12500	0.12500	-0.07162
MO3_MO3	2.8414(10)	5 1-1 0	0.87500	0.17838	0.37500
MO3_MO3	2.8414(10)	17 1 0-1	0.87500	0.37500	0.17838
MO3_MO3	2.8414(10)	-2 1 1 0	0.87500	0.07162	-0.12500
MO3_MO3	2.8414(10)	-3 1 0 1	0.87500	-0.12500	0.07162
MO3_MO3	3.0253(33)	111 1 0-1	1.12500	0.32162	0.12500
MO3_MO3	3.0253(33)	119 1-1 0	1.12500	0.12500	0.32162
MO3_N4	2.1392(23)	1 1 0 0	1.12500	0.12500	0.12500

Angle	Degrees	atom 1 loc	atom 3 loc
CO1_MO3_CO1	165.83(12)	107 1-1-1	111 1-1-1
CO1_MO3_N4	82.91(6)	107 1-1-1	1 1 0 0
CO1_MO3_N4	82.91(6)	111 1-1-1	1 1 0 0

Vector	Length	Optr Cell	Neighbor atom coordinates		
N4_MO3	2.1392(23)	1-1 0 0	-0.07162	0.12500	0.12500
N4_MO3	2.1392(23)	2 0-1 0	0.12500	-0.07162	0.12500
N4_MO3	2.1392(23)	3 0 0-1	0.12500	0.12500	-0.07162
N4_MO3	2.1392(23)	111 0 0-1	0.12500	0.32162	0.12500
N4_MO3	2.1392(23)	119 0-1 0	0.12500	0.12500	0.32162
N4_MO3	2.1392(23)	220 0 0-1	0.32162	0.12500	0.12500

Angle	Degrees	atom 1 loc	atom 3 loc
MO3_N4_MO3	90.000(0)	1-1 0 0	2 0-1 0
MO3_N4_MO3	90.000(0)	1-1 0 0	3 0 0-1
MO3_N4_MO3	90.000(0)	1-1 0 0	111 0 0-1
MO3_N4_MO3	90.000(0)	1-1 0 0	119 0-1 0
MO3_N4_MO3	180.000(0)	1-1 0 0	220 0 0-1
MO3_N4_MO3	90.000(0)	2 0-1 0	3 0 0-1
MO3_N4_MO3	180.000(0)	2 0-1 0	111 0 0-1
MO3_N4_MO3	90.000(0)	2 0-1 0	119 0-1 0
MO3_N4_MO3	90.000(0)	2 0-1 0	220 0 0-1
MO3_N4_MO3	90.000(0)	3 0 0-1	111 0 0-1
MO3_N4_MO3	180.000(0)	3 0 0-1	119 0-1 0
MO3_N4_MO3	90.000(0)	3 0 0-1	220 0 0-1
MO3_N4_MO3	90.000(0)	111 0 0-1	119 0-1 0
MO3_N4_MO3	90.000(0)	111 0 0-1	220 0 0-1
MO3_N4_MO3	90.000(0)	119 0-1 0	220 0 0-1